



LIBRARIES  
MICHIGAN STATE UNIVERSITY  
EAST LANSING, MICH. 48824

This is to certify that the

thesis entitled

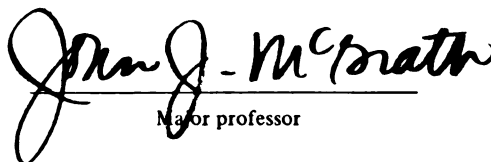
MICROCALORIMETRIC DETERMINATION OF THE  
THERMOELASTIC MEMBRANE PROPERTIES OF CELL-SIZE,  
UNILAMELLAR PHOSPHATIDYLCHOLINE LIPOSOMES

presented by

Thomas P. Gielda

has been accepted towards fulfillment  
of the requirements for

Master's degree in Mechanical  
Engineering

  
Major professor

Date 2-16-84



RETURNING MATERIALS:  
Place in book drop to  
remove this checkout from  
your record. FINES will  
be charged if book is  
returned after the date  
stamped below.

--	--	--

MICROCALORIMETRIC DETERMINATION OF THE  
THERMOELASTIC MEMBRANE PROPERTIES OF CELL-SIZE,  
UNILAMELLAR PHOSPHATIDYLCHOLINE LIPOSOMES

By

Thomas P. Gielda

A Thesis

Submitted to  
Michigan State University  
in partial fulfillment of the requirements  
for the degree of

MASTER OF SCIENCE

Department of Mechanical Engineering

1984

## ABSTRACT

### MICROCALORIMETRIC DETERMINATION OF THE THERMOELASTIC MEMBRANE PROPERTIES OF CELL-SIZE, UNILAMELLAR PHOSPHATIDYLCHOLINE LIPOSOMES

By

Thomas P. Gielda

The thermoelastic properties of large unilamellar egg and soy L- $\alpha$  phosphatidylcholine vesicles were determined experimentally. In these experiments the vesicles were formed in low concentrations (32 mosm) of sulpho rhodamine G ex dye. This was performed to allow observation under phase contrast illumination. The isothermal compressibility moduli,  $K_T$ , were found to be 80.0 and 52.0 dynes/cm for the egg and soy phosphatidylcholine respectively. These values were found to be statistically different than the results of Kwok and Evans (1981). The thermal expansion coefficient,  $C_T$ , of the soy L- $\alpha$  phosphatidylcholine vesicles was experimentally determined to be  $3.6 \times 10^{-3} \text{ } ^\circ\text{C}^{-1}$ . This result is in agreement with earlier investigators. The experimental results were then used in the formation of a state plane for the vesicle. The experimental data were collected on a micro-vesicle aspiration system. The apparatus was designed, fabricated and characterized during the course of the investigation.

## ACKNOWLEDGEMENTS

I would like to thank Dr. Robert Olien for his support in financing important equipment needs for this investigation. I would also like to recognize Dr. Bill Dunker, D.D. and Ms. Vicki Rakowski, R.N. Their friendship, understanding and professional skills have allowed me to complete this work. Special thanks go to my adviser, Dr. John McGrath for providing the direction and insight required in undertaking this adventure. I express my deep appreciation for always being there when I needed him. However, I owe the most to my loving wife, Peggy, and my son, Benjamin. They were constant reminders as to what is really important in life. Without their understanding and love this work would never have been completed.

## TABLE OF CONTENTS

		Page
	LIST OF TABLES .....	vi
	LIST OF FIGURES .....	vii
	NOMENCLATURE .....	x
 CHAPTER		
1	INTRODUCTION .....	1
	1.1 Early Work .....	2
2	MEMBRANE MECHANICS .....	7
	2.1 Derivation of Membrane Mechanical Properties .....	7
	2.1.1 Isothermal Compressibility Modulus of the Membrane .....	8
	2.1.2 Thermal Expansion Coefficient at Constant Tension .....	14
	2.1.3 Tension and Surface Pressure in the Vesicle .....	15
	2.1.4 Thermal Expansion Coefficient at Constant Surface Pressure .....	19
	2.1.5 Bending Modulus of the Membrane .....	20
	2.2 Tension and Pressure Differential Equations .....	23
	2.3 Summary .....	25
3	EQUIPMENT AND PROCEDURES .....	26
	3.1 Micropipette Fabrication .....	28
	3.1.1 Manufacturing Process Background .....	28
	3.1.2 Micropipette Manufacturing Process .....	30
	3.2 Micromanipulator System .....	32
	3.2.1 Integration of the Manipulator to the Microscope .....	32
	3.2.2 Liposome Aspiration System .....	36
	3.3 Test Stage .....	38
	3.3.1 Next Generation Test Stage .....	40

## TABLE OF CONTENTS (Continued)

CHAPTER		Page
	3.4 Liposome Formation .....	44
	3.4.1 Materials .....	44
	3.5 Bulk Compressibility Modulus Experimental Procedure .....	45
	3.6 Thermal Expansion Coefficient Experimental Procedure .....	48
	3.7 Experimental Sensitivity .....	49
	3.8 Summary .....	51
4	EXPERIMENTAL RESULTS .....	52
	4.1 Isothermal Compressibility Modulus .....	52
	4.2 Thermal Expansion Coefficient at Constant Membrane Tension .....	59
	4.3 Summary .....	60
5	PHASE TRANSITIONS IN LIPOSOMES .....	61
	5.1 Background Information .....	61
	5.2 Phase Change Experiments: Single-Component Systems .....	63
	5.3 Phase Transition: Two-Component Systems .....	64
	5.4 Limitations .....	65
6	RECOMMENDATIONS FOR FUTURE WORK .....	68
	6.1 Osmotic Shrinkage Experiments .....	68
	6.2 Ice-Water Interface Experiments .....	70
	6.3 Summary .....	73
	APPENDIX A--RELATION OF MEMBRANE TENSION TO SUCTION PRESSURE ..	75
	APPENDIX B--COMPUTER MODELLING AND DATA MANIPULATION .....	77
	B.1 Computer Modeling and Data Manipulation .....	77
	B.1.1 Computer Modeling .....	78
	B.1.2 Data Manipulation .....	78
	B1.2.1 Isothermal Compressibility Modulus .....	79
	B1.2.2 Coefficient of Expansion at Constant Membrane Tension .....	79
	B.1.3 User Notes .....	79



## TABLE OF CONTENTS (Continued)

	Page
APPENDIX C--TEMPERATURE CONTROL PROGRAM FOR THE SECOND GENERATION TEST STAGE .....	86
C.1 Introduction .....	86
C.2 Thermal Analysis .....	87
C.2.1 Cooling Cycle .....	87
C.2.2 Heating Cycle .....	89
C.3 Computer Modeling and Control .....	90
C.3.1 Computer Modeling of the Microscope Stage .....	90
C.3.1.1 Description of Error Analysis Figures .....	90
C.3.1.2 Summary of Parameter Studies .....	91
C.3.2 Computer Program for Temperature Control .....	98
C.4 Digital Control Hardware .....	102
C.4.1 Analog-to-Digital Thermocouple Amplifier .....	102
C.4.2 Digital-to-Analog Power Amplifier .....	108
C.5 Experimental Results .....	108
C.5.1 Microscope Stage Characteristics .....	108
C.5.2 Effect of Operation Parameter Variations .....	112
C.6 Conclusions .....	116
C.6.1 Correlation of the Model to Experiments .....	116
C.6.2 Error Sources and Reduction .....	116
APPENDIX D--EXPERIMENTAL UNCERTAINTY .....	118
D.1 Uncertainty Analysis for Isothermal Compressibility Modulus Experiment .....	118
D.2 Uncertainty Analysis for the Thermal Expansion Coefficient .....	119
APPENDIX E--STATE PLANE GENERATION .....	120
BIBLIOGRAPHY .....	121

## LIST OF TABLES

TABLE		Page
1.1	A Summary of Previous Results Describing Various Thermoelastic Membrane Properties .....	4
4.1	A Comparison of Current Results with Published Results for Isothermal Compressibility Modulus and Thermal Expansion Coefficient .....	53

## LIST OF FIGURES

FIGURE		Page
1.1	Cross Section of a Liposome Membrane .....	5
2.1	A Differential Membrane Element in the Plane of the Membrane Before and After Deformation .....	10
2.2	A Schematic Representation of the State Plane ( $\pi$ - $\bar{A}$ ) for a Typical Monolayer .....	17
2.3	Representation of Geometric Considerations Required to Determine the Membrane Bending Modulus from Micro-aspiration Experiments .....	22
3.1	Schematic of the Overall Experimental System .....	27
3.2	Micropipette Schematic Illustrating Typical Sizes and Geometries .....	29
3.3	Equipment Used to Produce Flat-Ended Micropipettes .....	31
3.4	Photograph of Micromanipulator System Mounted on Microscope .....	33
3.5	Photographic Detail of Manipulator, Micropipette and Sample Stage .....	35
3.6	Experimental Hydrostatic Set-Up Designed to Create and Measure the Suction Pressure Applied to Cells and Microvesicles .....	37
3.7	Schematic of the Sample Stage Used to Hold the Sample as Well as Control and Measure Temperature .....	39
3.8	Test Stage Open-Loop Transfer Function (Temperature Difference as a Function of Input Current) .....	41
3.9	Schematic of a Proposed Second-Generation Test Stage .....	43
3.10	Illustration of Membrane Deformation in a Micropipetting Experiment .....	47

## LIST OF FIGURES (Continued)

FIGURE		Page
4.1	A Typical Result for the Isothermal Compressibility Modulus Determination (Membrane Isotropic Tension as a Function of Normalized Area Change) .....	55
4.2	"State" Plane for the Liposome Membrane (Isotropic Tension as a Function of Temperature and Normalized Area Change) .....	57
4.3	State Plane for the Liposome Membrane (Membrane Surface Pressure as a Function of Temperature and Normalized Area Change) .....	58
5.1	Temperature of Onset and Completion of Solid-Liquid Separation in DMPC/DPPE Vesicles (Reproduced from Lee (1975)) .....	66
6.1	Schematic of the Interfacial Interaction between a Liposome and an Ice/Water Interface .....	72
A.1	Membrane Deformation Schematic Used for Performing Membrane Force Balance .....	76
C2.1	Schematic Representation of the First Law of Thermodynamics Applied to the Cryomicroscope Stage .....	88
C2.2	Schematic Representation of the First Law of Thermodynamics for the Cooling Process .....	88
C2.3	Schematic Representation of the First Law of Thermodynamics for the Heating Process .....	88
C3.1	Predicted Controller Steady State Error as a Function of Coolant Temperature .....	92
C3.2	Predicted Maximum Steady State Error as a Function of Temperature Sampling Rate .....	92
C3.2b	A Log-Log Representation of the Steady State Temperature Error as a Function of Temperature Sampling Frequency .....	93

## LIST OF FIGURES (Continued)

FIGURE		Page
C3.3	Predicted Maximum Steady State Error as a Function of Heater Input (HPC) .....	94
C3.4	Simulated Response of the Cryomicroscope Stage to a 10°C Temperature Change .....	94
C3.5	Simulated Response of the Cryomicroscope Stage to a Temperature Ramp of 80 C.min <sup>-1</sup> .....	95
C3.6	Pressure as a Function of Volume for the Coolant Fluid in the Cryomicroscope Stage .....	96
C3.7	Temperature Controller Flow Chart .....	103
C4.1	Electrical Schematic for Thermocouple Input Signal Conditioner .....	109
C4.2	Bode Plot for the Thermocouple Input Signal Conditioner (with Experimental Data) .....	110
C4.3	Overall Schematic of Temperature Controller .....	111
C5.1	Typical Experimental System Response to a Step Input Current to the Microscope Stage Heater .....	113
C5.2	System Response as a Function of the Microscope Heater Driver Voltage .....	114
C5.3	Maximum Temperature Rise as a Function of the Microscope Heater Driver Voltage .....	114
C5.4	Measured Steady State Temperature Error as a Function of Set Point Temperature with Proportional Control .....	115
C5.5	Effect of Different Thermal Sink Temperatures on the Stage Cooling Rate .....	115

## NOMENCLATURE

$C_p$	Specific Heat at Constant Pressure
$C_v$	Specific Heat at Constant Volume
$C_T$	Thermal Expansion Coefficient at Constant Membrane Tension
$C_\pi$	Thermal Expansion Coefficient at Constant Membrane Surface Pressure
$\tilde{F}$	Helmholtz Free Energy
$K_T$	Isotropic Compressibility Modulus
$Q$	Heat
$Q_T$	Membrane Transverse Shear
$S$	Entropy
$T$	Temperature
$T_i$	Principal Tension in the $i^{\text{th}}$ Principal Axis Direction
$\bar{T}$	Isotropic Membrane Tension
$T_S$	Maximum Membrane Shear Stress
$\alpha$	Nondimensional Area Change
$\beta$	Deformation Variable Associated with Membrane Shear
$\gamma$	Intramembrane Tension
$\lambda$	Membrane Extension Ratio
$\pi$	Membrane Surface Pressure

## CHAPTER 1

### INTRODUCTION

The purpose of this work was to determine the mechanical properties of egg and soy phosphatidylcholine (PC) cell-size, unilamellar vesicles: in particular, the isothermal compressibility modulus and the thermal expansion coefficient. This information is invaluable in the biophysical characterization of the lipid membrane. Once such properties of these simple model membrane systems are well-defined, the rationale is that these results and techniques can then be used in the study of much more complicated membrane systems such as actual biological membranes. Aside from determining the basic biophysical properties of membranes, this work also represents the first step in the research program of the Bioengineering Transport Processes (BTP) Laboratory aimed at understanding how the mechanical properties of cell membranes are related to freezing injury.

The results of this and future work in this area have many applications. By knowing the membrane properties of healthy biological cells, these techniques can be used as diagnostic tools in the detection of cell abnormalities (i.e., cell malignancies). The characterization of the cell membrane can also be used in the design of artificial organs. The designer must know the limits of stress which can be placed on the cell as it flows through the organ.

The membrane mechanical properties in this work were found by performing micropipette aspiration experiments on cell size, unilamellar

lipid vesicles (liposomes). This experimental technique was first developed in the early 1950s by Mitchison and Swan. A summary of earlier related work using micropipette aspiration techniques follows.

### 1.1 Early Work

Mitchison and Swan (1954) were the first investigators to implement micropipette aspiration techniques to determine the mechanical properties of biological systems. In their work they attempted to determine the "stiffness" of the sea urchin egg membrane. The term "stiffness" here refers to some measure of the membrane resistance to deformation. Further clarification of this point will be discussed below. Their experiments involved deformation of the egg at constant surface area. The results of their experiments yielded the shear modulus of the membrane, although they did not know it at the time. Instead, they stated that they had determined the elastic modulus of the membrane.

Rand and Burton (1964) applied the same techniques of Mitchison and Swan to the red blood cell (RBC). They too were interested in determining the "stiffness" of the membrane. The results of these earlier investigators were not clarified until Skalak et al., (1973) and Evans (1973) decomposed the membrane stiffness into the resistance to shearing deformation at constant area and the resistance to area dilatation or condensation. The theoretical basis for this decomposition is discussed in detail in Evans and Waugh (1977) and Evans and Skalak (1980). Steponkus (1982) determined the compressibility modulus of the *Secale Cereale* L. cv. Puma protoplast. He found the compressibility modulus to be 230.0 dynes/cm.



A summary of the results of the above-mentioned investigators are shown in Table 1.1. From the table it is observed that the early investigators, Mitchison and Swan as well as Rand and Burton, were determining the shear modulus of the membrane, where the shear modulus is the membrane resistance to shape changes while at constant area. This is apparent since the values they calculated for their compressibility moduli are much smaller than the values obtained for the compressibility moduli. This is consistent with their experimental procedures since they did not induce membrane tensions large enough to produce area dilatations.

Little work in this field has been done concerning liposomes, even though this represents an interesting and important model membrane since the membrane can be studied without the influence of the structure usually enclosed in a biological membrane. The membrane to be studied is shown in Figure 1.1 taken from Israelachvili et al., (1980). Kwok and Evans (1981) and Evans and Kwok (1982) have determined the compressibility moduli and the thermal expansion coefficients for egg PC and dimyristoyl PC (DMPC) vesicles. Their results are also in Table 1.1.

In addition to the membrane mechanical properties, Evans and Kwok (1982) have been able to determine the phase transition temperature of DMPC vesicles by measuring the changes in their compressibility moduli of the DMPC vesicles with temperature. They have demonstrated that by assuming a Gaussian distribution for the transition temperature and performing a convolution of an idealized first order phase transition, they obtain excellent correlation between predicted compressibility moduli and experimental data. They also report that by coupling

PREVIOUS WORK				
SYSTEM	COMPRESSIBILITY MODULUS (dynes/cm)	SHEAR MODULUS (dynes/cm)	THERMAL EXPANSION COEFFICIENT (1/°C)	INVESTIGATOR
Sea Urchin Egg	n/a	1.6-0.84	n/a	Mitchison and Swann (1954)
Red Blood Cell	Order 100	0.0019	n/a	Rand and Burton (1964)
Red Blood Cell	450.0	0.016	n/a	Evans, Waugh and Melnik (1976)
Plasma ** Membrane	230.0	n/a	n/a	Steponkus (1982)
Liposome Egg PC	140.0	n/a	0.0024	Kwok and Evans (1981)
Liposome DMPC	140.-128.	n/a	0.004-0.006	Evans and Kwok (1982)

\*\* Secale Cereale L. cv. Puma Protoplast

Table 1.1 A Summary of Previous Results Describing  
Various Thermoelastic Membrane Properties

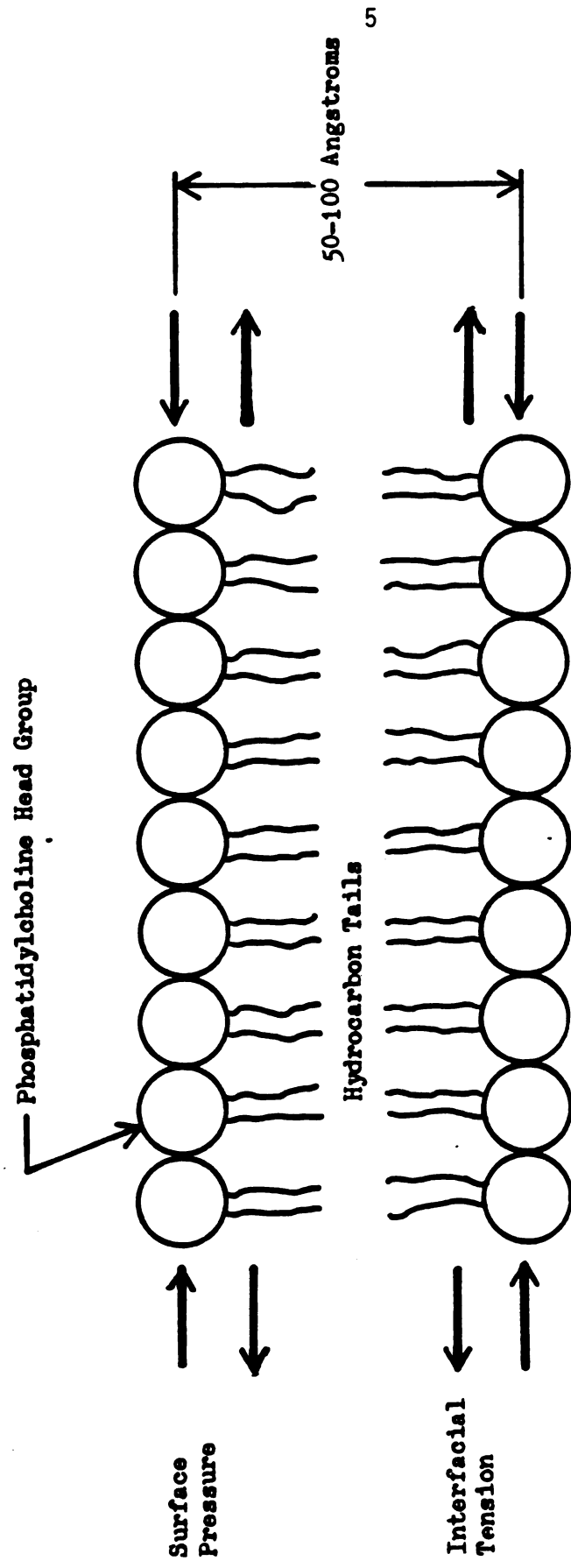


Figure 1.1 Cross Section of a Liposome Membrane

the convolution approach with the Clausius-Clapeyron equation for the membrane they can predict the transition temperatures of the vesicles.

This investigation is intended to be the foundation for future work related to membrane mechanics in the BTP laboratory. In order to perform such research a complete microcalorimetry system is required. This apparatus consists of the manipulator, data acquisition and temperature controlling systems. The experimental apparatus must be designed and fabricated. In addition the apparatus must have the capability to perform thermal transition temperature experiments similar to Evans and Kwok. Therefore, a major objective of the present research is the development of a complete microcalorimetry experimental apparatus. A second major objective is the reproduction of published data for representative types of major experiments of interest to verify that the experimental system yields acceptable data. Finally the system will be used to determine previously unpublished values of the isothermal compressibility modulus and the thermal expansion coefficient for soy PC vesicles. These data are useful with respect to defining the manner in which membrane composition affects membrane mechanical properties.

## CHAPTER 2

### MEMBRANE MECHANICS

The strategy of this chapter will be to relate the membrane mechanical properties to the thermodynamic state of the membrane. This will be accomplished by relating the change in energy of the membrane to the Helmholtz function. This information will then be coupled to the data provided by the solution of the differential equation for membrane surface pressure to yield the thermoelastic properties of the membrane, namely  $C_T$  and  $K_T$ . The integration of the differential equation for the membrane surface pressure yields the state plane for the membrane. The variables of the state plane equation are surface pressure, area and temperature. This is directly analogous to pressure, volume and temperature of the more common three-dimensional thermoelastic system.

#### 2.1 Derivation of Membrane Mechanical Properties

The function of this section is to relate theoretically the two membrane mechanical properties, isothermal compressibility modulus and the thermal expansion coefficient, to readily measured properties (i.e., isotropic tension and membrane area changes). In addition to the above, differential equations for the changes in isotropic tension and surface pressure will be derived. These equations will then be integrated in Chapter 4 to yield an equation of state for the vesicle membrane, where the variables of state are surface pressure, area and temperature. The following analysis is based primarily on the works of Evans and Skalak (1980) and Evans and Waugh (1977).

### 2.1.1 Isothermal Compressibility Modulus of the Membrane

This section will demonstrate the extraction of the membrane compressibility modulus from experimentally measured membrane tension data. The first law is written in integral and differential form for a reversible process as:

$$\int dE = \int (\delta Q + \delta W) \quad (2.1.1.1)$$

$$dE = \delta Q + \delta W \quad (2.1.1.2)$$

Where work done on the membrane brings about a positive change in energy.

For a reversible process the differential amount of heat transfer involved in a process can be calculated from the differential change in entropy:

$$\delta Q = TdS$$

From the second law of thermodynamics for a general process:

$$dS \geq \delta Q/T \quad (2.1.1.3)$$

Equation (2.1.1.2) is an exact differential in the energy  $E$ , and we assume that the process is energy conserving, therefore there exists a potential function as its solution. At this point a choice can be made as to what potential energy function will be used to describe the membrane system. The Helmholtz function will be used since the variables in Equation (2.1.1.2) are internal energy, heat flux and entropy. The Gibbs Function would be used if enthalpy were a variable instead of internal energy. The Helmholtz function is defined as:

$$\tilde{F} = \tilde{E} - T\tilde{S} \quad (2.1.1.4)$$

The  $\sim$  superscript defines the extensive property  $E$  or  $S$  taken on a per unit area basis. This is done since the first and second law are based on the entire liposome membrane system, while we are interested in elemental membrane area.

If Equation (2.1.1.4) is differentiated, and we assume an isothermal reversible process the equation can be written as:

$$d\tilde{F} = d\tilde{W} = d\tilde{E} - Td\tilde{S} \quad (2.1.1.5)$$

Figure 2.1 depicts an elemental membrane area undergoing a small deformation. At constant temperature the potential energy function is dependent on two membrane deformation variables. The potential energy function is independent of temperature. A useful analogy is energy stored in a spring, where the spring constant is constant at all temperatures.

Figure 2.1 represents an elemental membrane area at two different states. Note the two figures are related by:

$$dx_i = \lambda_i a_i$$

$$i = 1, 2$$

- (1)  $\alpha$  is the measure of the change of area to condensation or dilitation. It is defined as:

$$\alpha = \Delta A/A_0 = \lambda_1 \lambda_2 - 1 \quad (2.1.1.6)$$

- (2)  $\beta$  is defined as the measure of the change of the membrane shape, at constant area (i.e., change of aspect ratio of a rectangle). It is defined as:

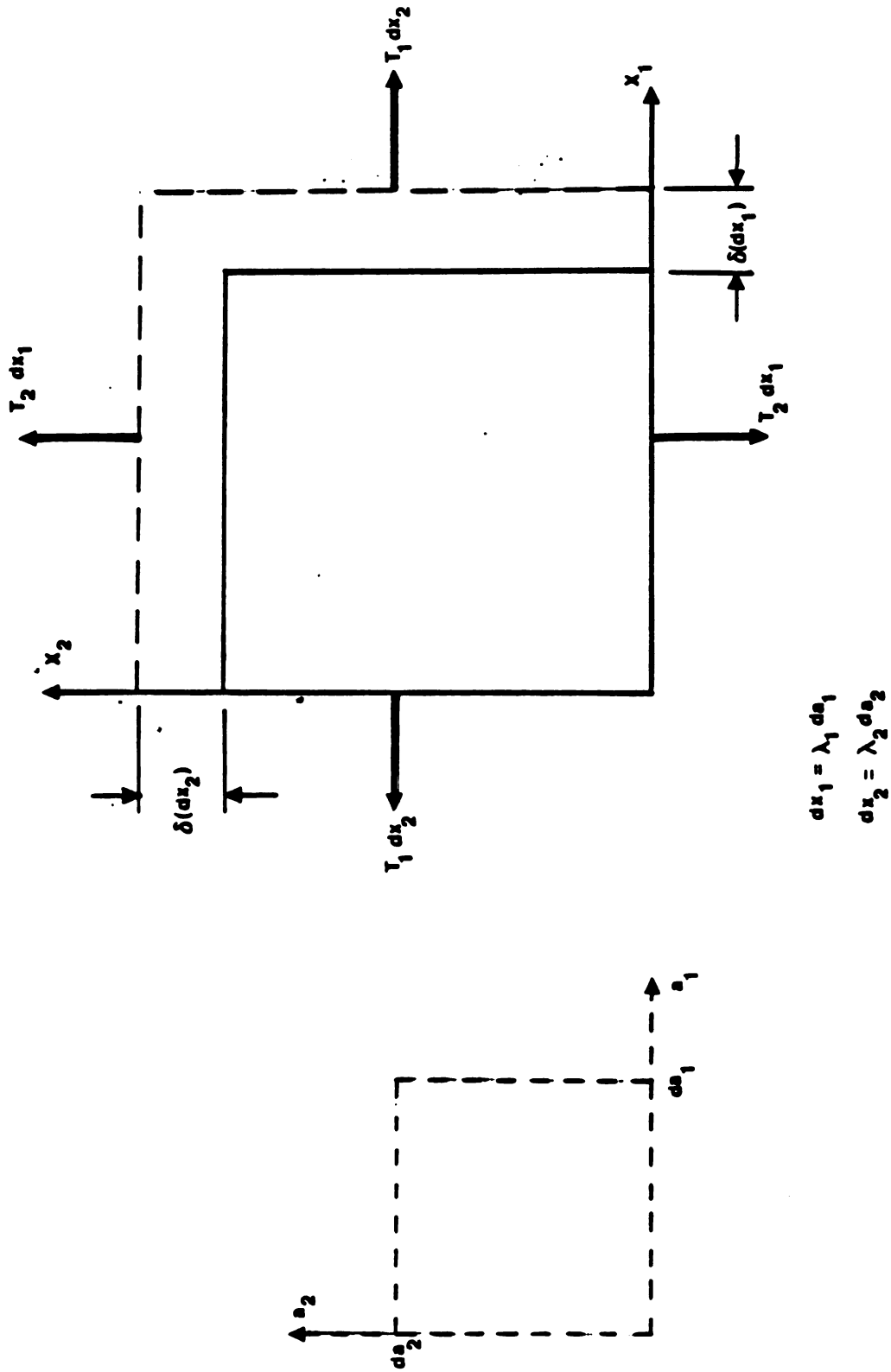


Figure 2.1 A Differential Membrane Element in the Plane of the Membrane Before and After Deformation



$$\beta = (\lambda_1^2 + \lambda_2^2)/(2\lambda_1\lambda_2) \quad (2.1.1.7)$$

where  $\lambda_1$  and  $\lambda_2$  are the principal extension ratios of the material defined by the following relations:

$$X_1 = \lambda_1 a_1 \quad (2.1.1.8)$$

$$X_2 = \lambda_2 a_2$$

The position of  $X_i$  at a different state than the initial position,  $a_i$ , is related by the extension ratio  $\lambda_i$ . That is to say:

$$X_i = f(a_i)$$

$$a_i = f^{-1}(X_i)$$

The two functions are the inverse of each other.

Incremental work was performed on the membrane. It was assumed that the work performed from state 1 to state 2 was isothermal and reversible.

For Figure 2.1 the equation for incremental work can be written as:

$$\delta W = [(T_1 dx_2) \delta(dx_1) + (T_2 dx_1) \delta(dx_2)] \quad (2.1.1.9)$$

Where  $T_1$  and  $T_2$  are the principal tensions in the membrane. Using the definitions of the extension ratios, Equation (2.1.1.9) can be rewritten as:

$$\delta W = [(T_1 \lambda_2 \delta \lambda_1) + (T_2 \lambda_1 \delta \lambda_2)] dA_0 \quad (2.1.1.10)$$

As a result, for an isothermal, reversible process the Helmholtz potential energy function is defined as:

$$(d\tilde{F})_T = (T_1 \lambda_2 d\lambda_1) + (T_2 \lambda_1 d\lambda_2) = \delta \tilde{W} \quad (2.1.1.11)$$

The differential change in the elastic potential energy function is dependent on the two deformation variables  $\alpha$  and  $\beta$ . Since  $\alpha$  and  $\beta$  are dependent on the extension ratios the following differential equations are formed:

$$d\alpha = [\partial\alpha/\partial\lambda_1]d\lambda_1 + [\partial\alpha/\partial\lambda_2]d\lambda_2 \quad (2.1.1.12)$$

$$d\beta = [\partial\beta/\partial\lambda_1]d\lambda_1 + [\partial\beta/\partial\lambda_2]d\lambda_2$$

For the isothermal case, the Helmholtz function is a function dependent only on  $\alpha$  and  $\beta$ . Equations (2.1.1.11) and (2.1.1.12) can be used to derive the relationships between the principal tensions and the derivatives of the Helmholtz function.

$$T_i \lambda_i = [(\partial\tilde{F}/\partial\alpha)_{T,\beta} (\partial\alpha/\partial\lambda_i) + (\partial\tilde{F}/\partial\beta)_{T,\alpha} (\partial\beta/\partial\lambda_i)] \quad (2.1.1.13)$$

$$i = 1, 2$$

Using the definitions for  $\alpha$  and  $\beta$  Equation (2.1.1.13) is rewritten as:

$$T_i = [(\partial\tilde{F}/\partial\alpha)_{T,\beta} + (-1)^{i+1} 1/(2\lambda_1^2 \lambda_2^2) (\partial\tilde{F}/\partial\beta)_{T,\alpha} (\lambda_1^2 - \lambda_2^2)] \quad (2.1.1.14)$$

$$i = 1, 2$$

The definitions of the isotropic tension and the maximum shear resultant are:

$$\bar{T} = 1/2 (T_1 + T_2) \quad (2.1.1.15)$$

$$T_s = 1/2 \| T_1 - T_2 \|$$

where the brackets denote the absolute value of the expression enclosed. Therefore:

$$\bar{T} = [\partial \tilde{F} / \partial \alpha]_{T, \beta} \quad (2.1.1.16)$$

$$T_s = 1/2(1+\alpha)[\partial \tilde{F} / \partial \beta]_{T, \alpha} \parallel \tilde{\lambda}^2 - \tilde{\lambda}^{-2} \parallel$$

Where:

$$\tilde{\lambda} = \lambda_1 / (\lambda_1 \lambda_2)^{.5}$$

Using the above relations the tension resultants can then be incorporated into the exact differential of the Helmholtz potential energy function, at constant temperature.

$$(d\tilde{F})_T = \bar{T}d\alpha + 2T_s(1+\alpha)d\tilde{\lambda}/\tilde{\lambda} \quad (2.1.1.17)$$

Equation (2.1.1.17) is then expanded in a Taylor series about  $\alpha$  equal to zero to yield:

$$(\tilde{F} - \tilde{F}_0)_T = \bar{T}_0 \alpha + K\alpha^2/2 + O(\alpha^3) \quad (2.1.1.18)$$

The shear term does not contribute toward the isotropic tension component. Isotropic tension in the membrane is a by-product of area dilitation or condensation only.

The membrane tension and the compressibility modulus of the membrane may then be defined as (assuming that  $\bar{T}_0$  is zero):

$$\bar{T} = \partial \tilde{F} / \partial \alpha = K_T \alpha$$

$$K_T \equiv [\partial \bar{T} / \partial \alpha]_{T, \alpha=0} = [\partial^2 \tilde{F} / \partial \alpha^2]_{T, \alpha=0} \quad (2.1.1.19)$$

The value of  $K_T$  is accurate only with  $\alpha$  values close to zero. This limitation is imposed by neglecting the second order terms in the tension Equation (2.1.1.18). This limitation does not reduce the effectiveness of the model. Evans and Waugh (1977), Evans and Skalak (1980) and Kwok and Evans (1981) report lysis of the membrane at  $\alpha$  values ranging from 2 to 3 percent. At values of  $\alpha$  at 3 percent the second order error term for the expression for  $K_T$  is approximately  $4.5 \times 10^{-9}$ .

### 2.1.2 Thermal Expansion Coefficient at Constant Tension

The surface area of a vesicle under tension is a function of temperature and isotropic membrane tension (see Section 2.2 for development):

$$d\alpha = \left(\frac{\partial \alpha}{\partial T}\right)_{\bar{T}} dT + \left(\frac{\partial \alpha}{\partial \bar{T}}\right)_T d\bar{T}$$

At constant tension,  $\bar{T}$ , this equation simplifies to:

$$d\alpha = \left(\frac{\partial \alpha}{\partial T}\right)_{\bar{T}} dT$$

or

$$\frac{d\alpha}{dT} = \left(\frac{\partial \alpha}{\partial T}\right)_{\bar{T}} \quad (2.1.2.1)$$

where  $C_{\bar{T}} (= \frac{\partial \alpha}{\partial T})_{\bar{T}}$  is the thermal expansion coefficient at constant membrane tension. Kwok and Evans (1981) and Evans and Kwok (1982) have found the value to be approximately  $2.4 \times 10^{-3}/^{\circ}\text{C}$  for egg lecithin. For DMPC they report expansion coefficients of  $.4 - .6 \times 10^{-3}/^{\circ}\text{C}$ .

It should be noted that Equation (2.1.2.1) cannot be used in the thermal transition region. Instead the Clausius-Clapeyron approach should be used as in Evans and Kwok (1982).

Evans and Kwok (1982) report changes in the compressibility modulus of an order of magnitude at the phase transition temperature. Evans and Kwok (1982) report that  $K_T$  is 140 dyne/cm above the transition point and 1100 dyne/cm below the transition point. This large change in the compressibility modulus at the phase transition emphasizes the need for the separate analysis performed by Evans and Kwok (1982) in the thermal transition region. Away from the thermal transition temperature  $C_T$  is given as:

$$C_T = \left( \frac{d\alpha}{dT} \right)_T \quad (2.1.2.2)$$

$C_T$  is a relatively easily obtainable quantity if the experiment is not performed in the thermal transition region. Later a relationship for the thermal expansion coefficient at constant surface pressure will be derived.

### 2.1.3 Tension and Surface Pressure in the Vesicle

Tension in the liposome is related to the Helmholtz free energy density through the relation:

$$[\partial \tilde{F} / \partial \alpha]_T = \bar{T} = \gamma - \pi \quad (2.1.3.1)$$

The tension in the membrane can be subdivided into two parts as in previous developments (Evans and Skalak (1980), Evans and Waugh (1977)).

$\gamma$  is taken to represent the intramembrane tension caused by the hydrophobic effect. The hydrophobic effect is defined as the interfacial tension between the hydrocarbon tails of the lipid molecule and the aqueous environment. It is independent of  $\alpha$ , but strongly dependent on temperature changes. The magnitude of  $\gamma$  is related to the interfacial geometry of the amphiphiles and the aqueous environment (Defay and Prigogine (1966)). See Figure 1.1.

$\pi$  is defined as the surface pressure. It will be assumed to obey the two-dimensional gas equation (Evans and Waugh (1977)):

$$\pi A = 4kT \quad (2.1.3.2)$$

The above assumption is based on the relation of the monolayer to the bilayer membrane.

It must be noted that this assumption assumes that the liposome is in a state where the  $\pi$ -A curve is a hyperbola. From Figure 2.2 taken from Fendler (1981), note that all portions of the curve do not fit the hyperbolic form. Please note that Figure 2.2 is taken from monolayer data, however monolayer data can yield bilayer data. This is discussed in Chapter 5. When the vesicle is in the thermal transition region the above analysis is not applicable since there can be area changes at constant surface pressure and temperature. Further study of the vesicle in the thermal transition region is required to yield a complete analysis for the membrane.

Tanford (1974) partitioned the Helmholtz free energy into two parts (see Figure 1.2).

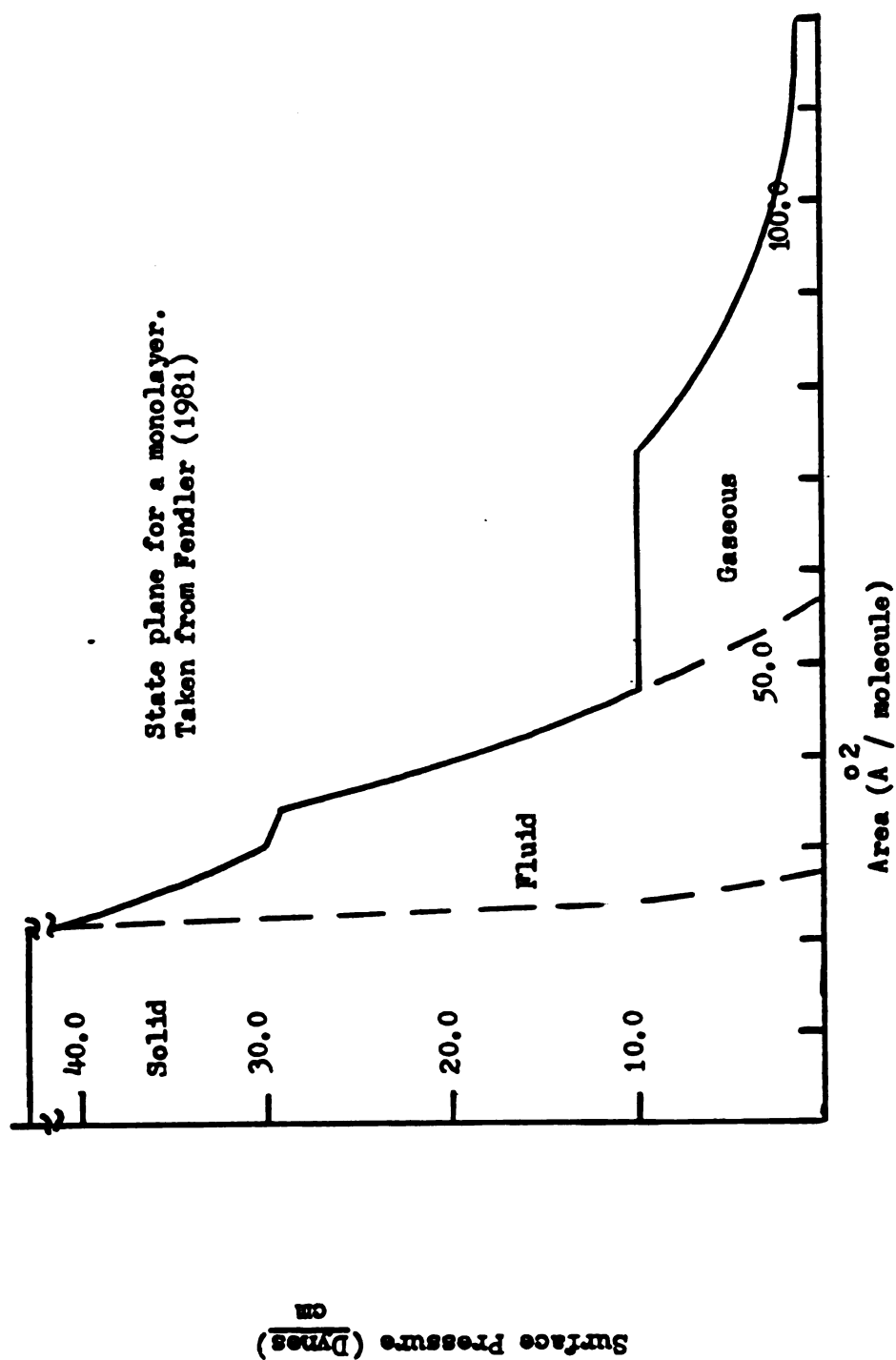


Figure 2.2 A Schematic Representation of the State Plane ( $\pi$ - $\bar{A}$ ) for a Typical Monolayer

$$\tilde{F} = \tilde{F}_p + \tilde{F}_w \quad (2.1.3.3)$$

Where  $\tilde{F}_p$  is the contribution to the free energy density from portions of the molecules not associated with the hydrophobic effect.

This portion of the free energy is defined as the free energy associated with the polar head group interactions, Van der Waals interactions and all other molecular interactions not associated with the hydrophobic effect. With this in mind the surface pressure is defined as:

$$-\pi = [\partial \tilde{F}_p / \partial \alpha]_T \quad (2.1.3.4)$$

$\gamma$  is defined as the free energy density associated with the interfacial exchange of the hydrocarbon tails of the lipid molecules with the aqueous environment:

$$\gamma = [\partial \tilde{F}_w / \partial \alpha]_T \quad (2.1.3.5)$$

By differentiating the free energy density we obtain:

$$[\partial \tilde{F} / \partial \alpha]_T = [\partial \tilde{F}_w / \partial \alpha + \partial \tilde{F}_p / \partial \alpha]_T = \bar{T} = \gamma - \pi \quad (2.1.3.5)$$

In the tension free state:

$$\bar{T}_0 = 0 = \gamma_0 - \pi_0 \quad (2.1.3.6)$$

Tanford (1973, 1974) and Reynolds et al., (1974) have shown  $\gamma$  to be dependent only on the interfacial geometry between the aqueous phase and the lipid membrane.  $\gamma$  is relatively constant for an isothermal process, therefore Equation (2.1.3.6) is rewritten as:



$$\bar{T} = \pi_0 - \pi \quad (2.1.3.7)$$

Now that a relationship exists between the isotropic membrane tension and the membrane surface pressure, expressions can be found for the thermal expansion coefficient while under constant membrane surface pressure.

#### 2.1.4 Thermal Expansion Coefficient at Constant Surface Pressure

As stated in Section 2.1.2, the thermal expansion coefficient at constant tension is an experimentally obtainable quantity. However, the thermal expansion coefficient at constant surface pressure,  $C_\pi$  cannot be directly obtained experimentally. This property is also useful in the characterization of the membrane.

From Evans and Waugh (1977):

$$C_\pi = [\partial\alpha/\partial T]_\pi \quad (2.1.4.1)$$

Note that in this case we cannot include changes in area due to the changes in the compressibility modulus due to temperature changes as was done in Equation (2.1.2.2). Such data required for determining  $(\partial K_T/\partial T)_\pi$  is not available at this time. By differentiating the membrane tension at constant area we obtain:

$$[\partial\bar{T}/\partial T]_\alpha = [d\gamma/dT]_\alpha - [\partial\pi/\partial T]_\alpha \quad (2.1.4.2)$$

where  $(d\gamma/dT)_\alpha = (\partial\gamma/\partial T)_\alpha$  because  $\gamma$  is assumed to be only a function of  $T$  and not area.

This can be rewritten as:

$$[\partial\bar{T}/\partial T]_\alpha = d\gamma/dT + [\partial\pi/\partial\alpha]_T [\partial\alpha/\partial T]_\pi$$

using the cyclic relationship where:

$$(\partial\pi/\partial T)_{\alpha}(\partial T/\partial\alpha)_{\pi}(\partial\alpha/\partial\pi)_{T} = -1$$

Using the definition of the compressibility modulus, (Equation (2.1.1.19)) this equation can be further rearranged to yield:

$$C_{\pi} = [\partial\alpha/\partial T]_{\pi} = -[1/K_T][\partial\bar{T}/\partial T]_{\alpha} + [d\gamma/dT][1/K_T] \quad (2.1.4.3)$$

All of the elements of the right hand side of Equation (2.1.4.3) can be measured experimentally, except  $d\gamma/dT$ . However  $d\gamma/dT$  can be approximated as:

$$d\gamma/dT \approx 2[d\sigma/dT] \quad (2.1.4.4)$$

where  $d\sigma/dT$  represents the temperature dependence of the surface tension, for the specific lipid material as a monolayer, at an oil water interface (Evans and Waugh (1977)).

### 2.1.5 Bending Modulus of the Membrane

The bending modulus of the membrane has considerable interest with respect to freezing injury. The characterization of this property is vital in biological cells. However, for this thesis these experiments will not be performed. The experimental apparatus does not have sufficient magnification to accurately measure this property. The mathematical analysis will be presented.

The bending modulus of the liposome membrane may be obtained, using the analysis presented in Evans and Waugh (1977), from photo image analysis of photographs taken during aspiration experiments. At the time of this investigation the Zeiss Universal Microscope did not

have an objective lens with sufficient magnification to resolve the contact radius as shown in Figure 2.3. The current objective is a 10x phase contrast lens. For adequate optical resolution the minimum lens objective should be 25x. Consider the Figure 2.3:

Performing a force balance, in the s direction, yields:

$$\Sigma F_x = 0 = d\bar{T}/ds + Q_T d\theta/ds \quad (2.1.5.1)$$

The term  $Q_T d\theta/ds$  is a resultant term from the reorientation of the transverse shear. The equation is valid for small values of  $d\theta/ds$ .

Assuming the membrane is an elastic material, the transverse shear may be written as a function of the bending moment.

$$Q_T = dM/ds = d/ds(\beta d\theta/ds) \quad (2.1.5.2)$$

Where  $\beta$  is defined as the bending modulus. Rewriting Equation (2.1.5.1) yields:

$$d\bar{T}/ds = - dM/ds \, d\theta/ds = - d/ds [\beta (d\theta/ds)^2] \quad (2.1.5.3)$$

The equation can now be solved if  $d\theta/ds$  is assumed constant at the bend. Therefore:

$$\bar{T} = \text{Constant} - \beta (d\theta/ds)^2 \quad (2.1.5.4)$$

where the constant is a by-product of the integration. By applying the boundary condition of isotropic tension away from the pipette entrance the constant is the isotropic tension. Performing a force balance in the axial direction inside the pipette, and assuming the pressure inside the liposome is equal to the ambient pressure, yields:

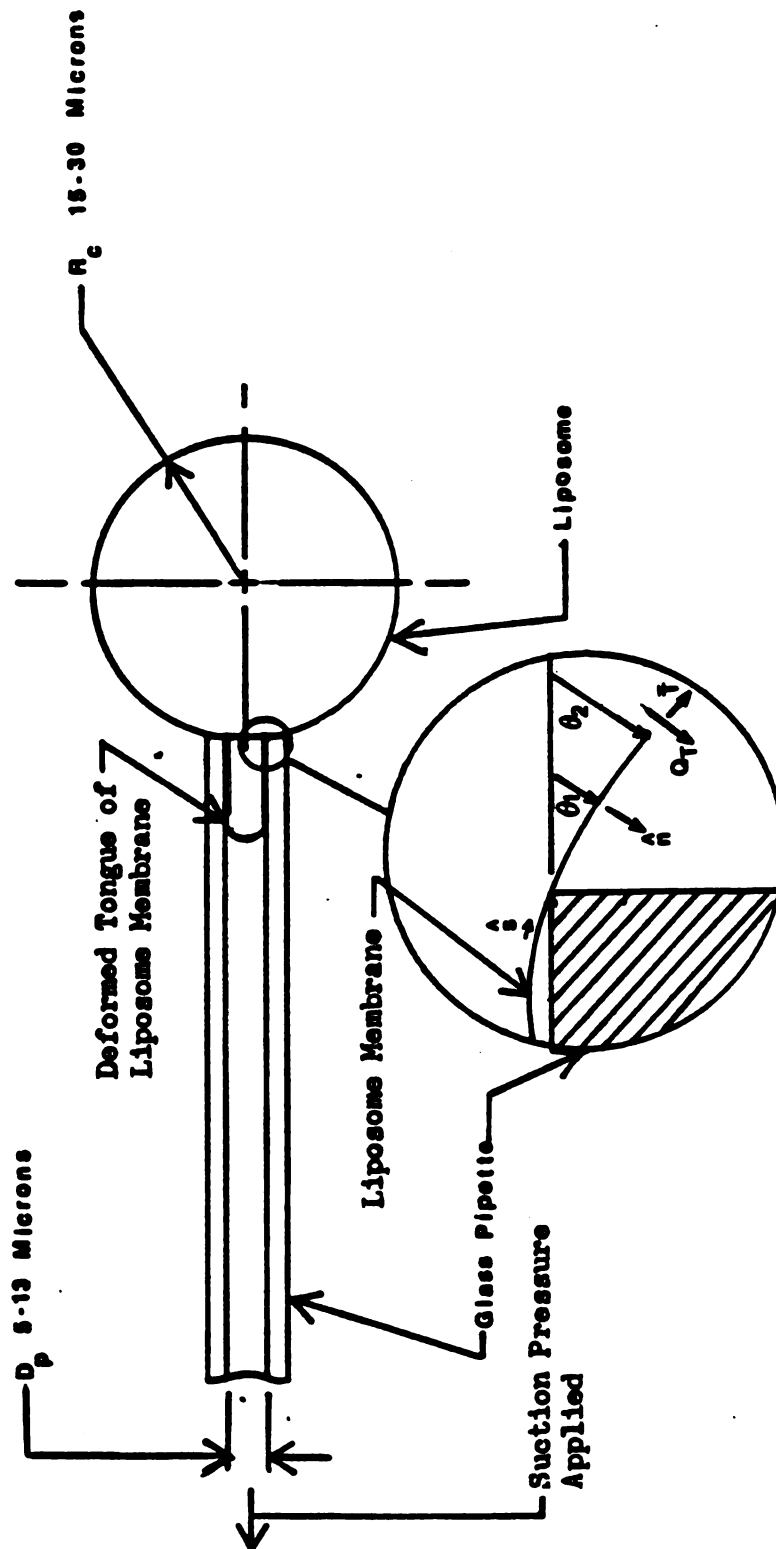


Figure 2.3 Representation of Geometric Considerations Required to Determine the Membrane Bending Modulus from Microaspiration Experiments

$$(P_p - P_{amb})\pi R_p^2 = 2\pi R_p [\text{Constant} - \beta(d\theta/ds)^2] \quad (2.1.5.5)$$

where  $R_p$  is the radius of the pipette and  $P_p$  and  $P_{amb}$  are the pressures inside and outside the pipette respectively.

$ds/d\theta$  is the radius of curvature at the point of contact with the pipette. Taking this into account, the bending modulus can be found experimentally as:

$$\beta = [\bar{T}_0 - \Delta P R_p/2] R_{\text{curvature}}^2 \quad (2.1.5.6)$$

where  $\bar{T}_0$  is the isotropic tension away from the pipette entrance and  $R_{\text{contact}}$  is the radius of curvature of the membrane at the region of contact with the pipette.

## 2.2 Tension and Pressure Differential Equations

It has been shown in the preceding sections that the membrane isotropic tension and surface pressure can be expressed as functions of membrane area changes and temperature. With this knowledge it is possible to form differential equations for the incremental changes in membrane tension and surface pressure ( $d\bar{T}, d\pi$ ).

Differential changes in surface pressure are defined as:

$$d\pi = (\partial\pi/\partial\alpha)_T d\alpha + (\partial\pi/\partial T)_\alpha dT \quad (2.2.1.1)$$

Since:

$$\bar{T} = \gamma - \pi$$

$$(\partial\bar{T}/\partial\alpha)_T = -(\partial\pi/\partial\alpha)_T = K_T \quad (2.2.1.2)$$

where  $(\partial\gamma/\partial\alpha)_T = 0$ .

We can now rewrite (2.2.1.1) as:

$$d\pi = -K_T d\alpha + (d\gamma/dT + K_T \partial\alpha/\partial T)_{\bar{T}} dT \quad (2.2.1.3)$$

where

$$(\partial\pi/\partial T)_{\alpha} = (d\gamma/dT)_{\alpha} - (\partial\bar{T}/\partial T)_{\alpha}$$

and

$$-(\partial\bar{T}/\partial T)_{\alpha} = [(\partial\bar{T}/\partial\alpha)_T (\partial\alpha/\partial T)_{\bar{T}}]$$

from the cyclic relation.

The differential equation for the change in isotropic tension is defined as:

$$d\bar{T} = (\partial\bar{T}/\partial\alpha)_T d\alpha + (\partial\bar{T}/\partial T)_{\alpha} dT \quad (2.2.1.4)$$

Substituting and rewriting:

$$d\bar{T} = K_T d\alpha - K_T C_T dT \quad (2.2.1.5)$$

Where  $C_T$  and  $K_T$  are the thermal expansion coefficient at constant tension and the isothermal compressibility modulus respectively. Equation (2.2.1.3) requires knowledge of the derivative with respect to temperature of the interfacial tension,  $\gamma$ , in order to be valuable. This information is presented in Section 2.1.5. However, Equation (2.2.1.5) can be used readily without requirements for additional information. The differential equations for the changes in membrane tension and surface pressure will be integrated to yield algebraic equations for tension and surface pressure.

### 2.3 Summary

The membrane isothermal compressibility modulus and the thermal expansion coefficients can now be determined from experimental tension and area change data. The experimental apparatus required to perform these experiments has been developed as part of this thesis and the development is described in the following chapter. One of the major difficulties with making experimental measurements is a result of the extremely small size of the experimental system (20 to 30 microns).

### CHAPTER 3

#### EQUIPMENT AND PROCEDURES

The majority of the effort in the present investigation was in the design and development of the experimental apparatus. The experimental system is shown in Figure 3.1. The experimental apparatus is subdivided into three sections: the micropipette, the manipulator system, the liposome aspiration system and the test stage.

The data acquisition system is driven by an LSI-11/02 microcomputer, with 12-bit analog-to-digital (A/D) and digital-to-analog (D/A) converters. The microcomputer also incorporates a 35 KHZ real time clock (RTC) which is used for data collection and temperature control.

The experimental testing apparatus also has the capability of digital temperature control for the test stage. Using the control program described in Appendix C and the second generation test stage described in Section 4.3, the test stage can achieve theoretical controller temperature accuracy of  $\pm 0.1^{\circ}\text{C}$ . The control program has been used with a new controller developed as part of this work to control an existing cryomicroscope conduction stage to  $\pm 0.5^{\circ}\text{C}$ . The difference between the theoretical and actual accuracy of the controller is discussed in Appendix C. This degree of accuracy is required for the thermal phase transition studies proposed in Chapter 5.





The experimental apparatus includes many improvements over the systems of previous investigators (Mitchison and Swan (1954), Rand and Burton (1964)). The current configuration is the first with on-line data acquisition and closed loop temperature control. However the system also has its shortcomings. Section 3.7 deals with the experimental uncertainties which are closely related to the shortcomings of the present system. At this time the experimental uncertainty is unacceptably high. The bulk of this uncertainty is due to the inability to accurately resolve the area changes in the liposomes. This effect will be discussed in detail in Section 3.7.

The description of the experimental apparatus is subdivided into four components for the purpose of discussion: the micropipette, the manipulator system, liposome aspiration system, and the test stage itself. The remainder of the section covers experimental procedures and uncertainties.

### 3.1 Micropipette Fabrication

#### 3.1.1 Manufacturing Process Background

The manufacturing of micropipettes, in the 7-13 micron inner diameter range, was a difficult task. The micropipettes must have a flat face on which the liposome must rest. (See Figure 3.2.)

Previous attempts to manufacture these pipettes by some other investigators have involved a quick fracture technique. This process is discussed in Evans, Waugh and Melnik (1976). Using this technique the stated production success percentage was less than 10 percent. Such high rejection rates led to alternative manufacturing processes.

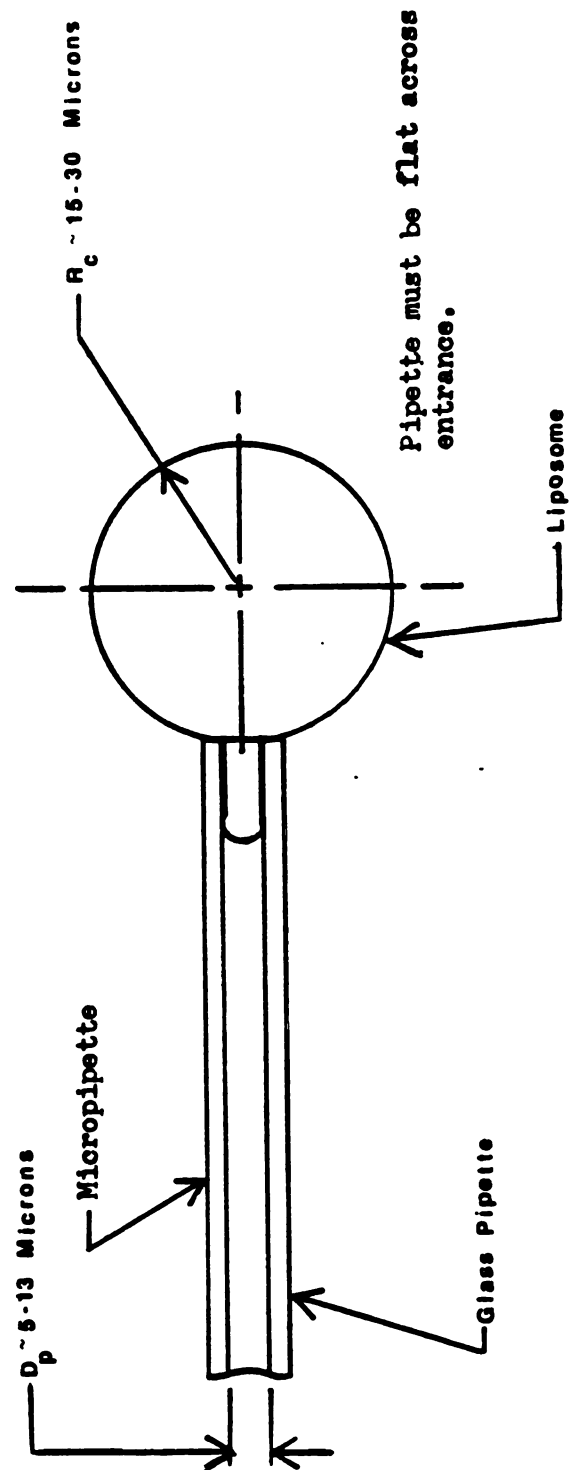


Figure 3.2 Micropipette Schematic Illustrating Typical Sizes and Geometries

Another manufacturing process, developed by the Fusion Research group of the University of Rochester and modified by Dr. R. Waugh, Radiation Biology and Biophysics Department of the University of Rochester Medical Center, was considered. Their technique involved the implementation of a sonicating bath to input ultrasonic energy into the glass pipette. This energy would then vibrate the glass tip, which was placed against a fine abrasive, and grind the tip to the desired diameter.

### 3.1.2 Micropipette Manufacturing Process

The first step in the pipette manufacturing process is the pulling down of the 20 microliter Dade Accupipettes, 1 millimeter nominal O.D., to needle tips. This task was accomplished at either of two locations on campus. The first was located at the Biochemistry Department Brown-Flaming horizontal pipette puller while the second was located at the Endocrine Research Laboratory. The Endocrine Research Laboratory Stoeling vertical pipette puller was shown to produce pipettes of more uniform and superior quality. This puller was therefore used routinely.

The second step in the manufacturing process involved the grinding of the needle pointed pipette to the desired inner diameter. Figure 3.3 depicts the necessary equipment and fixtures. The ultrasonic energy input into the glass pipette creates a vibration in the pipette, causing the tip to vibrate into a 600 grit aluminum oxide abrasive. The abrasive-glass interaction produced a grinding action which produces the desired flat-ended pipette. Typical sonification

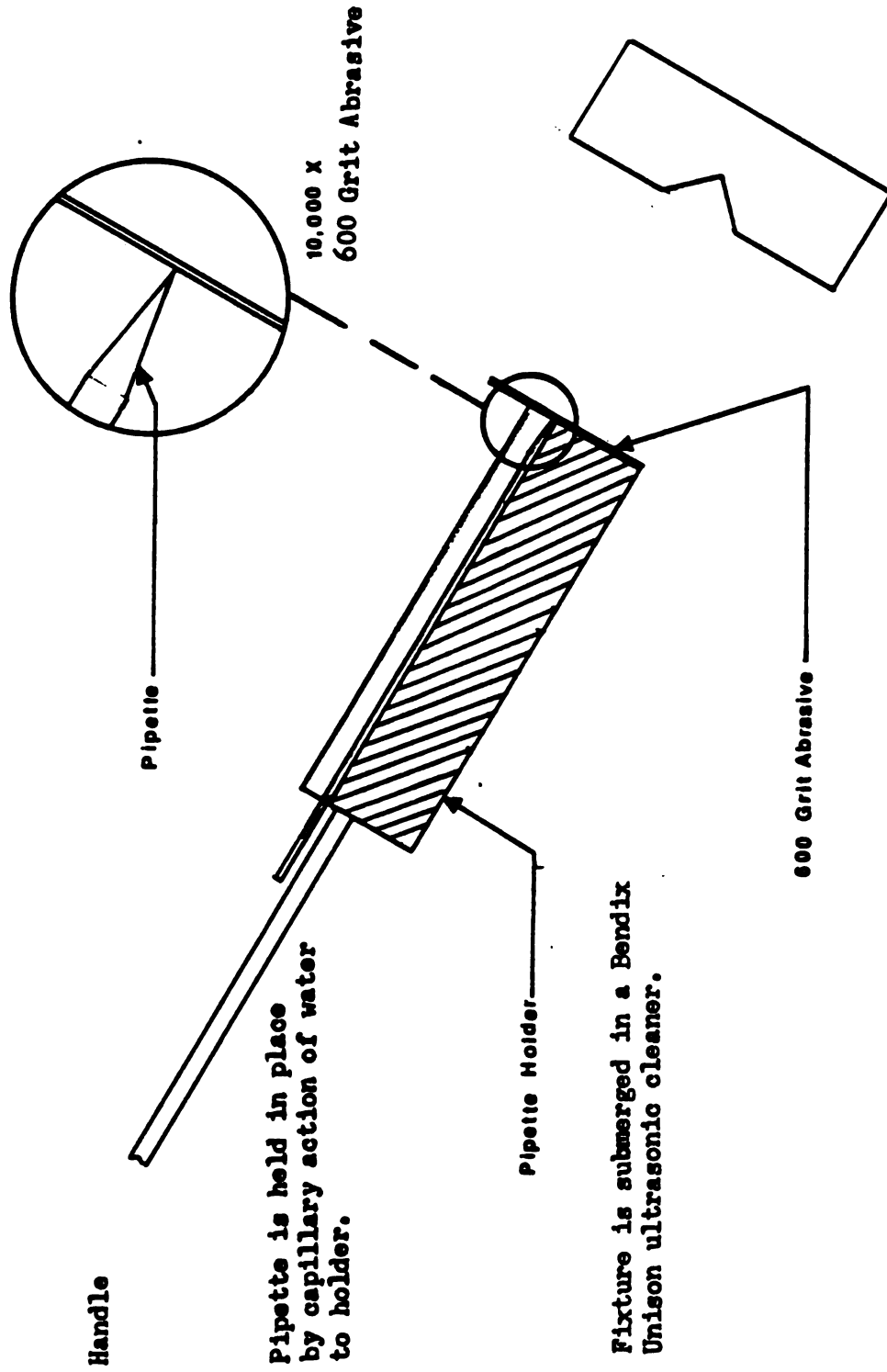


Figure 3.3 Equipment Used to Produce Flat-Ended Micropipettes

times for the system range from 2 to 10 seconds. The success rate of this process is slightly higher than 80 percent. Any pipette that was not flat-ended was rejected. This represents an increase of 700 percent from the previous quick-fracture method.

Once the pipettes are ground to the proper inner diameter all air must be excluded from the inside. Residual trapped air will cause compressibility problems in the pressure measurements which leads to erroneous measurements. All air is excluded from the micropipette by boiling the glassware for 20 minutes in distilled water. The pipettes must then be allowed to cool slowly to room temperature. The slow cooling ensured that all air was excluded from the interior of the pipette.

In the course of the mechanical properties experiments a frequently occurring problem was the lodging of lipid fragments in the pipette entrance. Previously this event would have required the changing of the pipette. However, this problem was solved by submerging the micropipette (without the holder shown in Figure 3.3) into the ultrasonic bath. The same level of ultrasonic energy which was used to grind the pipette can be used to free the lipid particles from the pipette entrance. This technique extends the working life of the pipette from a few hours to several weeks.

## 3.2 Micromanipulator System

### 3.2.1 Interfacing the Manipulator and the Microscope

The Duke model C micromanipulator was used in these experiments. The manipulator was built and obtained from the Physiology Instrument Shop of the Duke University Medical School. Figure 3.4 displays the manipulator system as it appears in place on the microscope system.

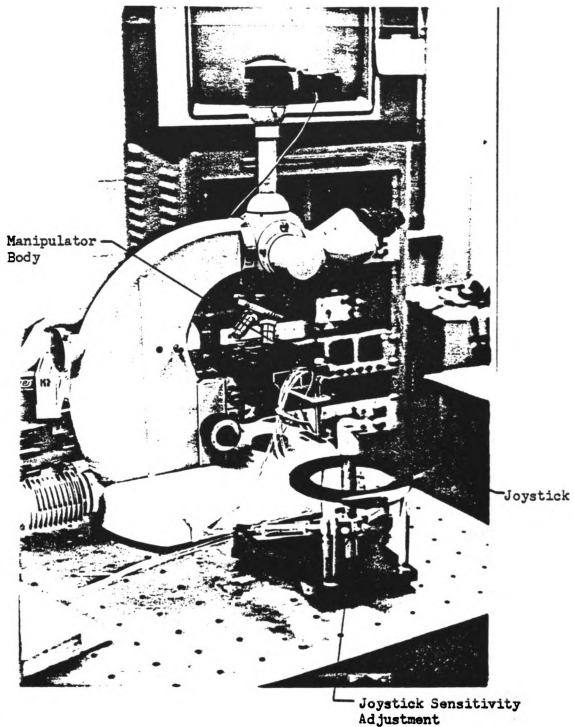


Figure 3.4 Photograph of Micromanipulator System Mounted on Microscope

The manipulator system consists of the joystick and the manipulator body shown in the foreground of Figure 3.4. The movement of pipettes, as shown in Figure 3.5, can be controlled in coarse and fine modes.

The coarse adjustment controls are located on the manipulator body. These screw-driven controls provide coarse adjustment in all three axes of motion. Care must be taken when performing coarse adjustments not to dislocate any of the adjustment pins. The adjustment pins are located under the adjustment screws. When the coarse adjustment screws are turned it forces the pin against a lever which in turn causes the pipette to pivot in a given direction. When an adjustment pin is dislocated the coarse adjustment in that direction does not function. When this occurs the manipulator outer covering must be removed and the adjustment pin realigned. This operation usually takes three or four hours to perform.

The Duke manipulator also has a joystick sensitivity adjustment (see Figure 3.4). By sliding the adjustable yoke of the joystick up or down the sensitivity of the pipette to joystick movements can be increased or decreased. This is a valuable tool when one is scanning the test chamber for suitable liposomes for experimentation. By keeping the joystick sensitivity high one can reduce the need for coarse adjustments. This allows for smoother system adjustment and reduces the induced vibrations from coarse adjustment.

Figure 3.5 depicts the manipulator body attached to the Zeiss Universal Microscope. The plexiglass support fixture was specially designed for the Duke manipulator. The fixture allows rotation of the manipulator about its support rod and it keeps the manipulator



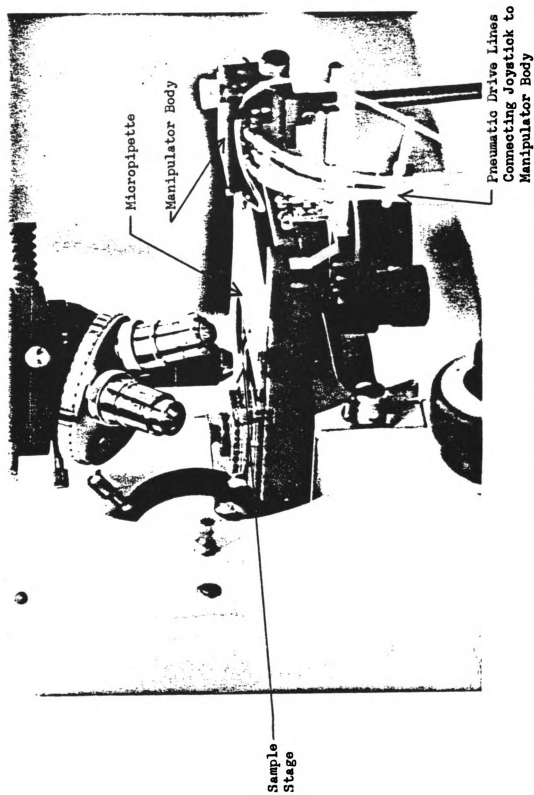


Figure 3.5 Photographic Detail of Manipulator,  
Micropipette and Sample Stage

sufficiently removed from the microscope stage to eliminate physical interference problems.

The plexiglass support is bolted to the microscope stage by two mounting screws. Care must be taken not to exert too great a load on the support fixture. Failure to do so will result in damage to the microscope stage and the support fixture (i.e., do not rest your hand on the support).

### 3.2.2 Liposome Aspiration System

The suction pressures required for the compressibility modulus experiments were generated by the system shown in Figure 3.6.

The suction pressures were measured by a Validyne DP-103-32 pressure transducer, coupled to a Validyne CP-15 carrier demodulator. The output of the transducer was  $\pm 5V$  over a pressure range of  $\pm 35.0$  inches of water ( $\pm 8.72 \times 10^4$  dyne/cm<sup>2</sup>;  $\approx \pm 0.1$  atm). The output of the demodulator was then interfaced to the LSI-11 thru the I/O box and the A/D converter and to a panel meter for display. The pressure transducer was calibrated according to manufacturers specifications using a water manometer before the experiments were started. The accuracy of the pressure measurements was  $\pm 140$  dynes/cm<sup>2</sup>. The accuracy of the pressure measurements is based on the uncertainty of the transducer and the uncertainty of the relative levels of the two reservoirs.

The two-reservoir system was used to eliminate compressibility errors associated with a working fluid such as air. The system was shown to be reliable in producing low suction pressures. The suction pressure was adjusted to the 1 cc syringe.

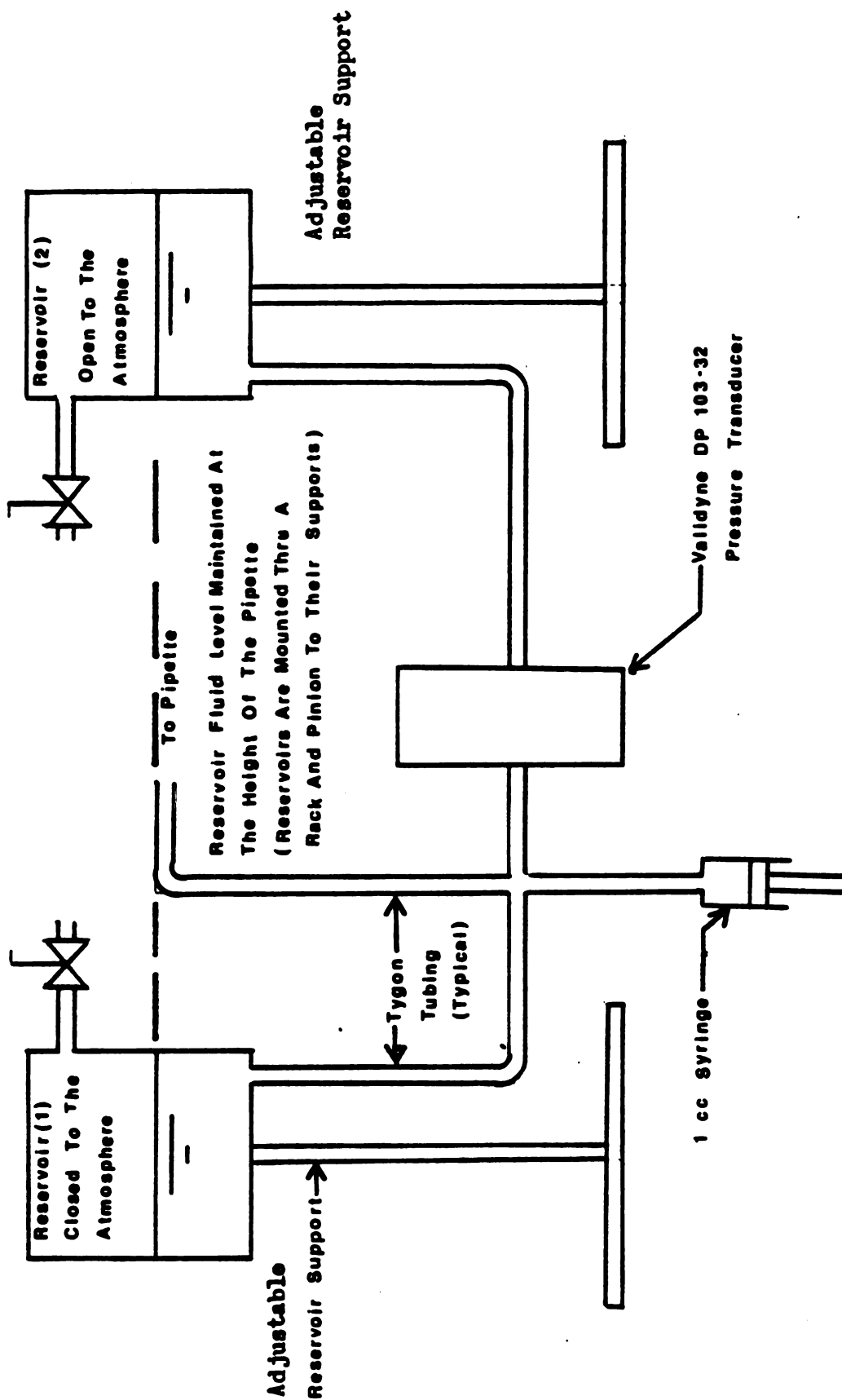


Figure 3.6 Experimental Hydrostatic Set-Up Designed to Create and Measure the Suction Pressure Applied to Cells and Microvesicles

Prior to each run the two reservoirs were open to the atmosphere. Then the air-water interface level in the reservoirs was brought to the height of the micropipette tip. This was a cumbersome and tedious process which could be eliminated with the incorporation of an inverted microscope. By incorporating an inverted microscope the level of the test chamber does not move with respect to the air-water interface in the reservoirs. With the current system, every time the sample is changed the water levels in the reservoirs must be realigned. When the reservoirs were brought to the proper height the pressure transducer read zero volts. With rebalancing complete the valve to reservoir one was closed. The experiments could then begin.

### 3.3 Test Stage

The test stage used in this investigation is shown in Figure 3.7. Brass was chosen as the stage material since it has good thermal conductivity. The test chamber itself is located in the lower left hand corner as seen from the top view of the test stage. The 7x12 mm. test chamber could hold a 40  $\mu$ l liposome sample. During operation the undersurface of the test chamber was covered with a 18x18 mm. coverslip. The coverslip was held in place by capillary action and a light coat of vacuum grease between the brass stage and the glass coverslip. The liposome sample was then placed on the lower coverslip in the test chamber and then covered with a 12 mm. dia. coverslip. The micropipette was then positioned in the test chamber through the 1 mm thick opening in the y-z plane.

Located to the side of the test chamber is the temperature heating/cooling source. The Cambion model 801-1006-1 ceramic cascade module

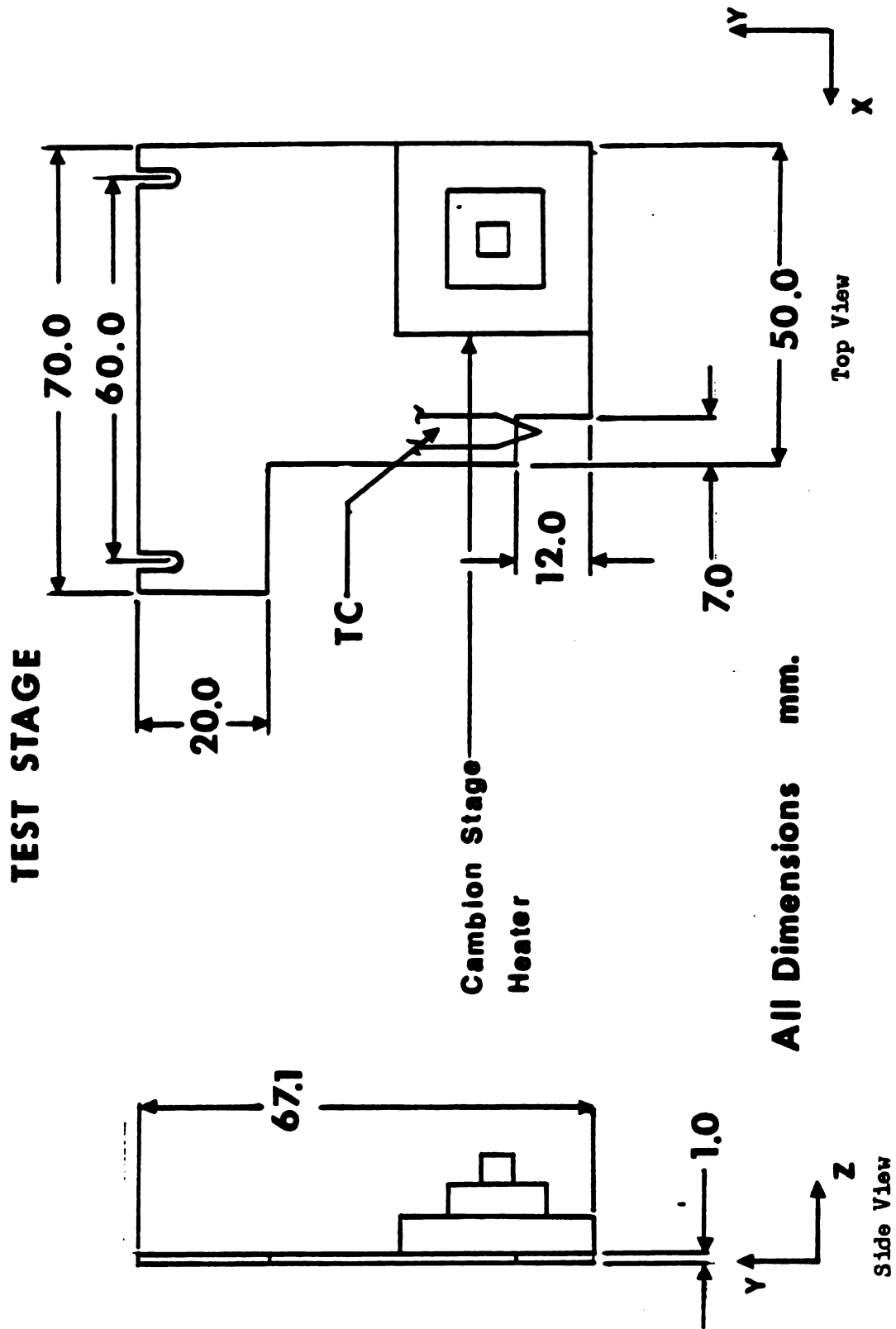


Figure 3.7 Schematic of the Sample Stage Used to Hold the Sample as well as Control and Measure Temperature

is a thermoelectric refrigeration device which acts as a heat pump. Since the stage was constructed from brass and the cross sectional area is small, it was assumed that temperature gradients in the y and z directions were small. In any case, all of the experiments were conducted in close proximity to the copper-constantan thermocouple.

Temperature control for this stage was provided via open-loop control. Figure 3.8 represents the open-loop transfer function of the test chamber thermocouple temperature as a function of the input current to the Cambion module. Using Figure 3.8 it was possible to control the test chamber thermocouple temperature with an accuracy of  $\pm 2^{\circ}\text{C}$ . This type of temperature control made it impossible to conduct accurate thermal transition experiments. To perform thermal transition experiments temperature resolution and control must be at least  $\pm .25^{\circ}\text{C}$  (Evans and Kowk (1982)). This shortcoming of the test stage led to a different method of temperature control.

### 3.3.1 Next Generation Test Stage

The test stage described in the preceding section did not have the temperature resolution and control required to perform thermal transition experiments. These experiments are important for the characterization of the membrane in the thermal transition region. In order to conduct these experiments the temperature must be controllable down to  $\pm .25^{\circ}\text{C}$ . This section proposes a test stage which can be used for such experiments. The computer program required to control the test stage is described in detail in Appendix C.

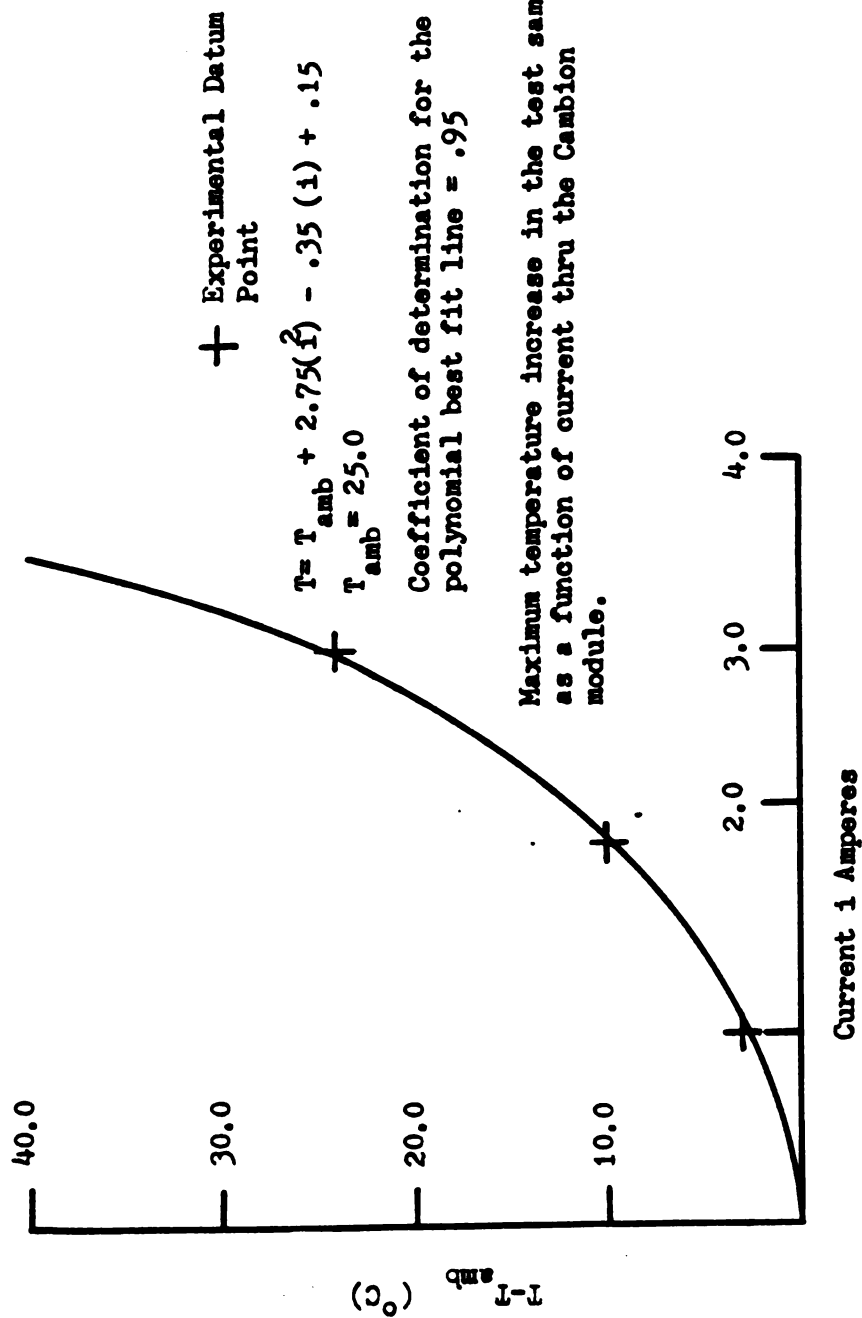


Figure 3.8 Test Stage Open-Loop Transfer Function  
 (Temperature Difference as a Function  
 of Input Current)

Figure 3.9 depicts a recommended next generation test stage. The next generation test stage should be constructed from copper for good thermal response. A cooling channel flows around the viewing area/test chamber. The coolant can either be liquid or gas. However, it has been observed in previous testing that liquid tends to create too much flow-induced vibrations. To either side of the viewing area are glass slides coated with an electrical resistant coating. The glass slides are fixed to the test stage by the electrode heater supports. The test chamber is formed by the gap between the two glass slides (viewing area).

Unlike the stage previously described, the next generation test stage has independent heating and cooling sources. The heat source is formed by Joule heating of the glass slides coated with the resistant film, while the cooling is provided by convection/conduction of the coolant in the cooling channel. The independent heating/cooling sources allow the test stage a faster response time to control signal inputs.

The computer control program described in Appendix C was tested on a stage similar to Figure 3.9 (Shabana (1983)). The temperature offset (desired temperature - actual temperature) of the stage ranged from  $\pm (.1-.5)^{\circ}\text{C}$ .

The actual dimensions of the next generation test stage are not given. The computer simulation of Tu (1983) should be employed to obtain optimum performance of the test stage. Once the simulations are complete and the recommendations made in Appendix C regarding the controller hardware are executed, the test stage can obtain a temperature controller accuracy of  $\pm .1^{\circ}\text{C}$ .





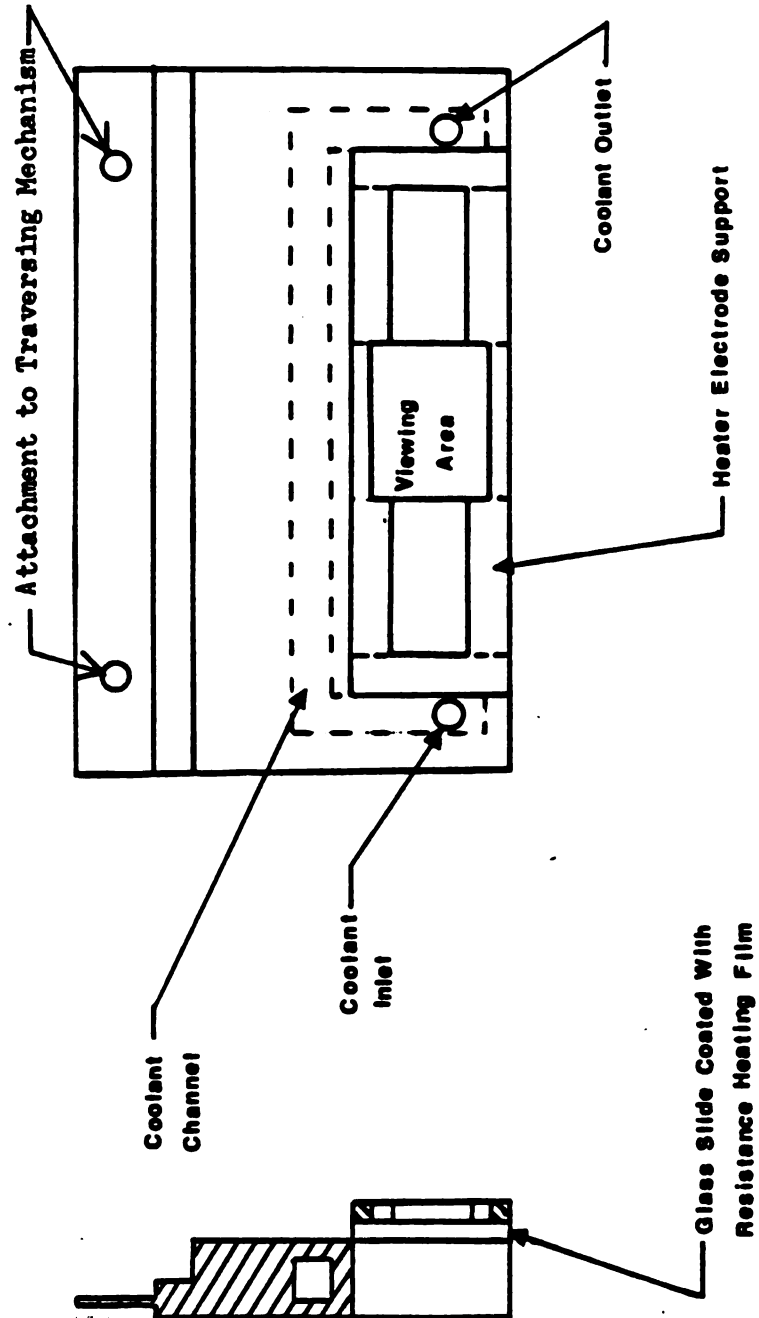


Figure 3.9 Schematic of a Proposed Second-Generation Test Stage

### 3.4 Liposome Formation

#### 3.4.1 Materials

In this study four lipid materials were considered, DMPC, dipalmitoyl phosphatidylcholine (DPPC), Soy L- $\alpha$  PC and ultra pure Egg PC. All of the materials were provided by Sigma Chemical and used without further processing. In the experiments, dyes were used to enhance the vesicular image. In the work of Kwok and Evans, and Evans and Waugh a Hoffman modulation optical system was used to enhance the vesicular or RBC image. Hoffman modulation was unavailable to this laboratory during the course of this investigation. Therefore, it was decided to use a dye to stain the inside of the liposome. With the dye incorporated in the liposome, the projected length of the liposome inside the micropipette could be seen under bright field and phase contrast illumination. The image observed under the phase contrast objective was superior to bright field and phase contrast was used during the course of this investigation. However, these dyes would not incorporate into the DPPC and DMPC liposome during formation. Therefore the mechanical properties of their respective membranes could not be determined using this method.

The dye used in all of the experiments was Sulpho Rhodamine G EX, provided by Pylam products. No detailed data were available from the manufacturer on this material.

#### 3.4.2 Liposome Formation Techniques

The liposome formation technique used was a modified version of Callow (1983).

A 100 mg. sample of lecithin was dissolved in 30 ml. of 10:1 Chloroform-methanol solution. The lipid solvent mixture was then placed in vacuo for a period of one hour. When the solvent was completely evaporated from the evaporation flask, the flask was then filled with 40 ml. of a 22-32 mosm solution of Sulpho Rhodamine dye and distilled water. All solution osmolarities were determined by a Precisions Systems Inc. Osmette S. Automatic Osmometer. The sample was then placed in a recirculating water bath for one hour at 60°C. At the end of the first hour the bath was turned off and the sample was allowed to cool slowly to room temperature over a period of several hours in the recirculating bath. During this time a lipid cloud containing liposomes formed.

A 100  $\mu$ l sample of the cloud was then removed from the dye solution and placed in 40 ml. of slightly hypertonic sucrose solution (32-37 mosm.). The solution was then gently swirled to disperse the liposome cloud evenly. Vigorous swirling was avoided to reduce the opportunity for the liposome membranes to break.

### 3.5 Bulk Compressibility Modulus Experimental Procedure

A 40  $\mu$ l sample of the dispersed liposome cloud was placed in the test chamber. The sample temperature was then recorded after the sample came to thermal equilibrium. The contents of the test chamber was then scanned with the microscope for a large unilamellar liposome of diameter larger than 20 microns. The location of suitable liposomes was a major obstacle in this investigation. It was not uncommon to spend several hours searching for one suitable liposome. There was great difficulty locating large liposomes, without encountering

large areas of dispersed lipid. The dispersed lipid degraded the quality of the image observed through the microscope. At times the degradation became so great that the liposome could not be observed in the micropipette. Clearly, another method of liposome formation is needed to eliminate the great amounts of dispersed lipid.

Once a suitable liposome was found it was then aspirated at low pressure into the pipette (100-200 dynes/cm.<sup>2</sup>). The low suction pressure corresponded to a carrier demodulator voltage of 0.01 to 0.02 V DC. The projected length of the liposome was then measured from the video monitor along with the liposome diameter. The liposome was also moved into close proximity to the thermocouple using the micromanipulator prior to making measurements.

The suction pressure was then raised to increase the projected length of the liposome. (See Figure 3.10.) After several seconds at the higher, steady suction pressure, the new equilibrium liposome diameter and projected length were recorded. This process was repeated several times with increasing suction pressures. It was found that one could obtain approximately four data points per run. Usually the maximum suction pressure applied was 7,000 dynes/cm.<sup>2</sup> (0.5 VDC on the carrier demodulator). The number of data points taken was limited by the size of the suction syringe. During this investigation a 1 cc syringe was used. The number of data points taken could be increased in the future if greater resolution were possible in producing the suction pressures. Several possibilities suggest themselves, including: a thinner longer syringe, a micrometer driven syringe and a stepper-motor-driven syringe. The current syringe was drawn back by hand.

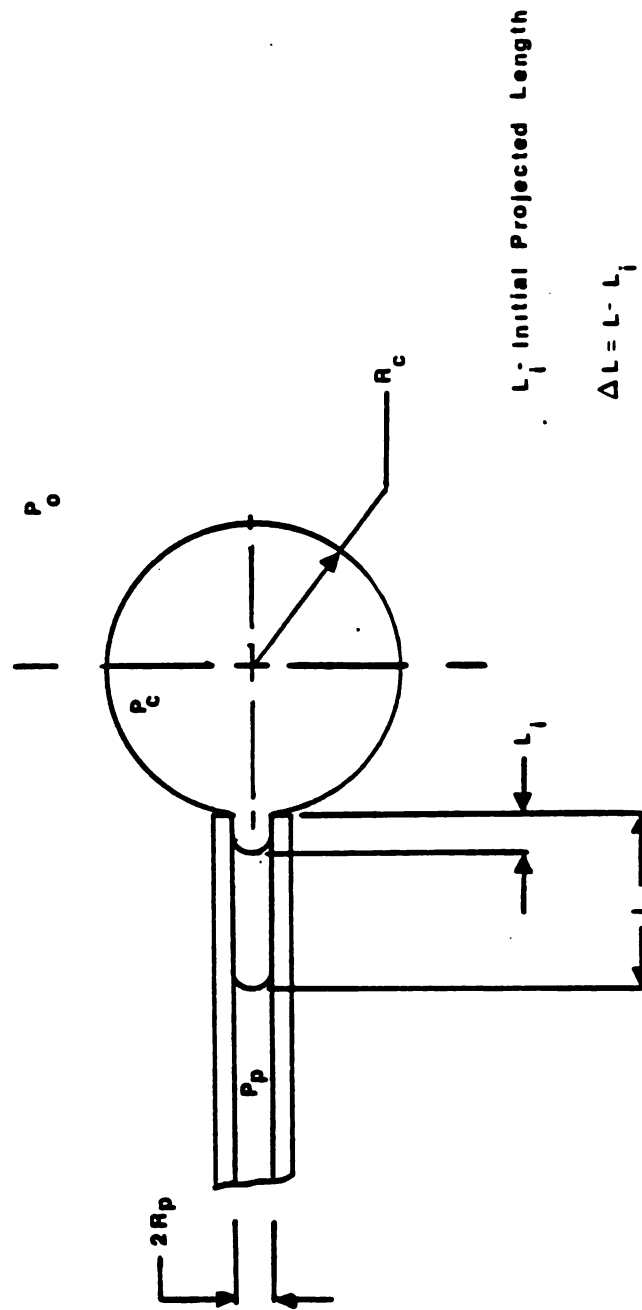


Figure 3.10 Illustration of Membrane Deformation in a Micropipetting Experiment

After the last data set the liposome was expelled from the pipette. If the liposome had any surface defects the data were not used. A typical defect observed in the liposome was a necking of the projected length in the pipette. This would result in the loss of lipid material from the membrane. The general check which was used for the testing of process reversibility was that the liposome return to its original shape and size prior to aspiration. This return to the original shape usually took 5-6 seconds before it was completed. It was typical to perform this experiment on 10 to 12 liposomes over a period of several hours and only obtain 3 or 4 good data sets. The poor success rate was due to frequent irreversible runs. The process must be reversible for the analysis to be valid since reversibility has been assumed in the derivation of the expressions for the isothermal compressibility modulus of the liposome.

### 3.6 Thermal Expansion Coefficient Experimental Procedure

For these experiments the liposome was found and captured in a manner similar to that described in the previous section. It was critical that the liposome be located as close to the thermocouple as possible to insure experimental accuracy. Once the liposome was located near the thermocouple the diameter, initial projected length, temperature, and suction pressure were recorded. The heat source was activated. Once the system came to thermal equilibrium (i.e., no convection currents visible and a stable temperature) the new projected length was measured from the video monitor with a scale accurate to  $\pm .1$  inches ( $\pm 1.2$  microns). The process was repeated once more. Two data

points for each run, 5°C apart. Only two data points were taken since the temperature control of the stage was not as accurate as desired which limited the minimum  $\Delta T$ . Also we did not wish to make  $\Delta T$  too large since we did not know how the thermal expansion coefficient varied with temperature. This limited the maximum  $\Delta T$ .

After the two data points were taken the system was allowed to cool to room temperature. The liposome was then expelled. If the liposome had any surface defects the data were not used. The process must be reversible for the analysis to be accurate as described in the previous section.

### 3.7 Experimental Sensitivity

In any experiment there is a device-dependent experimental uncertainty of the measurements. This section will determine the experimental uncertainty associated with calculating the isothermal compressibility modulus and the thermal expansion coefficient from experimental data. The uncertainty values are based upon the average operating conditions at which the experiments were conducted.

The expressions for the experimental uncertainties of the isothermal compressibility and the thermal expansion coefficient are:

$$dK_T = (\partial K_T / \partial T) dT + (\partial K_T / \partial \alpha) d\alpha \quad (3.6.1)$$

$$dC_T = (\partial C_T / \partial \alpha) d\alpha + (\partial C_T / \partial T) dT \quad (3.6.2)$$

The experimental uncertainty associated with the isothermal compressibility modulus is a function of the membrane tension and the fractional change in area. The relationships for  $dT$  and  $d\alpha$  are:



$$d\bar{T} = (\partial\bar{T}/\partial\Delta P)d\Delta P + (\partial\bar{T}/\partial R_p^{-1})dR_p^{-1} + (\partial\bar{T}/\partial R_c^{-1})dR_c^{-1} \quad (3.6.3)$$

$$d\alpha = (\partial\alpha/\partial\Delta L)d\Delta L + (\partial\alpha/\partial(R_p R_c^{-1}))d(R_p R_c^{-1}) \quad (3.6.4)$$

The results of Equations (3.6.3) and (3.6.4) are combined with:

$$\bar{T} = K_T \alpha$$

to yield the experimental uncertainty.

The experimental uncertainty for the isothermal compressibility modulus experiments was found to be  $\pm 19.0$  dynes/cm. (See Appendix D.) It is interesting to note that 84.6 percent of the experimental uncertainty is due to the inability to accurately measure the changes in the surface area of the liposome. This error can be reduced substantially by incorporating higher power objective lenses into the microscope.

The experimental uncertainty for the thermal expansion coefficient is calculated in a similar fashion to that of the isothermal compressibility modulus. Again the major source of error was found to be the inability to measure the change in surface area of the vesicle (i.e., the projected length in the pipette). The experimental uncertainty of the thermal expansion coefficient under constant membrane tension was  $1.6 \times 10^{-3}^\circ\text{C}$ . Ninety-five percent of the experimental uncertainty was from the measurements of the change in the vesicle surface area. Again, this experimental uncertainty can be greatly reduced by incorporating higher power magnification in the microscope.

### 3.8 Summary

The experimental apparatus to measure two important thermo-mechanical properties of liposome membranes has been constructed. The system works reasonably well for this preliminary investigation. Suggestions have been made for improving the system performance and accuracy. It has been found that the major source of improvement would come from higher power magnification in the objective lenses of the microscope. Other high priorities for future improvements would include an inverted microscope to improve the liposome aspiration system performance, and an image analysis system to decrease the experimental uncertainty of the area change measurements.

The results of this investigation will be presented in the following chapter.

## CHAPTER 4

### EXPERIMENTAL RESULTS

#### 4.1 Isothermal Compressibility Modulus

The isothermal compressibility modulus experiments were performed on two lipid materials. The compressibility moduli for egg and soy PC vesicles are found in Table 4.1.

It is interesting to note that the standard deviation of the sample was almost equal to the experimental uncertainty. The experimental uncertainty for the compressibility experiments, as stated in Section 3.7, was  $\pm 19.0$  dynes  $\text{cm}^{-1}$ . The major source of the experimental uncertainty was from the inability to measure the projected length of the liposome in the micropipette with a high degree of accuracy. Since there was a substantial amount of experimental uncertainty it was difficult to determine if hysteresis was present in the data. Six percent of the liposomes were checked for hysteresis. Of the 6 percent checked, none displayed any discernable hysteresis. Therefore all tests were assumed to be reversible.

A total of 29 reversible runs were conducted on the soy PC, while 13 runs were done on the egg. It was observed that after 10 runs the standard deviation of the compressibility modulus data was relatively invariant. This observation lends strong support to the argument that the standard deviation of the data collected was dependent on the uncertainty of the experiment, and the true standard deviation of the

RESULTS FOR LIPOSOME SYSTEMS			
SYSTEM	ISOTHERMAL COMPRESSIBILITY MODULUS (dynes/cm)	THERMAL EXPANSION COEFF. (1/C°)	AUTHOR
Egg PC	80.0 ± 14.0	NOT PERFORMED	Gielda*
Egg PC	140.0 ± 16.0	0.0024 ± 0.002	Kwok & Evans
Soy PC	52.0 ± 17.0	0.0036 ± 0.002	Gielda*

\* -- Liposomes were incorporated with Sulpho Rhodamine dye during formation.

Table 4.1 A Comparison of Current Results with Published Results for Isothermal Compressibility Modulus and Thermal Expansion Coefficient

compressibility moduli is unknown. The experimental uncertainty must be smaller than the standard deviation of the measured quantity to make accurate statements as to the distribution of the property measured.

Figure 4.1 depicts a typical result for the compressibility modulus experiments. The coefficient of determination for the least squares fit of the tension as a function of  $\alpha$  data ranged from .9 to 1.0. Note that the tension as a function of  $\alpha$  curve does not pass through the origin. This is a resultant of the initial, although small, tension (i.e., 0.4 dynes/cm. as in Figure 4.4) which is imposed upon the liposome in order to aspirate it into the pipette.

As stated in Chapter 2, Equation (2.2.1.5) is useful in integrated form. The result of this integration is an algebraic equation which relates the membrane isotropic tension to temperature and change in the fractional area of the membrane.

$$d\bar{T} = K_T d\alpha - K_T C_T dT$$

Assuming that  $K_T$  and  $C_T$  are relatively constant with temperature, the above equation can be integrated very easily leaving an algebraic equation of state for the isotropic tension in the membrane. If the parameters  $K_T$  and  $C_T$  were both functions of  $\alpha$  and  $T$  and their functions were known this equation could still be used but the integration would be more complex. However, this assumption has been verified by data collected here and the work of Evans and Kwok (1982). If the lower limit of the integration is assumed to be the liposome in the tension free state, where  $\bar{T}$  and  $\alpha$  are equal to zero, the equation for the isotropic membrane tension is:

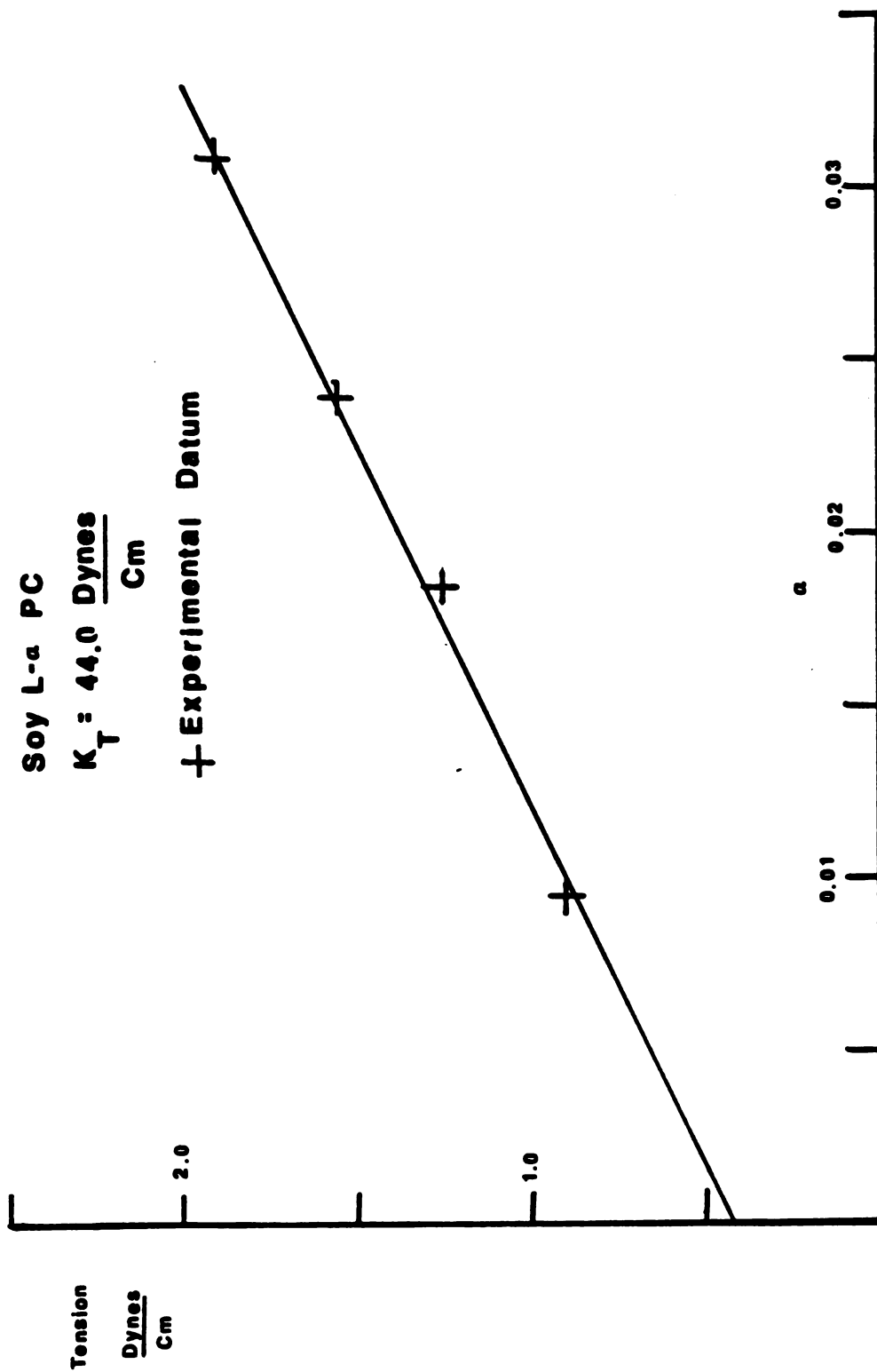


Figure 4.1 A Typical Result for the Isothermal Compressibility Modulus Determinations (Membrane Isotropic Tension as a Function of Normalized Area Change)

$$\bar{T} = K_T \alpha - K_T C_T (T - T_{Ref}) \quad (4.1.1)$$

The state plane generated by Equation (4.1.1) is shown in Figure 4.2.

Equation (4.1.1) is very useful in comparing the membrane isotropic tension data to the theoretical results. However, knowledge of the membrane tension is not as desirable as the membrane surface pressure. Substituting:

$$\bar{T} = \gamma - \pi$$

into Equation (2.2.1.5) one can rewrite Equation (4.1.1) to yield:

$$d\pi = d\gamma - K_T d\alpha + K_T C_T dT \quad (4.1.2)$$

The above equation is integrated below. The lower limit is assumed to correspond to the liposome in the tension-free state.

$$\pi - \pi_0 = (\gamma(T) - \gamma_0) - K_T \alpha + K_T C_T (T - T_{Ref}) \quad (4.1.3)$$

This equation is the algebraic equation of state for the liposome which relates  $\pi$  to  $\alpha$  and  $T$ . (Note the analogy to the pressure, volume and temperature case.) Note that  $\gamma$  is a function of temperature only, and in the tension free state  $\pi_0$  is equal to  $\gamma_0$ . The values for  $\gamma$  can be approximated from existing monolayer data by employing equation (2.1.4.4). Figure 4.3 depicts the state plane created when the values for  $\gamma$  are approximated. It is interesting to note that if one takes the intersection of a plane of constant surface pressure and the state plane the resultant is the thermal expansion coefficient at constant surface pressure  $C_\pi$ . The state plane shown in Figure 4.2 is an expansion of a small segment of the Equation (2.1.4.2) ( $\pi A = 4KT$ ) to form a state plane.

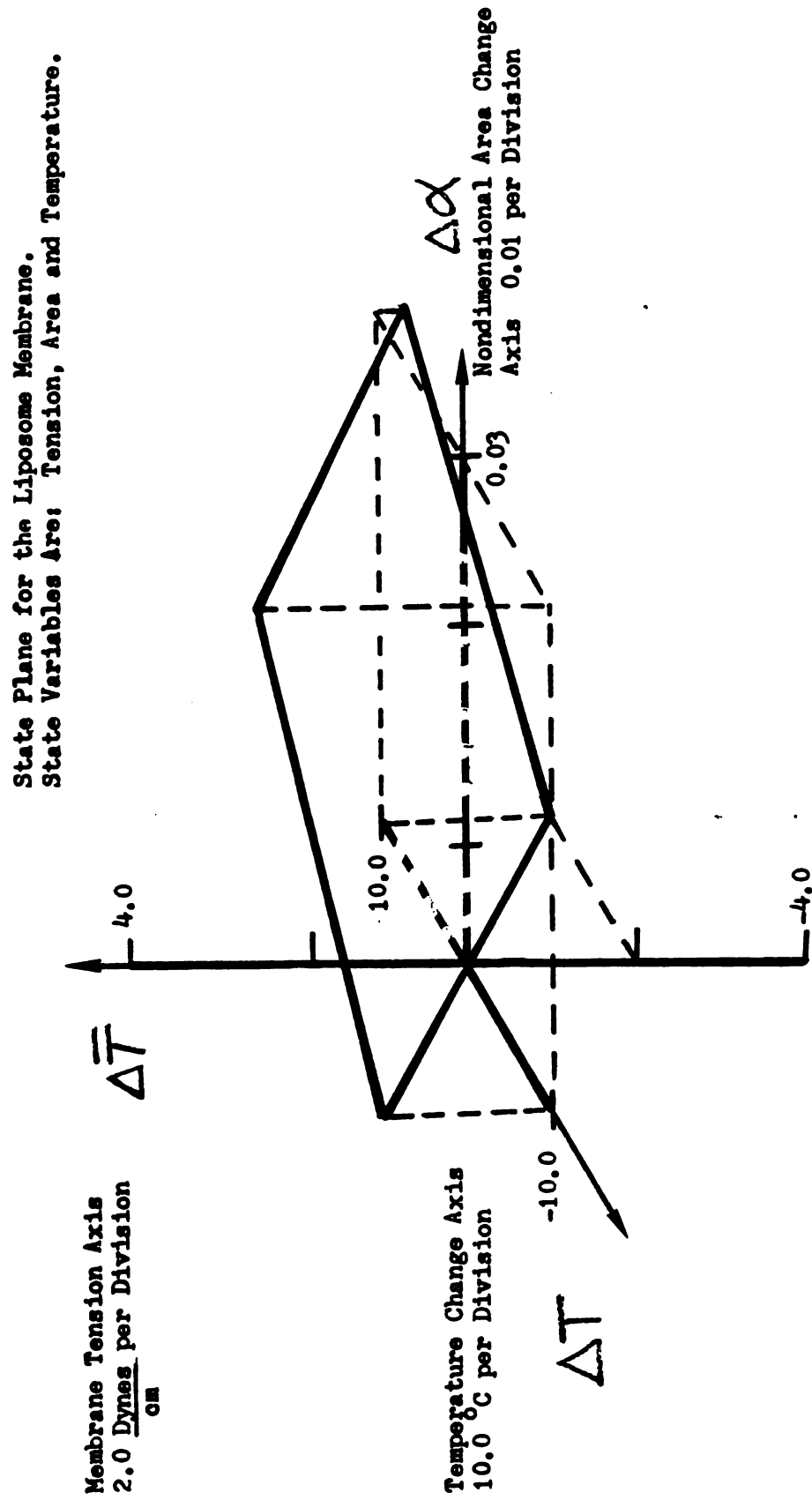


Figure 4.2 State Plane for the Liposome Membrane (Isotropic Tension as a Function of Temperature and Normalized Area Change)



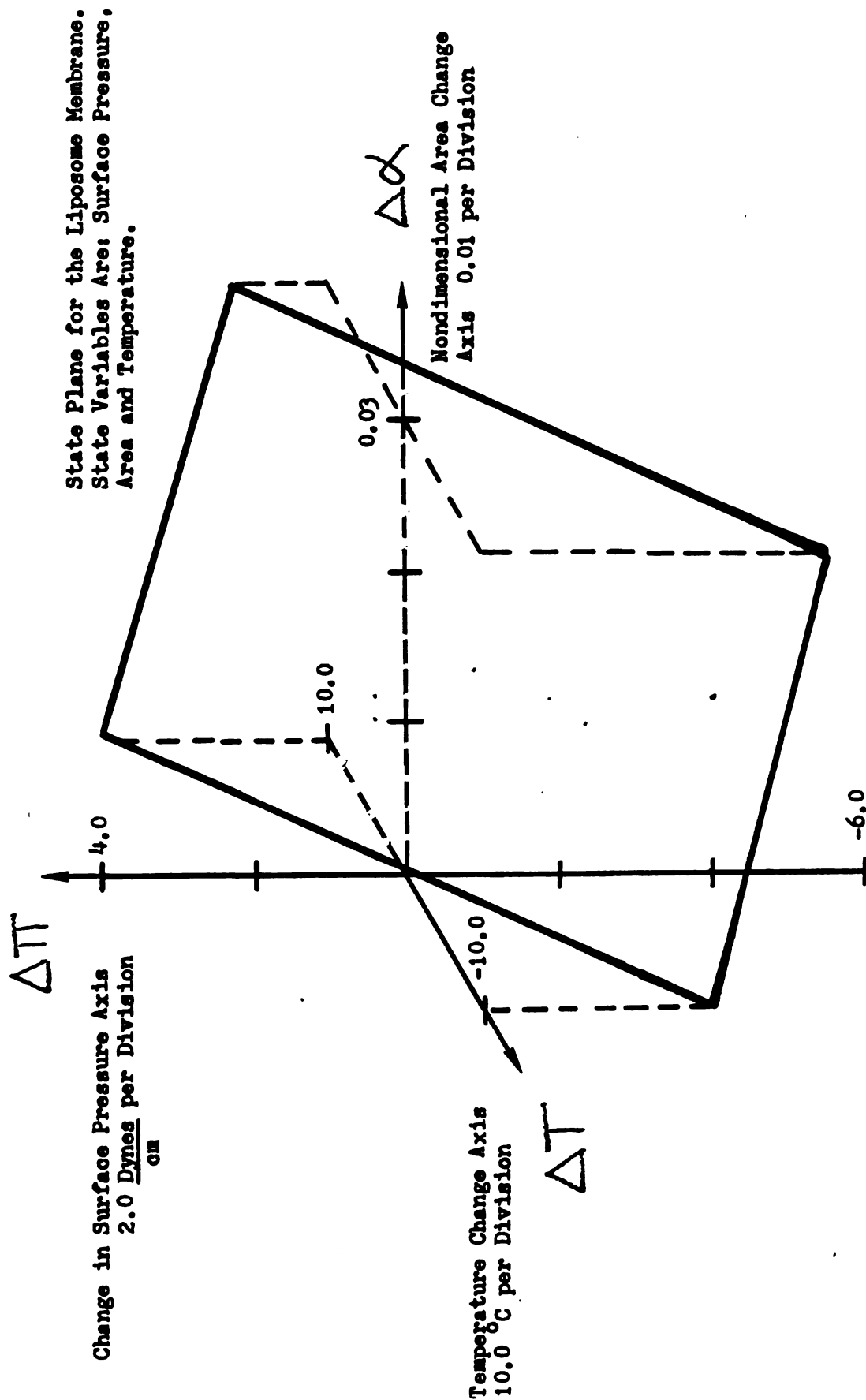


Figure 4.3 State Plane for the Liposome Membrane (Membrane Surface Pressure as a Function of Temperature and Normalized Area Change) (See Appendix E for Sample Calculation)

Again it must be reiterated that the state plane created is only valid when the vesicle is not in its thermal transition region. In this analysis the vesicle cannot have changes in area without changes in pressure or temperature.

The effect of the Sulpho Rhodamine dye on the compressibility modulus of the liposomes was an apparent reduction in the membrane stiffness. Kowk and Evans (1981) report an average compressibility modulus for egg PC of  $140 \text{ dynes cm.}^{-1}$ . This value is 75 percent greater than the average value found in this investigation. Performance of a null hypothesis test on the two compressibility moduli revealed they were statistically different at the 0.05 level of significance (Miller and Freund (1965)). The same type of statistical test was performed comparing the soy and egg compressibility moduli. The results revealed that the two moduli are statistically different at the 0.05 level of significance.

#### 4.2 Thermal Expansion Coefficient at Constant Membrane Tension

The thermal expansion coefficients as detailed in Chapter 3 were conducted on the soy PC lecithin. The results of these experiments are shown in Table 4.1. A total of 19 runs were conducted. Again the calculated experimental uncertainty was as large as the standard deviation of the sample. This result strongly suggests that before any further investigations are conducted higher power objective lenses should be employed with the microscope.

The data for the soy PC suggest that the dye used has no effect on the thermal expansion coefficient. It is also apparent that the expansion coefficient does not vary appreciably with various lipid

materials. However, these conclusions cannot be asserted with confidence because the standard deviations are nearly as large as the measured average values (see Table 4.1).

#### 4.3 Summary

The isothermal compressibility modulus experiments were conducted on two lipid materials, egg and soy PC. The results were found to be statistically different from the work of Kwok and Evans (1981). They were also found to be different from each other. This finding suggests that the sulpho rhodamine dye used for liposome visualization is affecting the liposome membrane mechanical properties. Since there are no manufacturer's data available on the dye, the mechanism of change is unknown at this time. However, when the dye was used in the thermal expansion coefficient experiments it did not seem to change this membrane property. Clearly further work is needed to characterize the effect of the dye.

## CHAPTER 5

### PHASE TRANSITIONS IN LIPOSOMES

The purpose of this section is to form an outline for experiments leading to a greater understanding of phase transitions in liposomes. The development will not be limited to one-component systems. Two-component lipid mixtures will be studied, and a method to construct their phase diagrams will be discussed.

Baret (1981) compiled thermal phase transition data for many lipid materials. In his work he determines the thermal phase transition temperature by many different techniques: differential scanning calorimetry, electron spin resonance, nuclear magnetic resonance, fluorescence, light absorption and scattering, X ray diffraction, dilatometry and Raman and infrared spectroscopy. In his work he studies both single and multi-component lipid systems. Baret also reports on the effect of lipid-protein interactions in the membrane.

#### 5.1 Background Information

Information on the phase transition of bilayer membranes is difficult to determine experimentally due to the nature of the liposome system. Therefore it is desirable to relate the wealth of available data concerning monolayers to the bilayer.

Nagle (1976), Blume (1979) and Gruen (1982) have developed analogies for the relation of the bilayer system to the monolayer. Nagle and Gruen suggest that a bilayer in the tension-free state is

similar to a monolayer with an externally applied pressure of 50 dynes  $\text{cm}^{-1}$ . The criteria used to equate the bilayer system to the monolayer system involves matching the area per molecule of each system. In addition, Gruen suggested that monolayers on an oil/water interface will not represent as close an analogy as a monolayer on an n-alkane/water interface. Blume (1979) suggests that the lateral pressure in the monolayer be 30 dynes  $\text{cm}^{-1}$  for an analogy between the monolayer and the bilayer. He reasons that at this surface pressure the absolute areas per molecule are equal for the monolayer and the bilayer.

Lee (1975) performed fluorescence studies using chlorophyll a on small sonicated liposomes of various compositions, to determine their phase transition temperatures. Lee also demonstrated a method to construct phase diagrams, for two component systems, from fluorescent intensity measurements. Evans and Kwok (1982) studied the phase transition of large unilamellar DMPC vesicles employing mechanical calorimetry. Their results were in close correlation with previously existing bilayer transition data (Lee (1975)).

Evans and Kwok (1982) employed a micromanipulator system to study the membrane phase transition. In their investigation they measured the relationship between the isothermal compressibility modulus and temperature. By monitoring the isothermal compressibility modulus and assuming a Gaussian thermal transition temperature distribution they predicted the thermal transition temperature. They verified their mechanical calorimetry study with differential scanning calorimetry.

## 5.2 Phase Change Experiments: Single Component Systems

The phase change experiments should be conducted on pure lipids with sharply defined phase transition temperatures because the sharp phase transition will allow a clearer definition of the phase transition temperature.

Yeager, et al., (1982) studied phase changes in cell-sized vesicles using light microscopy. His method involved determining the area changes by changes in the diameter of the liposomes. They report area changes of 23 percent during phase transition. However their method may miss the true onset of phase transition simply by not having sufficient optical resolution. (Note that their investigation was only interested in the main transition of the vesicle.) In contrast the manipulator system and the micropipette act as a mechano-optical amplifier. Very minute changes in the vesicle area will be apparent in the pipette. An area change of 0.5 percent can be resolved, for a 30  $\mu\text{m}$  diameter vesicle and a 6  $\mu\text{m}$  radius pipette.

These experiments must be conducted on a test stage which has fine temperature control in order to achieve the temperature resolutions on the order of 0.1°C normally reported in phase transition work (Evans and Kwok (1982)). As the vesicle is warmed from below the phase transition temperature one would expect to see the vesicle area increase. In the phase transition region, the vesicle area would increase markedly. As the vesicle passed out of the upper bound of phase transition the vesicle would increase its surface more slowly. By monitoring the increase in vesicles surface area one can determine the vesicle phase transition temperatures. By employing this technique the effect of the external environment on the phase transition of the liposome may be directly measured, instead of inferred from monolayer data.

To serve as a check on the method outlined above, the liposome could be tagged with a fluorescent probe which fluoresces in the solid or liquid phase only. Therefore as the liposome was warmed above the phase transition temperature, the fluorescent intensity could be monitored with a photomultiplier yielding the phase transition temperature. This type of technique has been used by Lee for bulk samples of small (nm) sonicated liposomes. It has never been applied to a cell sized liposome. Cell sized liposomes and fluorescent probes offer the additional advantage that the fraction of surface in the solid or liquid state could be ascertained visually using the segregation of phase-specific fluorescent probes as outlined above. These data could then be checked against data collected using the manipulator mechano-optical-amplifier.

### 5.3 Phase Transition: Two Component Systems

Lee (1975) performed a series of experiments to determine the phase diagrams of multicomponent systems. His experiments, which were conducted on small sonicated vesicles, could be modified by using area change data from the manipulator system instead of fluorescent data. The new test system requires the mechano-optical amplifier detailed in Section 5.2.

Lipid mixtures at various concentrations could be tested similarly to those in Section 5.2. During phase transition the temperature and the area would be measured. Since the thermal expansion coefficient is greater during phase change, by approximately one order of magnitude (Evans and Kwok (1982)), the onset and completion of transition is apparent.

By determining the onset and completion of phase transition at various lipid concentrations a phase diagram similar to Figure 5.1 from Lee (1975) can be constructed. Note that the ends of the diagram are not closed. This is expected since the process does not occur isothermally which means that some degree of uncertainty in determining the initial onset and final completion of the phase transition will be included.

By incorporating different fluorescent probes, which are lipid and phase selective, into the solid and liquid phase the composition of any phase and temperature could be found. This would be accomplished by scanning the liposome with the photomultiplier and determining the composition of the liposome by PMT output. Further investigation into this phenomena is warranted.

#### 5.4 Limitations

At present the microscope system used does not have the necessary optics to observe the phase transition. Since the dye used in Chapter 3 will not incorporate into the pure compound liposomes Hoffman modulation optics are required.

The liposomes can be formed at the desired molar ratios (Lee (1975)). However, the actual composition of the liposomes proposed for the studies outlined in Section 5.3 should be verified experimentally. It is possible that the liposomes may not form as homogeneous mixtures. The liposomes may form configurations similar to bedquilts with patches of pure lecithin dispersed throughout. Or the lipids may not mix at all and form liposomes only of a specific lipid such that the liposome



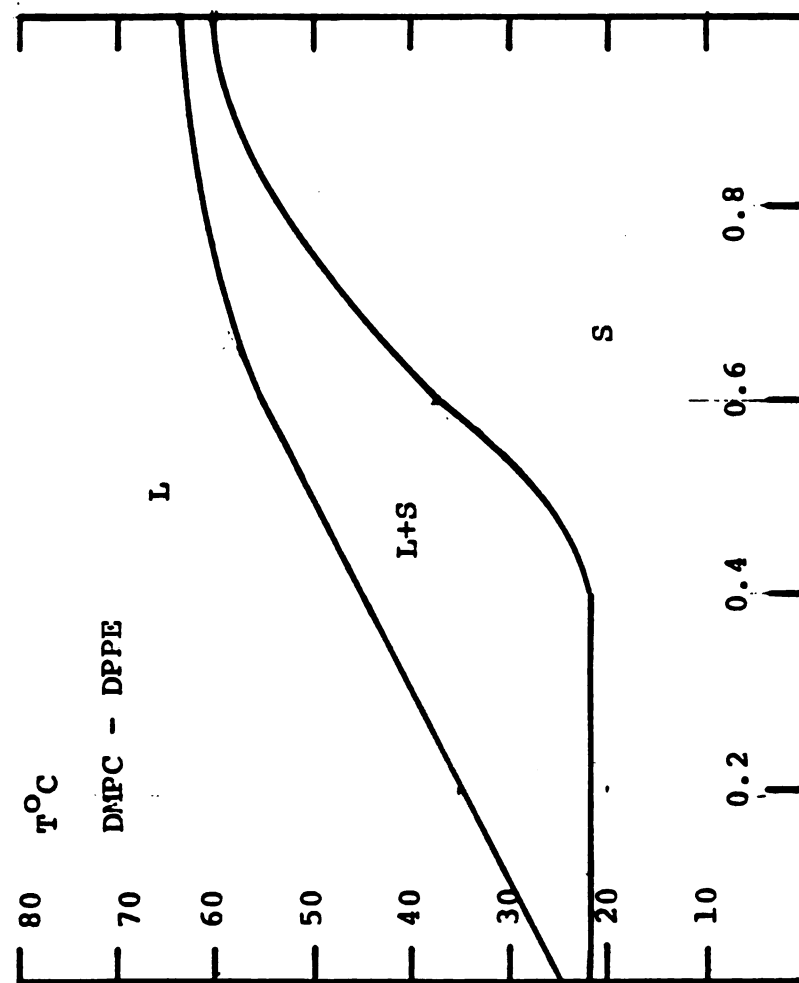


Figure 5.1 Temperature of Onset and Completion of Solid Lipid Separation in DMPC/DPPE Vesicles (Reproduced from Lee (1975))

membrane structures formed are at a different molar ratio than the initial bulk solution ratios used to form them.

In order to experimentally verify the composition of the multi-component liposomes an electrophoresis apparatus should be constructed. However, since the PC head groups are zwitterionic (Lehninger (1970)) a probe must be attached to the specific lipids to allow phoresis. This is not an easy task, and much more consideration is warranted.

In order to perform the experiments suggested in this section, the second generation test stage and its temperature controller must be employed. This controller has shown  $\pm .5^{\circ}\text{C}$  accuracy on the BTP Lab conduction stage and would need to be debugged further to allow realization of the theoretical accuracy of  $\pm 0.1^{\circ}\text{C}$  predicted for this device. See Appendix C.

## CHAPTER 6

### RECOMMENDATIONS FOR FUTURE WORK

The micromanipulator system is an excellent tool to measure the volume and surface area changes in microscopic objects. This system should be employed to further the osmotic shrinkage work of Callow (1983) and Nowlen (1983). It can also be used in the fluorescence studies proposed in this thesis. Lastly, the system should be used to examine liposomes and other biological membranes at the ice-water and ice-aqueous solution interfaces.

#### 6.1 Osmotic Shrinkage Experiments

Nowlen (1983) reported difficulties in measuring the volume changes of liposome vesicles in osmotic shrink-swell experiments. He calculated the volume changes by measuring the changes in the liposome diameter. The liposome diameters were measured from photographs taken during the course of the experiment.

The recommended experiments would be conducted in a modified diffusion chamber, to allow admittance of the pipette. Since the volume of the chamber will be greater than previous models, there may be significant concentration gradients in the sample chamber. To alleviate this problem it is suggested that two membranes be employed instead of one. By locating the dialysis membranes on the upper and lower surface of the chamber the concentration gradients may be reduced. (See Nowlen (1983) for a complete description of the diffusion chamber.)

Once the pipette is in the chamber and a suitable liposome is found, it would be aspirated into the pipette at a low suction pressure. Then the initial diameter and projected length of the liposome would be recorded. Once the experiment is started the suction pressure in the pipette would take up all the excess membrane area produced by the liposome as a result of osmotic shrinkage. This accommodation of the excess membrane material would prevent necking of the liposome and it would always keep the liposome in spherical form. If the membrane area of the liposome is assumed constant the following relation can be used for the radius of the liposome at any time  $t$ :

$$R_L(t) = [(A(0) - 2\pi R_p \Delta L(t)(1 - R_p R_C^{-1}))/4\pi]^{.5} \quad (6.1.1)$$

Where  $A(0)$  is the surface area of the liposome at time  $t=0$ .

Equation (6.1.1) depicts how the changes in volume can be measured much more accurately than in previous investigations. Equation (6.1.1) yields the radius of the liposome at any time  $t$  based upon the projected length and the radius of the pipette. The proposed system does have one feasibility problem. In this system the test chamber must be open to the environment to allow entrance of the pipette. Further work is needed in characterizing the solute time history in the proposed chamber. Another question is whether the mechano-optical system will react fast enough to keep up with the dynamics of the system. In the compressibility modulus experiments it was observed that the liposome reacted almost instantaneously to an increase in the suction pressure. As long as the increase in pressure

was not large enough to perform irreversible work on the membrane (i.e., in regimes where membrane viscosity, plasticity or failure occur). Therefore it is felt that if the suction pressure is sufficiently high to provide minimal membrane tension the system will react fast enough to accurately measure the changes in volume of the liposome. Also the effects of friction between the liposome and the glass micropipette can be minimized if the glassware is kept ultraclean. This can be accomplished by sonicating the micropipette in distilled water prior to use. In any case the osmotic dynamics have been reported by several investigators (Boroske, et al., (1981) and Callow (1983)) and these data could serve to check the possible deleterious effects of friction on the experiments suggested above.

## 6.2 Ice-Water Interface Experiments

These experiments will be invaluable in determining the stresses a biological membrane undergoes during freezing. They will attempt to yield the adhesion forces and the adhesion energies the membrane senses while in contact with an ice front (Olien (1972) and Olien and Smith (1977)).

The first task involved in these experiments is the formation of the ice front. The ice front must be planar with respect to the liposome. This is essential in order to measure the contact angle between the ice and the membrane. The generation of such an ice front can be accomplished with the second generation test stage. This task can also be accomplished on some of the other conduction stages (Shabana (1983)), but these stages have no access site for the micropipette.

Once the ice front is established the liposome can be captured in a large bore pipette. Then the remaining liquid in the chamber can be drawn off and replaced with an inert fluid such as 3M FC-47. With this accomplished the liposome can be expelled from the pipette into the inert fluid and then captured again with a small bore pipette similar to those used in the previous experiments.

Thus the temperature of the test chamber can then be lowered further as desired without further propagation of the ice front. Care must be taken not to form ice crystals in the liposome. The liposome can then be placed against the ice front and the contact angles measured (see Figure 6.1). The contact angle data can then be put into the equation:

$$\cos(\theta) = \frac{((0.0015\gamma_{i-w} - 2.00)(\gamma_{i-w}\gamma_{m-w})^{.5} + \gamma_{m-w})}{(\gamma_{m-w}(0.015(\gamma_{i-w}\gamma_{m-w})^{.5} - 1.))} \quad (6.2.1)$$

taken from McGiver (1981) to yield the interfacial tensions of the various interfaces. Where  $\gamma_{m-w}$  is the interfacial tension at the water-membrane interface, and  $\gamma_{i-w}$  is the interfacial tension at the ice-water interface.  $\gamma_{i-w}$  must be available or determined independently to allow the solution of Equation (6.2.1). This analysis was applied to a video tape sequence of an egg PC liposome in distilled water in contact with an ice front (Callow (1983)). The value for  $\gamma_{i-w}$  was given by Dr. D. McGiver (1983) of the University of Western Ontario, as approximately 5.0 dynes/cm. When Equation (6.2.1) was solved for  $\gamma_{m-w}$

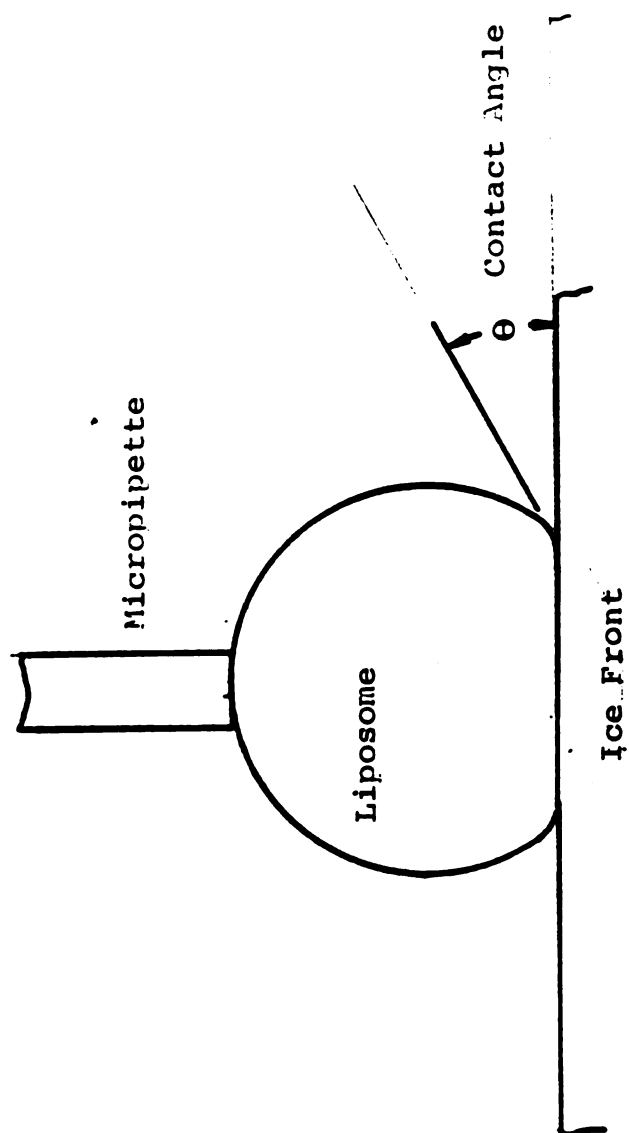


Figure 6.1 Schematic of the Interfacial Interaction between a Liposome and an Ice/Water Interface

the result was 77.0 dynes/cm. This is approximately twice the interfacial tension of a monolayer on an oil-water interface. The value for  $\gamma$  is in accordance to that predicted by Evans and Skalak (1980). The contact angles used in the calculation differed on each side of the membrane by no more than 3 degrees.

The existence of possible adhesion forces between the membrane and the ice front can be tested by attempting to pull the vesicle from the ice front. By increasing the suction pressure the membrane tension is increased. If an attempt is made to pull the liposome off the ice front, and it just breaks away, a force balance can be performed to calculate the adhesive forces between the ice front and the liposome.

The result of this type of proposed study would be a tabulation of the adhesive force as a function of the ice front temperature at the membrane-ice interface. These data would be useful for comparison with theory (Olien and Smith (1977)). These experiments could then be performed in various cryoprotective agents and their effects on the adhesive forces measured.

Preliminary experiments were attempted using the existing test stage. However the test stage did not have the capability to form the ice front required. The test stage could not reach the low temperature required.

### 6.3 Summary

The micromanipulator system offers an excellent opportunity to study the physical properties of the bilayer membranes in biological



cells and liposomes. It also allows one to observe how the membrane reacts to perturbations of its environment. This research has been intended to open the door to the characterization of the membrane and the relationship between the membrane state and the state of its environment. The experimental system has been developed and suggestions as to its further refinements and use have been made.

## APPENDICES

APPENDIX A  
RELATION OF MEMBRANE TENSION TO SUCTION PRESSURE

This appendix demonstrates the relation of suction pressure to the membrane isotropic tension. It will also relate the projected length of the aspirated vesicle to the change in area.

Performing a force balance, in the axial direction, on Figure (A.1) yields:

$$(P_p - P_c)\pi R_p^2 = \bar{T}2\pi R_p \quad (A.1)$$

$$(P_o - P_c)\pi R_c^2 = \bar{T}2\pi R_c$$

Subtracting the two equations eliminates the pressure inside the liposome to yield the following equation.

$$\Delta P = 2\bar{T}[1/R_p - 1/R_c] = (P_o - P_p) \quad (A.2)$$

which can be solved for  $\bar{T}$  in terms of measured data ( $P_o$ ,  $P_p$ ,  $R_p$ ,  $R_c$ ).

The area change is related to the projected length (and other measured data) (Evans, Waugh and Melnik (1976)) by:

$$\Delta A = (2\pi R_p)\Delta L[1 - R_p/R_c] \quad (A.3)$$

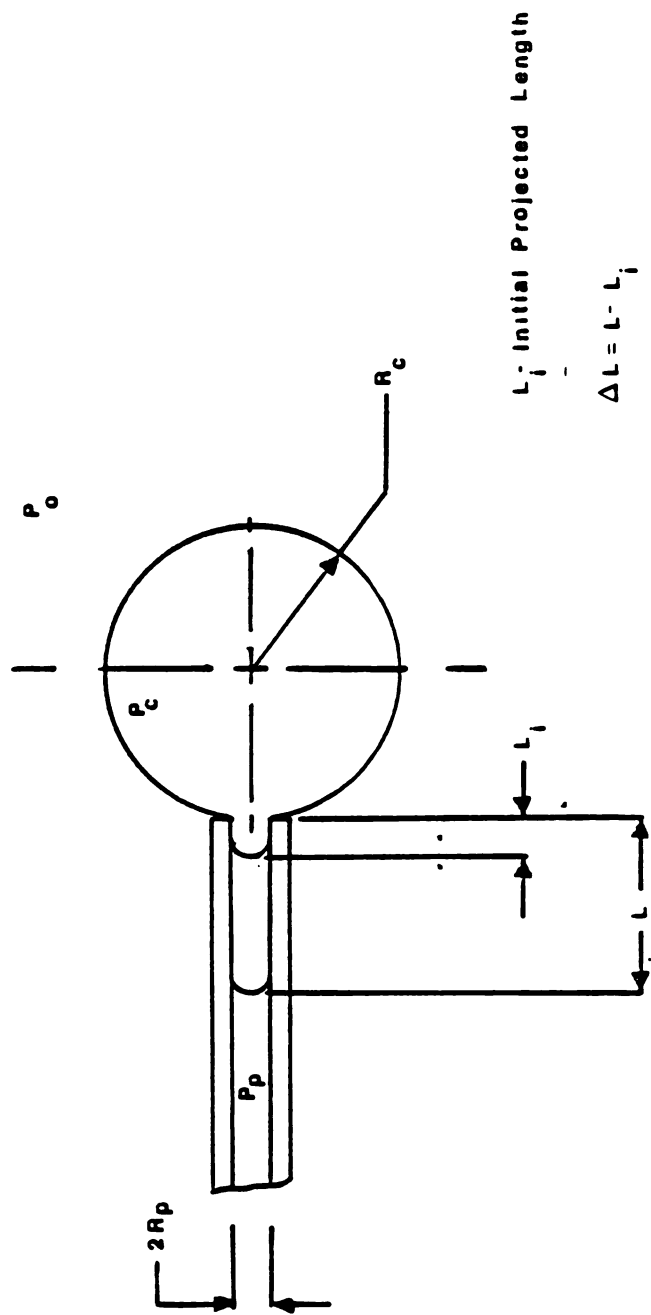


Figure A.1 Membrane Deformation Schematic Used for Performing Membrane Force Balance

## APPENDIX B

### COMPUTER MODELING AND DATA MANIPULATION

#### B.1 Computer Modeling and Data Manipulation

In the course of this investigation, several computer programs were written to perform various tasks. Early in the study the finite element program ELAS was used in an attempt to model the beam compression test as described by Evans and Skalak (1980). This was attempted to allow greater understanding of the membrane and to attack the modeling problem from a finite element point of view.

This effort failed since the program was not adaptable to the volume constraint inside the vesicle. During the beam compression experiments the vesicle can only deform in a way such that its volume remains constant. This volume constraint could not be satisfied in any finite element codes. The results produced from this effort was similar to that of placing a compression load on a thin hoop. The membrane deformed in such a way that there was a sharp bend or buckling at one point. This was not consistent with the experimental results of Evans and Skalak (1980). Therefore this effort was terminated.

In the course of this investigation two main computer programs were written. One program was written to perform data reduction, while the other was written to act as a digital temperature controller. Both of the programs will be discussed in detail.

The Fortran program DRED.FOR was written to reduce vesicle area, temperature and membrane tension data to allow calculation of the mechanical

properties of the membrane. The program was also designed to perform parameter variation studies on the isothermal compressibility modulus.

Fortran program HTRCON.FOR was written to provide the control logic for temperature control of the second generation test stage. This program requires an LSI-11 with A/D, D/A and RTC capability. This temperature control system was not operational at the time the experiments in this study were performed.

A new test stage employing this control program is in development and is discussed in detail in Chapter 3 and Appendix C. The control program HTRCON.FOR has been tested on the stage used by Shabana (1983) and proven useful.

#### B.1.1 Computer Modeling

At the present, DRED.FOR will do parameter studies on the isothermal compressibility modulus. The user inputs compressibility moduli and the program will construct the tension versus nondimensional area curves. Figure 4.1 represents the tension as a function of the nondimensional area change of the membrane. The curve is generated from Equation (2.1.1.19).

The  $\alpha$  values range from 0 to 3 percent. The upper limit was chosen based on the results of Evans and Kwok (1981). They report membrane lysis at values of 3 percent.

#### B.1.2 Data Manipulation

This section of the program DRED.FOR calculates the isothermal compressibility modulus ( $K_T$ ) and the thermal expansion coefficient, at constant tension ( $C_T$ ) from experimental data.

#### B.1.2.1 Isothermal Compressibility Modulus

The user inputs the suction pressure and the projected length of the vesicle in the pipette at several points. The program will then transform the raw data to tension and nondimensional area changes (Appendix A). The tension data is then input to a least squares routine to find the best fit straight line. The slope of this line is defined as the compressibility modulus. The program also performs statistical analysis to determine the coefficient of determination for the least squares linear fit.

#### B.1.2.2 Coefficient of Expansion at Constant Membrane Tension

The coefficient of expansion is calculated using Equation (2.1.2.2). The user inputs two operation temperatures along with the corresponding compressibility moduli, suction pressures and projected lengths. With these data the coefficient of expansion at constant tension ( $C_T$ ) is determined.

#### B.1.3 User Notes

The driver program is DRED.FOR. Subroutine Comp.FOR is also required. The program is user-friendly and will prompt for all necessary data. Sample output and program listings follow.

```

0001      PROGRAM DRED
C
C-----
C
C      This program will calculate membrane mechanical properties
C      using data taken from mechanical experiments in the BTP lab
C      The program operates in two modes. Mode 1 being calculation
C      of membrane conditions, (ie. Tension and projected length of
C      vesicle aspiration), the other will calculate the bulk
C      compressibility, shear modulus, and thermal expansion
C      coefficient from experimental data.
C
C-----
C
C      Dimension arrays and make declarations.
C
0002      DIMENSION X(360), Y(360), XB(100), YB(100), ALPHA(30), TENSIN(30)
0003      DIMENSION DELTAL(30)
0004      LOGICAL IANS
0005      REAL K, MU
0006      COMMON/BLK1/TENSIN, NPTS, ALPHA, K, YINTRS, RP, RC, A, DELTAL, PI
0007      COMMON/BLK2/EXPANS, IRUNS
C
C      Define variables.
C
C      X = Position of vesicle in x direction.
C      Y = Position of vesicle in y direction.
C      XB = Position of vesicle in micro-pipette.
C      YB = Position of vesicle in micro-pipette.
C      ALPHA = Nondimensional area change.
C      TENSIN = Isotropic tension in vesicle.
C      K = Bulk compressibility modulus.
C      MU = Shear modulus.
C      A = Area of vesicle.
0008      PI = 3.141592654
0009      IRUNS = 1 !Run counter.
C
C-----
C
0010      1 WRITE(7,*) 'DO YOU WANT A PARAMETER STUDY OR ARE YOU GOING'
0011      WRITE(7,*) 'TO INPUT EXPERIMENTAL DATA. IF THIS IS A'
0012      WRITE(7,*) 'PARAMETER STUDY TYPE YES.'
0013      READ(7,10) IANS !Check if user is doing param. stdy.
0014      10 FORMAT(A1)
0015      IF(IANS.NE.'Y') GOTO 55
C
C-----
C
C      Parameter study section. The user may vary the values of
C      the mechanical properties of the membrane and then watch the
C      variation in the expected experimental output.
C
C-----
C

```



```

      C      Read in physical parameters of experiment.
      C
0017      WRITE(7,*) 'ENTER BULK COMPRESSIBILITY: DYNE/CM. '
0018      READ(7,*) K
0019 55      WRITE(7,*) 'ENTER VESICLE RADIUS IN MICRO METERS. '
0020      READ(7,*) RC
0021      WRITE(7,*) 'ENTER PIPETTE RADIUS IN MICRO METERS. '
0022      READ(7,*) RP
      C
      C      Calculate tension and projected length of aspirated vesicle.
      C
0023      RP=RP*.0001 !Convert to centimeters.
0024      RC=RC*.0001 !Convert to centimeters.
0025      NPTS=30
0026      A=4.*PI*RC**2.      !Calculate area of vesicle.
      C
      C
      C
0027      IF(IANS.NE. 'Y') GOTO 300
0029      DO 20 I=1,30
0030          ALPHA(I)=I*.001
0031          TENSIN(I)=K*ALPHA(I)
0032          DELTA(I)=(A*ALPHA(I)/(2.*PI*RP*(1.-RP/RC)))*10000.
0033 20      CONTINUE
0034      GO TO 700
0035 300      WRITE(7,*) 'DO YOU WANT TO INPUT DATA TO CALCULATE '
0036          WRITE(7,*) 'THE COMPRESSIBILITY MODULUS. TYPE YES OR NO: '
0037          READ(7,250) IANS
0038 250      FORMAT(A1)
0039          IF(IANS.EQ. 'N') GOTO 1100
0041      CALL COMP
      C
      C-----
      C
      C      Calculate coefficient of determination.
      C
      C-----
      C
      C      DO 260 I=1,NPTS
      C          SUMX= ALPHA(I) + SUMX
      C          SUMY= SUMY + TENSIN(I)
      C          SUMXY= SUMXY + ALPHA(I)*TENSIN(I)
      C          SUMXSQ=SUMXSQ + ALPHA(I)**2.
      C          SUMYSQ=SUMYSQ + TENSIN(I)**2.
C260      CONTINUE
      C      XNUM=(SUMXY-SUMX*SUMY/NPTS)**2.
      C      XDENOM=(SUMXSQ-((SUMX**2.)/NPTS))
      C      XDEN2 = SUMYSQ-((SUMY**2.)/NPTS)
      C      COEDET= XNUM/(XDENOM*XDEN2)
      C      SUMX=0.
      C      SUMY=0.
      C      SUMXY=0.
      C      SUMXSQ=0.
0042      IDATF=1

```

```

C      SUMYSQ=0.
C
C-----
C
C      Write results.
C
C-----
C
0043 700  WRITE(6,800) IRUNS
0044 800  FORMAT('///// Run number ',I2)
C      IF(IDATF.EQ.1) WRITE(6,805) COEDET
0805  FORMAT('/// The coefficient of determination = ',F10.3)
0045      if(IDATF.EQ.1) WRITE(6,806)
0047 806  FORMAT('/// Experimental results!!!!')
0048      WRITE(6,810) K
0049 810  FORMAT(' Bulk compressibility = ',F10.3, ' Dyne/cm. ')
0050      RP=RP*10000.
0051      WRITE(6,811) RP
0052      RC=RC*10000.
0053 811  FORMAT(' Pipette radius=',F5.1, ' Micro meters. ')
0054      WRITE(6,812) RC
0055 812  Format(' Vesicle radius = ',F5.2, ' Micro meters')
0056      WRITE(6,820)
0057 820  FORMAT('///// ')
0058      WRITE(6,850)
0059 850  FORMAT(' Alpha ',5x, ' Tension ',5x, ' Proj. Lng')
0060      WRITE(6,860)
0061 860  FORMAT(15X, ' Dyne/Cm. ',5X, ' Micro-Metrs. ')
0062      WRITE(6,870)
0063 870  FORMAT('/// ')
C
C
C
0064 900  DO 920 I=1,NPTS
0065      WRITE(6,910) ALPHA(I),TENSIN(I),DELTA(I)
0066 910  FORMAT(3(F10.3,5X))
0067 920  CONTINUE
0068      GOTO 950
C
C-----
C
C      Calculate thermal expansion coefficient.
C
C-----
C
0069 1100 WRITE(7,*) 'ENTER INITIAL TEMPERATURE. '
0070      READ(7,*) T1
0071      WRITE(7,*) 'ENTER FINAL TEMPERATURE. '
0072      READ(7,*) T2
0073      WRITE(7,*) 'ENTER COMPRESSIBILITY MODULUS AT INITIAL TEMP. '
0074      READ(7,*) XK1
0075      WRITE(7,*) 'ENTER COMPRESSIBILITY MODULUS AT FINAL TEMP. '
0076      READ(7,*) XK2
0077      WRITE(7,*) 'ENTER DELTA P IN DYNE/CM**2. '

```

```

0078      READ(7,*)DELTAP
0079      WRITE(7,*)'ENTER INITIAL PROJECTED LENGTH IN MICRONS.'
0080      READ(7,*) XLINIT
0081      WRITE(7,*)'ENTER PROJ. LENGTH AFTER TEMP INCREASE: IN MICRONS.'
0082      READ(7,*) DELX
0083      DELX=DELX-XLINIT
0084      DELX=DELX*.0001                                !CONVERT TO CENTIMETERS
0085      ADDA = 2.*PI*RP*XLINIT*.0001
0086      A=A + ADDA
0087      WRITE(7,*) A, ADDA
0088      TENS=(DELTAP/2.)/(1./RP - 1./RC)
0089      ALPH1=TENS/XK1
0090      ALPH2=TENS/XK2
0091      DA=2.*PI*RP*DELX*(1. - RP/RC)
0092      ALPHT=DA/A
0093      EXPANC=ALPHT - (ALPH2-ALPH1)
0094      EXPANC=EXPANC/(T2 - T1)

      C
      C
      C

0095      WRITE(6,1110) IRUNS
0096      1110  FORMAT(///// 'Run number', I4)
0097      write(6,1120) T1,T2
0098      1120  FORMAT(// 'Initial temp = ', F5.1, 'SX', ' Final temp = ', F5.1)
0099      WRITE(6,1130) TENS
0100      1130  FORMAT(// 'Isotropic tension = ', f10.3, ' Dyne/cm.')
0101      WRITE(6,1135) XK1,XK2
0102      1135  FORMAT(// 'Bulk compressibility: Initial ', f9.3, ' Final', f9.3,
      .       ' Dyne/cm.')
0103      WRITE(6,1140) EXPANC
0104      1140  FORMAT(// 'Thermal expansion coefficient = ', f10.7, ' /C deg')

      C
      C-----
      C
      C      Check if user wants another run.
      C
      C-----
      C

0105      950  WRITE(7,*)'DO YOU WANT ANOTHER RUN: TYPE YES OR NO'
0106      READ(7,1000) IANS
0107      1000  FORMAT(A1)
0108      IRUNS=IRUNS + 1                                !Increment run counter.
0109      IF(IANS.EQ. 'Y') GOTO 1

      C
      C
      C

0111      200  STOP
0112      END

```

```

0001      SUBROUTINE COMP
      C
      C      This subroutine will calculate the compressibility modulus
      C      for a cell or liposome. The input data required is the
      C      delta P across the membrane and the projected length of the
      C      aspirated vesicle in the pipette.
      C
      C-----
      C
      C      Dimension arrays and make declarations
      C
0002      DIMENSION AT(2,25), ATAINV(2,2), INTM(2,2), C(2), DELTAL(30)
0003      DIMENSION TENSIN(30), ALPHA(30), ATA(2,2), XM(2,25), FR(3)
0004      COMMON/BLK1/TENSIN, NPTS, ALPHA, K, YINTRS, RP, RC, A, DELTAL, PI
0005      DOUBLE PRECISION DELTAA
0006      REAL K
      C
      C-----
      C
      C      Set initial values.
      C
0007      WRITE(7,*) 'ENTER NUMBER OF DATA PONTS, UP TO 25. '
0008      READ(7,*) NPTS
0009      WRITE(7,*) 'ENTER INITIAL PROJECTED LENGTH: MICRO-MTRS '
0010      READ(7,*) XINITL
0011      ADDA = 2.*RP*.0001*XINITL*PI
0012      A = A + ADDA
0013      WRITE(7,*) A, ADDA
      C
      C-----
      C
      C      Enter data.
      C
0014      DO 20 I=1,NPTS
0015          WRITE(7,*) 'ENTER DELTA P IN DYNE/CM. '
0016          READ(7,*) DELTAP
0017          WRITE(7,*) 'ENTER PROJECTED LENGTH IN MICRONS '
0018          READ(7,*) DELTAL(I)
0019          DELTAL(I)=DELTAL(I)-XINITL
      C
      C      Calculate tensions and alpha.
      C
0020          TENSIN(I)= (DELTAP/2.0)/(1./RP - 1./RC)
0021          DELTAA= 2.*PI*RP*DELTAL(I)*.0001*(1.-RP/RC)
0022          ALPHA(I)= DELTAA/A
0023      20  CONTINUE
      C
      C-----
      C
      C      Use least squares to get compressibility modulus.
      C
0024      DO 30 I=1,NPTS
0025      30  AT(1,I) = 1.
0026          XI = 0.

```

```

0027      XISQ = 0.
      C
      C      Enter alphas for x axis.
      C
0028      DO 40 I=1,NPTS
0029      40      AT(2,I) = ALPHA(I)
      C
      C
      C
0030      DO 50 I=1,NPTS
0031      XI = XI + ALPHA(I)
0032      XISQ = XISQ + ALPHA(I)**2.
0033      50      CONTINUE
      C
      C
      C
0034      ATA(1,1) = NPTS
0035      ATA(1,2) = XI
0036      ATA(2,1) = XI
0037      ATA(2,2) = XISQ
0038      DETA      = ATA(1,1)*ATA(2,2) - ATA(1,2)**2.
      C
      C
      C
0039      ATAINV(1,1) = ATA(2,2)/DETA
0040      ATAINV(1,2) = - ATA(2,1)/DETA
0041      ATAINV(2,1) = - ATA(1,2)/DETA
0042      ATAINV(2,2) = ATA(1,1)/DETA
      C
      C
      C
0043      DO 60 I=1,NPTS
0044      60      XM(1,I)=ATAINV(1,1)*AT(1,I) + ATAINV(1,2)*AT(2,I)
0045      DO 70 I=1,NPTS
0046      70      XM(2,I)=ATAINV(2,1)*AT(1,I) + ATAINV(2,2)*AT(2,I)
      C
      C
      C
0047      DO 80 I=1,NPTS
0048      SUM = SUM + XM(1,I)*TENSXN(I)
0049      SUM1 = SUM1 + XM(2,I)*TENSXN(I)
0050      80      CONTINUE
0051      WRITE(7,*) SUM, SUM1
0052      K=SUM1
0053      SUM = 0.
0054      SUM1 = 0.
0055      RETURN
0056      END

```

APPENDIX C  
TEMPERATURE CONTROL PROGRAM FOR THE  
SECOND GENERATION TEST STAGE

C.1 Introduction

The temperature controller for the cryomicroscope in the BTP lab is an analog device. At present, its accuracy is not more than  $\pm 1^{\circ}\text{C}$ . Furthermore the offset is not constant. To reduce the tolerance to  $\pm .1^{\circ}\text{C}$  a digital temperature controller was designed. The principal advantage of the digital controller was the increased flexibility gained by incorporating the LSI-11 as the control driver.

The present analog device contains eight operational amplifiers, each with its own offset adjustment. In the current controller configuration, the offset adjustments are not used. Physical location and wiring problems prevent the offset adjustment. The offsets must be adjusted each time the device is powered up, and then they must be monitored frequently to reduce drift errors.

To alleviate this offset problem the digital controller contains only three operational amplifiers, and only two require offset adjustment. The offset adjustment is performed by two high precision potentiometers. The offset will be displayed on panel meters for inspection. The present breadboard device can read the thermocouple temperature into the A/D converter to  $.01^{\circ}\text{C}$  accuracy.

## C.2 Thermal Analysis

To model the performance of the cryomicroscope stage a lumped parameter system was used. Figure C2.1 depicts the microscope stage system. Please note convection to the atmosphere has been neglected.

The heat flux into the microscope stage is controlled by the LSI-11. If the sample temperature is too low the heater is activated, likewise if the temperature is too high the heater is deactivated. This type of temperature control is frequently used in commercial temperature controllers. The key to accuracy is the rate of temperature sampling. Employing the LSI-11 greatly increases the accuracy of the controller.

### C.2.1 Cooling Cycle

Figure C2.2 depicts the lumped parameter system in the cooling cycle.

Applying the first law of thermodynamics to the system the following equation is formed.

$$MC_p \, dT/d\theta = -hA(T_B - T_{\text{coolant}}) \quad (\text{C2.1.1})$$

Where  $\theta$  is time and  $C_p$  is the capacitance for the stage.  $M$  is the thermal mass of the system, and  $h$  is the convective heat transfer coefficient.

To solve this equation a variable transformation is required.

Let:

$$\bar{T} = T_B - T_{\text{coolant}} \quad (\text{C2.1.2})$$

Equation (C2.2.1) can now be solved in terms of the new variable  $\bar{T}$ .

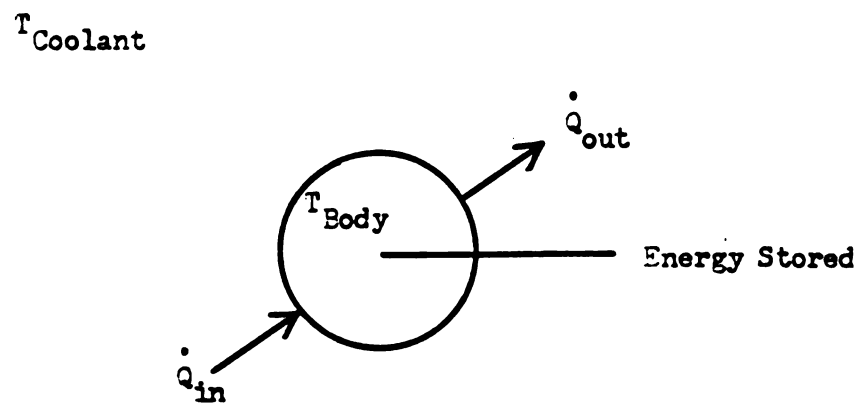


Figure C2.1 Schematic Representation of the First Law of Thermodynamics Applied to the Cryomicroscope Stage

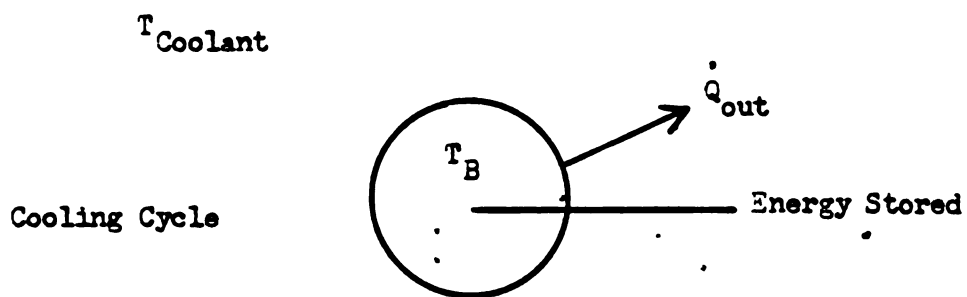


Figure C2.2 Schematic Representation of the First Law of Thermodynamics for the Cooling Process

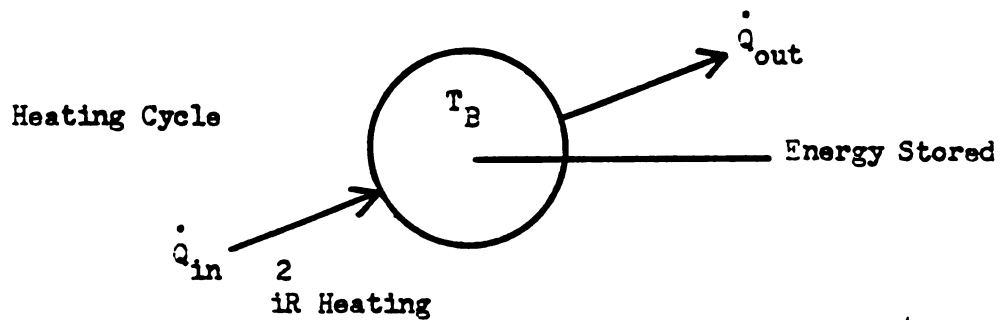


Figure C2.3 Schematic Representation of the First Law of Thermodynamics for the Heating Process



The solution for the cooling cycle is:

$$\bar{T}(\theta) = Ke^{-(hA/MC_p)\theta} \quad (C2.1.3)$$

By definition the time constant for the system in the cooling mode is:

$$T_{CC} = MC_p/hA \quad (C2.1.4)$$

However it is nearly impossible to predict what the time constant of the system is. Tu (1983) performed numerical analysis on the stage and found the time constant to be 52 seconds.

Using the results of Tu, the solution to the cooling cycle differential equation is:

$$\bar{T}(\theta) = Ke^{-(.0192)\theta} \quad (C2.1.5)$$

Where K is equal to the temperature difference between the sample and the coolant at time equal to zero.

### C.2.2 Heating Cycle

Figure C2.3 depicts the heating cycle. The differential equation derived from the first law is:

$$MC_p d\bar{T}/d\theta = \text{Constant} - hA\bar{T} \quad (C2.2.1)$$

The constant is the  $i^2R$  heating of the microscope stage. The solution to this differential equation is:

$$\bar{T} = \bar{T}(0) + (\text{Constant})(T_{CH}/MC_p) (1 - e^{-(1/T_{CH})\theta}) \quad (C2.2.2)$$

Where  $T_{CH}$  is the system time constant for heating of the stage. It was determined by Tu (1983) to be approximately 32 seconds.

### C.3 Computer Modeling and Control

#### C.3.1 Computer Modeling of the Microscope Stage

The computer simulation of the stage predicted an obtainable accuracy of  $\pm .03^\circ\text{C}$  for steady and dynamic operation. The Fortran program HTRSIM, written for the BTP lab LSI -11, modeled the cryomicroscope stage as a lumped parameter system. The computer model is separated into two parts, heating and cooling cycles. In the heating cycle Equation (C2.2.2) is used to determine the temperature history.  $\bar{T}(0)$ , of the heating cycle, is determined by the final value of  $\bar{T}$  from the previous cooling cycle. In the cooling cycle Equation (C2.1.3) is used. The constant  $K$  is the final  $\bar{T}$  from the previous heating cycle.

The value for  $\theta$  is reset to zero each time the program switches from heating to cooling cycles, or vice-versa.

The two system time constants, heating and cooling, along with the temperature sampling rate, coolant temperature, the amount of power to the heater and the final target temperature are input by the user. With this input data the program can perform in two modes, steady state or dynamic.

##### C.3.1.1 Description of Error Analysis Figures

Figure C3.1 represents the controller steady state error as a function of the coolant temperature. In this series of runs the heater power coefficient (HPC) is defined by:

$$\text{HPC} = i^2 R T_{CH} / (MC_p) \quad (\text{C2.1.1.1})$$

was held constant at 50. The HPC is a ratio of the  $i^2R$  heat input multiplied by the heating cycle time constant, and then divided by the thermal mass and capacitance. The HPC is the maximum possible  $\Delta T$  that the heater can input into the system. Typical values for the microscope stage were 200°C. The temperature sampling rate was 100 Hz. In these simulations the program was operated in the steady state mode.

Since the main application of the temperature controller, in this work, applies to an isothermal process, (constant sample temperature) the value of the HPC was set at 50. The coolant temperature was also set at -10°C for this work.

Figure C3.2 depicts the maximum steady state error as a function of the temperature sampling rate. In this series of runs the HPC was 50, and the coolant temperature was held at -10°C. Figure (C3-2B) depicts the steady state temperature error as a function of temperature sampling frequency.

Figure C3.3 represents the maximum steady state error as a function of the HPC. In these simulations, the sampling rate was 100 Hz, and the coolant temperature was -10°C.

Figure C3.4 is the plot for a simulated 10°C step change of the desired temperature of the stage induced by a step change in heater input. The HPC is 50, sampling rate is 100 Hz and the coolant temperature is -196°C.

Figure C3.5 Depicts the simulated response to a temperature ramp of 80°C per minute. The solid line is the target temperature. The dots represent the temperatures predicted by the simulation program.

#### C.3.1.2 Summary of Parameter Studies

The parameter studies depicted in Figures C3.1 to C3.5 yielded the following trends.

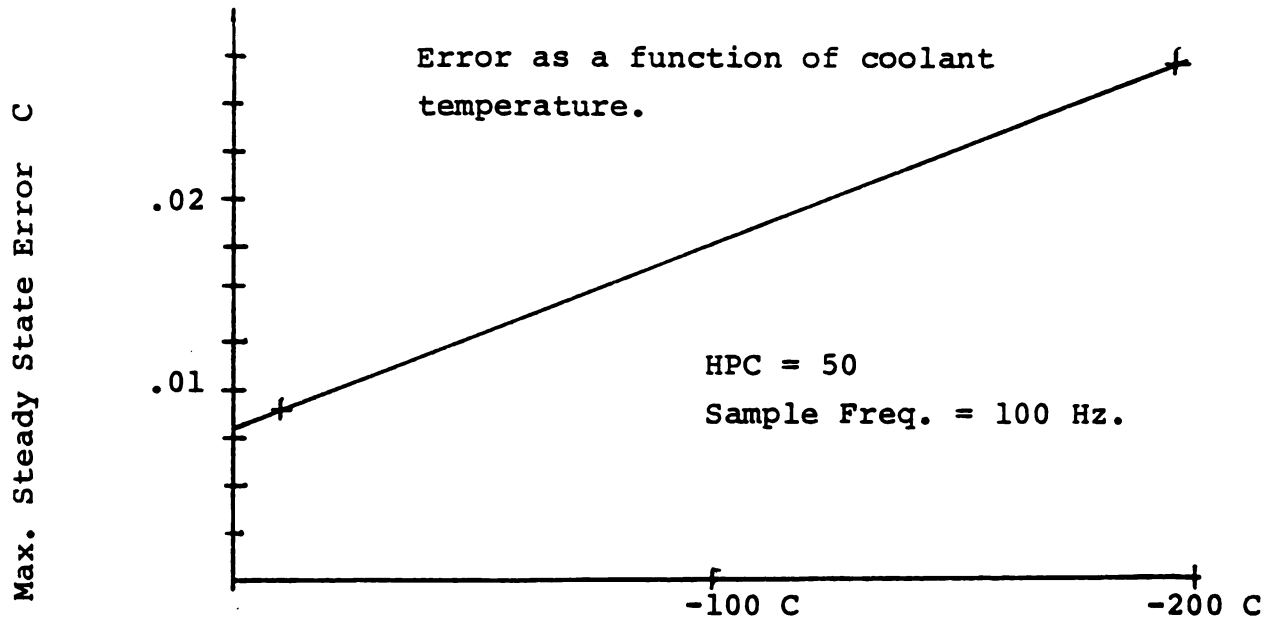


Figure C3.1 Predicted Controller Steady State Error as a Function of Coolant Temperature

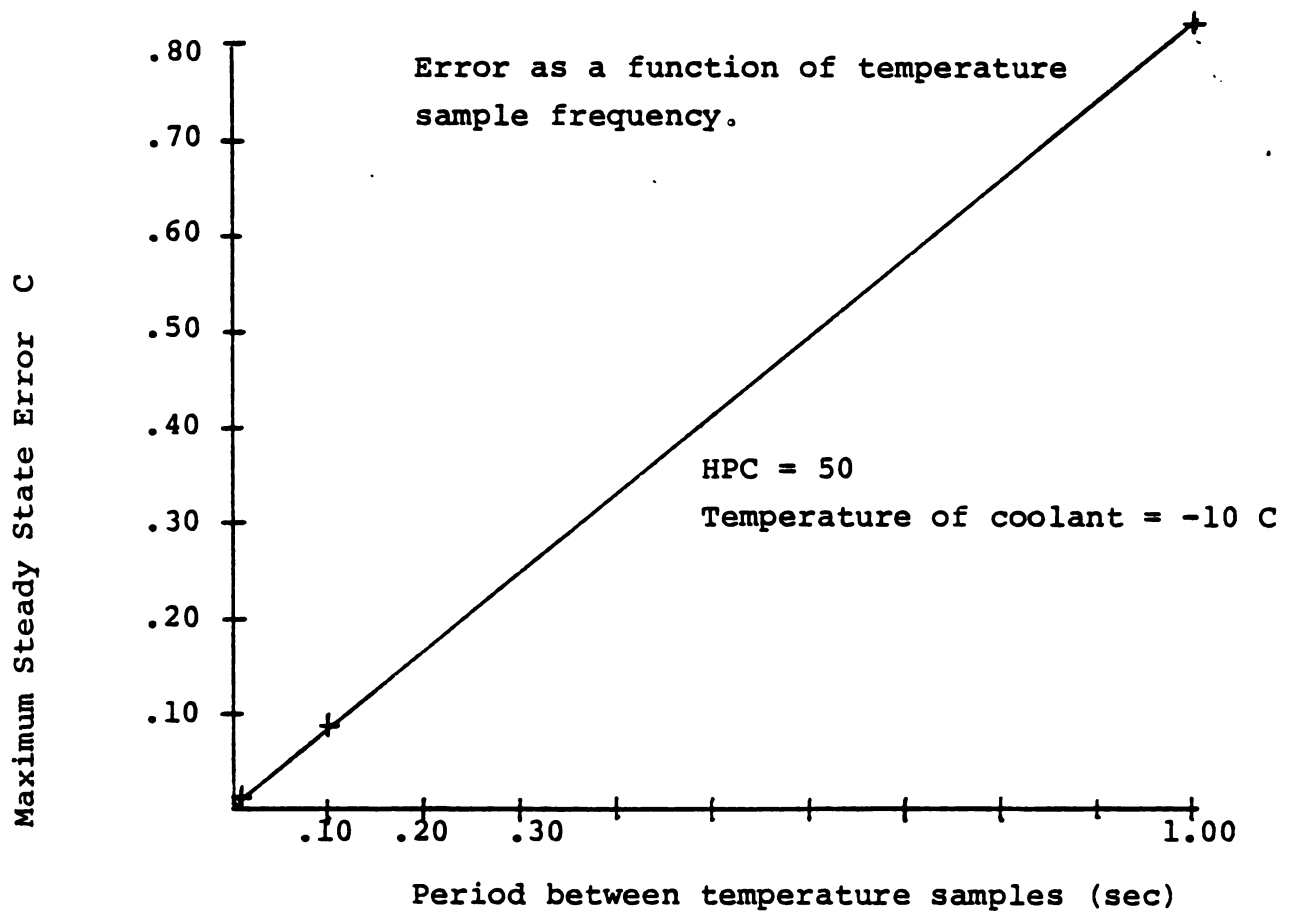


Figure C3.2 Predicted Maximum Steady State Error as a Function of Temperature Sampling Rate

Error as a function of A/D sampling rate.

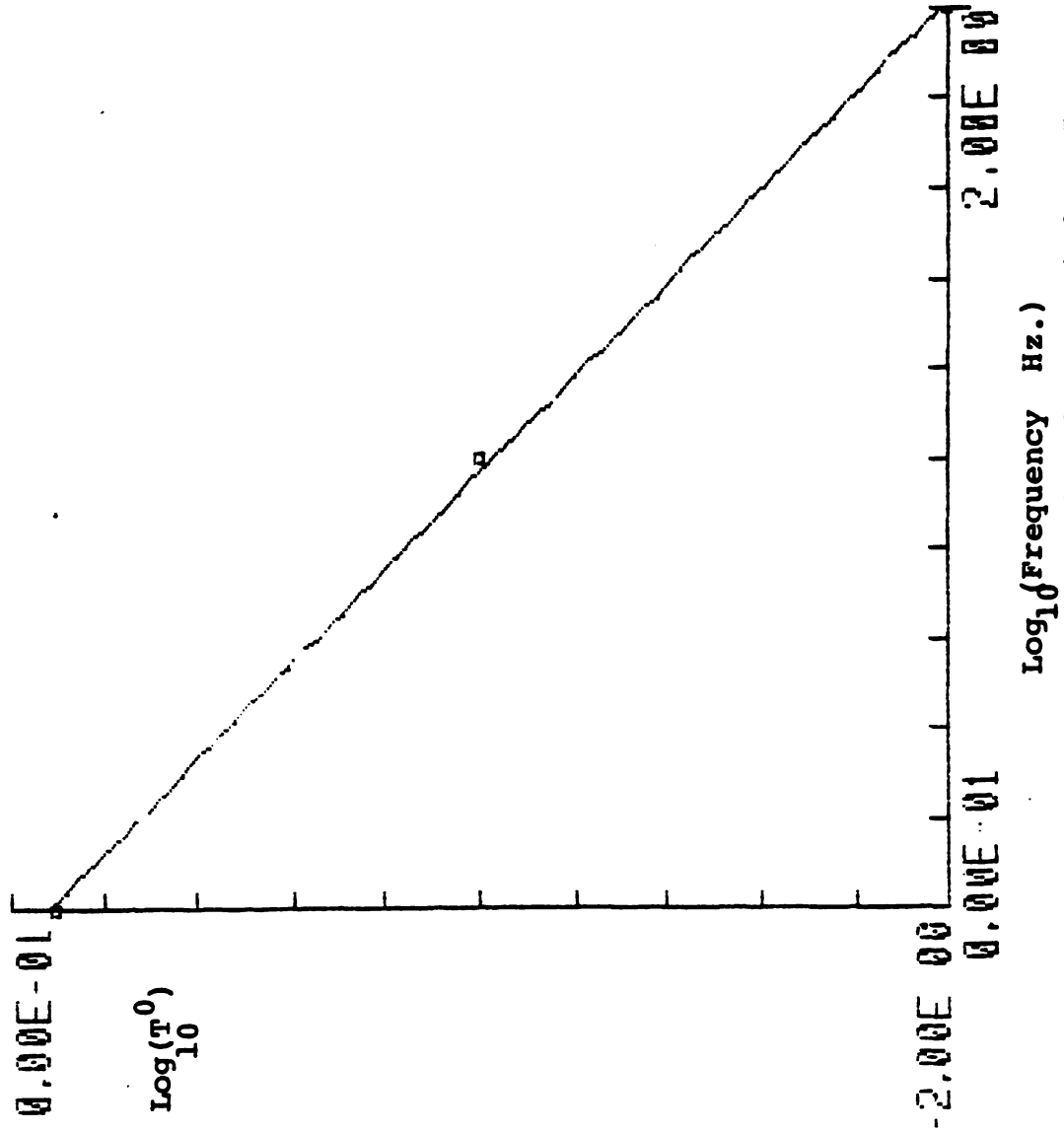


Figure C3.2b A Log-Log Representation of the Steady State Temperature Error as a Function of Temperature Sampling Frequency

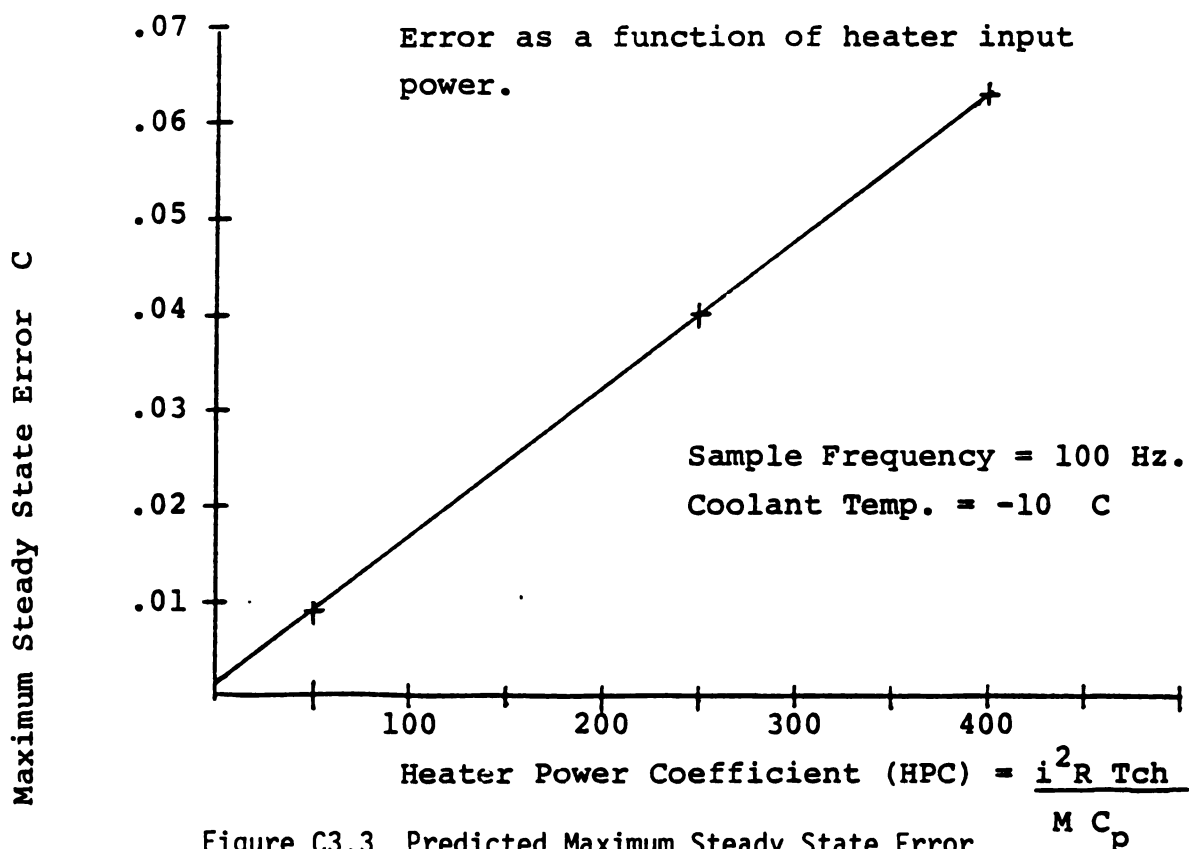


Figure C3.3 Predicted Maximum Steady State Error as a Function of Heater Input (HPC)

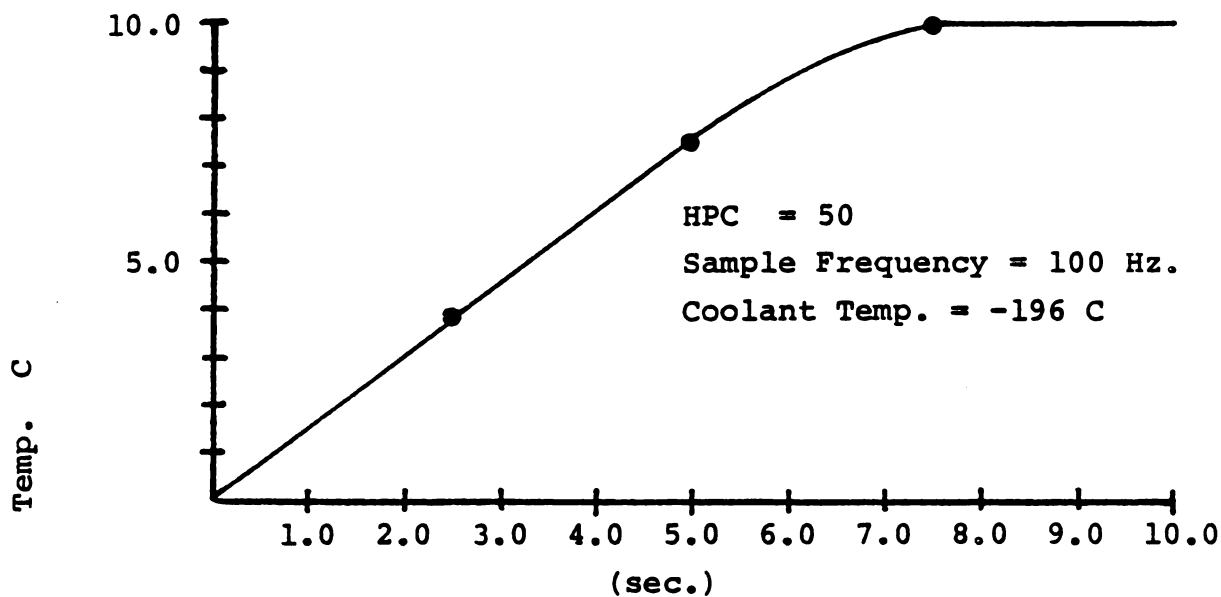


Figure C3.4 Simulated Response of the Cryomicroscope Stage to a 10°C Temperature Change

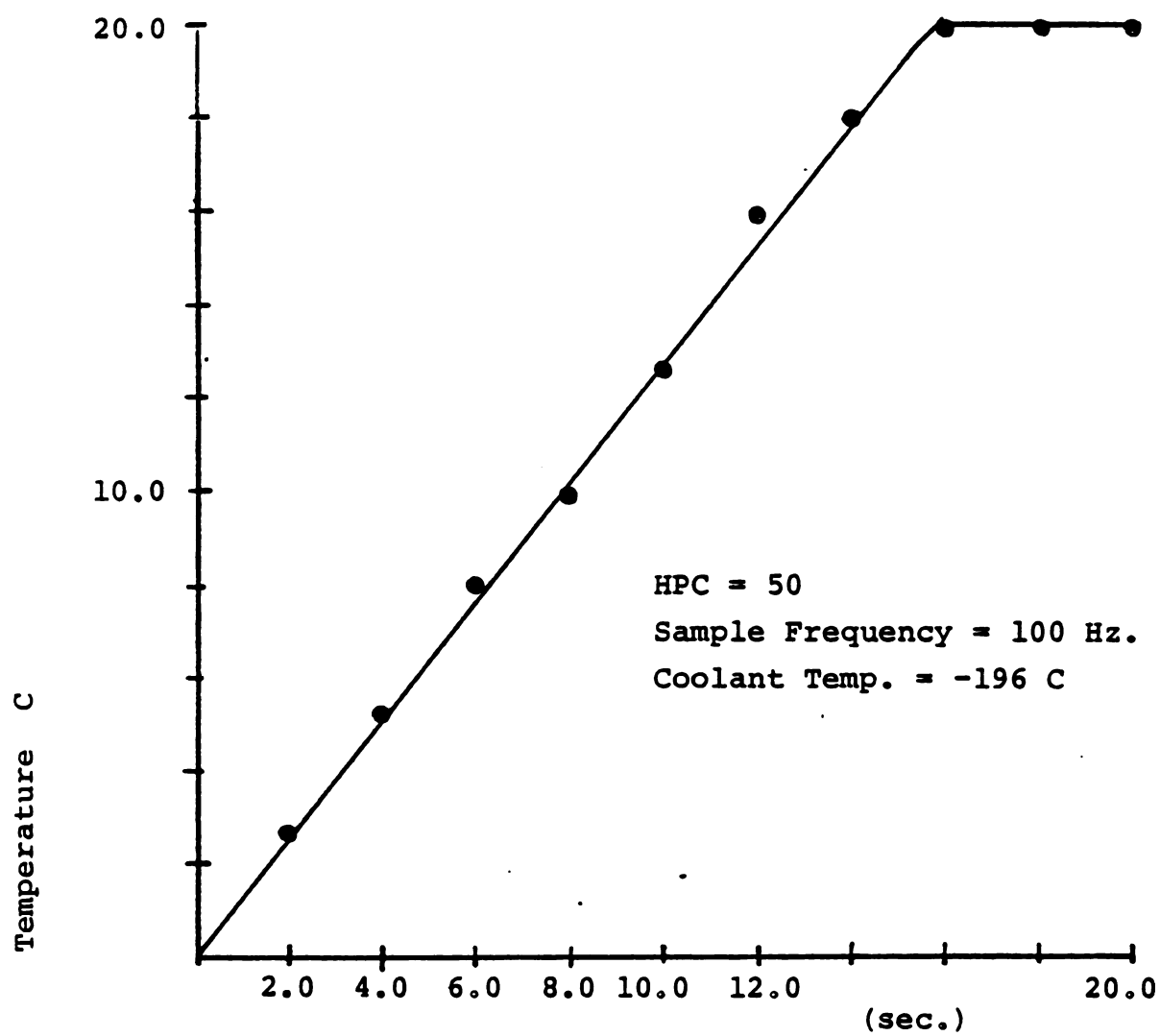


Figure C3.5 Simulated Response of the Cryomicroscope Stage to a Temperature Ramp of  $80 \text{ C.min}^{-1}$

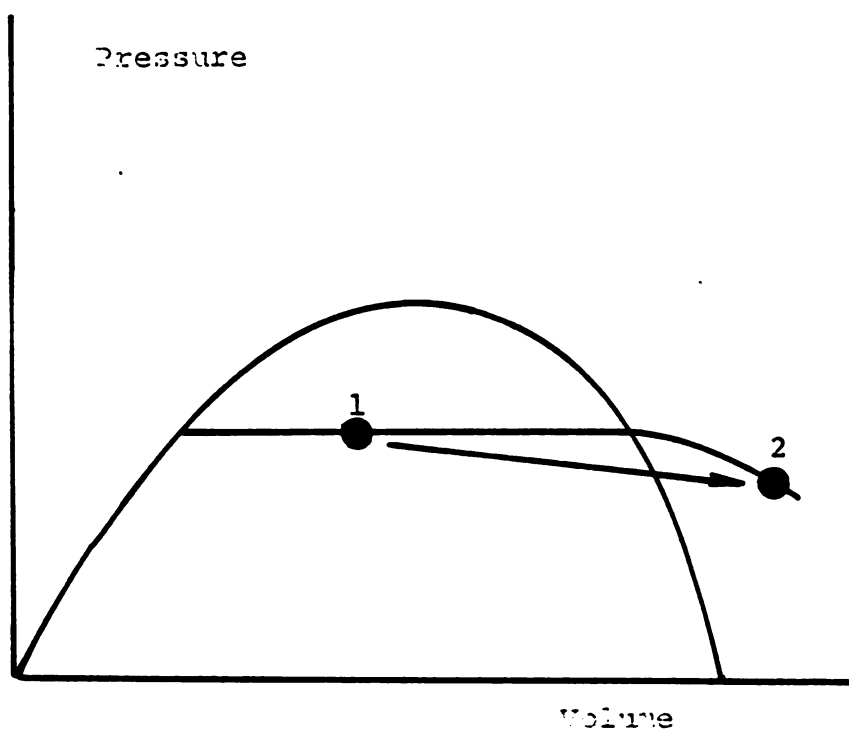
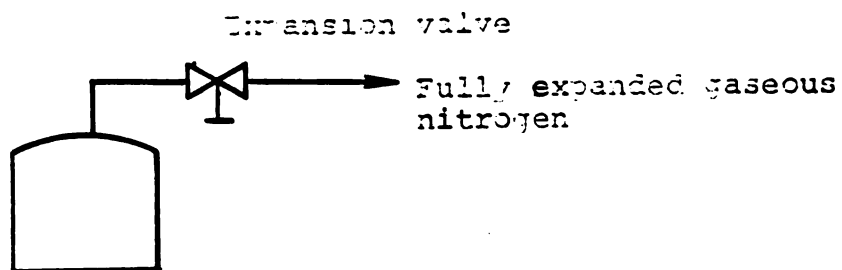


Figure C3.6 Pressure as a Function of Volume  
for the Coolant Fluid in the  
Cryomicroscope Stage



Accuracy was increased as the ratio between system time constants and A/D sample time interval was increased. This suggested that the sampling should be conducted as fast as possible. The optimum achievable sampling rate was, limited by the response time constant of the thermocouples, 100 Hz. This value was approximately twice the time constant of the thermocouples.

Accuracy was also increased when the temperature difference between the desired temperature and the coolant temperature was decreased. An undesirable side effect of this was a slower cooling rate. This effect caused the system to be sluggish. This can be shown analytically from Equation (C2.1.5):

$$\bar{T}(\theta) = Ke^{-(.0192)\theta}$$

When the coolant temperature was increased, the value for K decreases. Therefore:

$$d\bar{T}/d\theta = -(.0192)Ke^{-(.0192)\theta}$$

When the heater power coefficient HPC was reduced

$$HPC = i^2 R T_{CH} / MC_p \quad (C3.1.1)$$

the accuracy was also increased. However, again the system became sluggish. This can be shown analytically from Equation (C2.2.2).

$$\bar{T} = \bar{T}(0) + (\text{Constant}) (T_{CH} / MC_p) (1 - e^{-(1/T_{CH})\theta})$$

This is reduced to:

$$\bar{T} = \bar{T}(0) + HPC (1 - e^{-(1/T_{CH})\theta})$$

Therefore:

$$d\bar{T}d\theta = HPC e^{-(1/T_{CH})\theta}$$

It was found through these parameter studies that the microscope stage should operate under two completely different sets of conditions for the steady state and dynamic modes.

In the dynamic mode, the HPC and the sample/coolant temperature difference should be large. This will give the system the amount of power and heat flux required to drive dynamic operations.

In the steady state mode the HPC and the sample/coolant temperature difference should be small. These conditions will slow the response time, but once the system is at its operating condition it will remain extremely stable.

In addition, the liquid nitrogen coolant used for dynamic studies should have the following valving depicted below (Fig. C3.6) to increase its accuracy. Gaseous nitrogen should be drawn from the tank and fed to the regulator. The regulator will then meter the flow to the stage. The optimal flow condition would be to have the coolant be in the completely gaseous region of the P-V diagram. This will eliminate changes in the convective heat transfer coefficient due to mixed phase boiling. A small heater may be needed in the liquid nitrogen tank to insure an adequate supply of gaseous nitrogen.

Parameter study results and the simulation program listing follows.

### C.3.2 Computer Program for Temperature Control

The following flow chart depicts the computer controlled temperature controller. The computer program utilizes quasi-proportional control.

```

0001      PROGRAM HTRSIM
      C
      C      THIS PROGRAM WILL MODEL A DIGITAL CONTROLLED PULSE HEATER
      C      SYSTEM TO BE USED IN THE BTP LAB.  THE MICROSCOPE STAGE IS
      C      MODELED A LUMPED PARAMETR SYSTEM.
      C
0002      DIMENSION TB(2501),T(2500)
0003      LOGICAL IANS
      C
      C      READ IN PARAMETERS
      C
0004 10    WRITE(7,*)'ENTER THE COOLING TIME CONSTANT IN SECONDS. '
0005      READ(7,*) TCC
0006      WRITE(7,*)' '
0007      WRITE(7,*)'ENTER THE HEATING TIME CONSTANT IN SECONDS. '
0008      READ(7,*) TCH
0009      WRITE(7,*)'ENTER THE PERIOD BETWEEN TEMPERATURE SAMPLES. (TWICE '
0010      WRITE(7,*)'THE TIME CONSTANT OF THE THERMOCOUPLES'
0011      READ(7,*) DT
0012      WRITE(7,*)' '
0013      WRITE(7,*)'ENTER HEATER POWER: HP*TCH/(Mt*Cp)'
0014      READ(7,*) HP
0015      WRITE(7,*)' '
0016      WRITE(7,*)'ENTER THE TEMP OF COOLANT STREAM, DEGREES C '
0017      READ(7,*) TN2
0018      WRITE(7,*)' '
0019      WRITE(7,*)'ENTER THE DESIRED TEMPERATURE OF THE SAMPLE'
0020      READ(7,*) TDES
0021      WRITE(7,*)'ENTER STARTING TEMPERATURE OF SAMPLE'
0022      READ(7,*) TSTR
0023      WRITE(7,*)' '
0024      WRITE(7,*)' '
0025      WRITE(7,*)' ENTER 1 OR 0 FOR LONG OR SHORT OUTPUT'
0026      READ(7,*) IOUT
0027      IF(IOUT.EQ.1) IP=50
0029      IF(IOUT.EQ.0) IP=250
0031      IF(IOUT.EQ.5) IP=5
      C
      C
      C
0033      TBDES=TDES-TN2
0034      TBINIT=TSTR-TN2
0035      TTTT=TBINIT
0036      ITIME= 0
0037      ISTAT=0
0038      TTT=20.
      C
      C
      C
0039      DO 40 I=1,2500
      C      IF(I.LT.1500) TBDES= TTTT + (TTT/1500.)*I      !for ramps
      C
      C
0040 20    IF((TB(I-1).LT.TBDES).AND.(I.GT.1)) GO TO 30

```

```

0042      IF(I.EQ.1) GOTO 30
      C
      C      TURN OFF HEAT.
      C
0044      IF(ISTAT.EQ.1) ITIME=1
0046      IF((ISTAT.EQ.1).AND.(I.GT.1)) TBINIT=TB(I-1)
0048      IF((ISTAT.EQ.1).AND.(I.EQ.1)) TBINIT=TBINIT
0050      TB(I)=TBINIT*(EXP((-1.)/TCC * (DT*ITIME)))
0051      ISTAT=0
0052      ITIME=ITIME + 1
0053      GOTO 40
      C
      C      TURN ON HEAT
      C
0054  30    IF(ISTAT.EQ.0) ITIME=1
0056      IF((ISTAT.EQ.0).AND.(I.GT.1)) TBINIT=TB(I-1)
0058      IF((ISTAT.EQ.0).AND.(I.EQ.1)) TBINIT=TBINIT
0060      TB(I) = TBINIT + HP*(1. - EXP((-1.)/TCH * (DT*ITIME)))
0061      ISTAT=1
0062      ITIME=ITIME+1
      C
      C
      C
0063  40    CONTINUE
      C
      C      WRITE RESULTS
      C
0064      WRITE(6,45) HP,TN2
0065  45    FORMAT(///' HEATER POWER = ',F8.1,5X,' N2 TEMP= ',F8.1,' F.')
0066      WRITE(6,48) TCH,TCC,DT
0067  48    FORMAT(// ' HEAT TC =',F8.2,5X,' COOL TC =',F8.2,5X,' DT=',F5.3)
0068      WRITE(6,47)
0069  47    FORMAT(///' TEMP',20X,' TIME')
0070      DO 50 I=1,2501,IP
0071          TEMP=TB(I)+TN2
0072          TIME=I*DT
0073          WRITE(6,60) TEMP,TIME
0074  60    FORMAT( F10.2,20X,F10.4)
0075  50    CONTINUE
      C
      C      CALCULATE DEVIATIONS
      C
0076      DO 100 I=1,2500
0077          T(I)=TB(I)+TN2
0078          IF(I.LT.1000) GO TO 100
0080          IF(I.EQ.1000) TMAX=TDES
0082          IF(I.EQ.1000) TMIN=TDES
      C
      C
0084      IF(T(I).GT.TMAX) GOTO 90
0086      IF(T(I).LT.TMIN) GOTO 95
0088      GOTO 100
      C
      C

```

FORTRAN IV

V02.5-2

Tue 27-Dec-83 14:42:46

PAGE 003

```
0089  90      TMAX=T(I)
0090          GOTO 100
      C
      C
0091  95      TMIN=T(I)
      C
      C
0092  100     CONTINUE
      C
      C
0093          TDEV=TMAX-TMIN
0094          TDEV=TDEV/2.0
0095          WRITE(6,110) TDEV
0096  110     FORMAT(/' MAXIMUM ERROR = ',F10.3,' DEGREES C. ')
      C
      C      DO YOU WANT ANOTHER RUN
      C
0097          WRITE(7,*) ' DO YOU WANT ANOTHER RUN. '
0098          READ(7,70) IANS
0099  70      FORMAT(A1)
0100          IF(IANS.EQ.'Y') GOTO 10
      C
      C
      C
0102          STOP
0103          END
```

That is to say that the temperature is sampled, and then compared to the desired temperature. If the actual temperature is too high, the heater is turned off. If the temperature is ten degrees lower than the desired, then the D/A voltage is set to allow maximum power through the heater. If the temperature is five degrees lower than desired, then a lower power is sent through the stage heater (see Figure C3.7). The current configuration of the program allows for three separate power inputs into the heater. It should be noted that the more power settings there are in the program, the longer it takes to execute a data sample.

The program is user friendly and will prompt for all input required.

Note: DO NOT ATTEMPT TO RUN THE PROGRAM WHEN THE INPUT AND OUTPUT DEVICES ARE NOT CONNECTED. THIS ACTION MAY CAUSE DAMAGE TO THE A/D AND D/A COMPONENTS AND WILL ALSO CAUSE THE HEATER ON THE STAGE TO BEHAVE ERRATICALLY.

The program listing follows.

## C.4 Digital Control Hardware

### C.4.1 Analog to Digital Thermocouple Amplifier

The function of this device is to take the output of the existing Action Pac and process it for input into the A/D converter. The device consists of a double-ended input to single-ended output converter coupled to a noninverting amplifier with a gain of 100. The thermocouple input signal conditioner, shown in Figure C4.1, was built to boost the output of the Action Pac ( $1\text{mV}/^{\circ}\text{C}$ ) to  $.1\text{V}/^{\circ}\text{C}$ . This will give a temperature operation band of  $\pm 50^{\circ}\text{C}$ . The temperature operation band is limited by

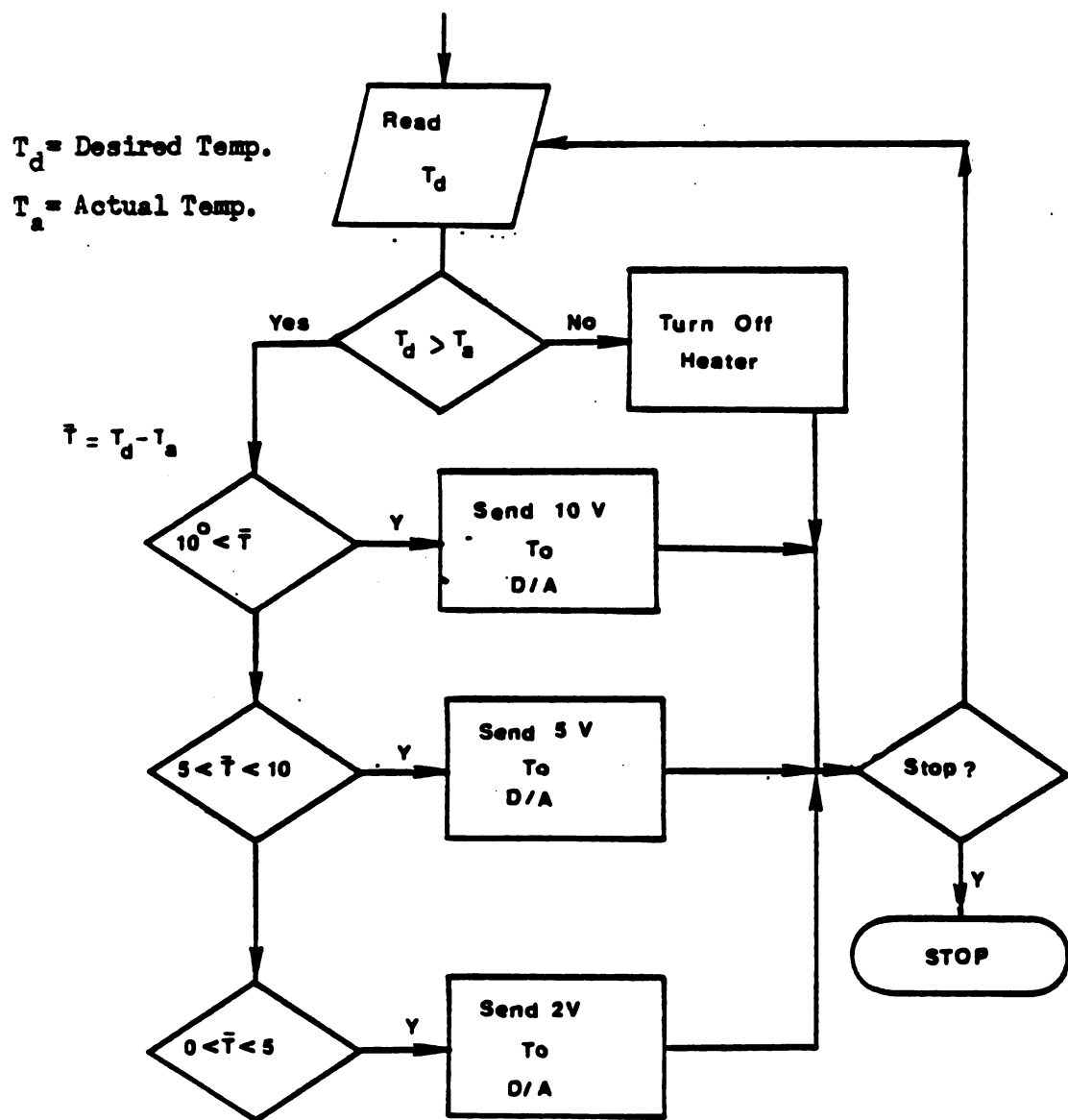


Figure C3.7 Temperature Controller Flow Chart

0001       PROGRAM HTRCON

C

C

C

C

C

C

C

C

C

C

C

C

C

C

C

C

-----  
This program was written to operate as a digital controller for  
the cyromicroscope stage. The program uses two A/D channels  
and one D/A channel.

A/D Channel 3 is the aspiration pressure.

A/D Channel 4 is the stage temperature.

D/A Channel 1 is the stage heater amplifier signal.

C

C

C

C

C

Declare externals and set up IDLIST

0002       DIMENSION IDLIST(13)

0003       EXTERNAL ISR

0004       LOGICAL IANS

0005       COMMON TARTEM, ICNT, TSTART, TFINAL, IFLAGR, TEMPR, DT

C

C

C

C

C

Set up IDLIST for the call to device.

0006       IDLIST(1) = "177000           !Location of A/D CSR.

0007       IDLIST(2) = IPEEK("177000)   !Contents of A/D CSR.

0008       IDLIST(3) = "177002           !Location of A/D DR.

0009       IDLIST(4) = IPEEK("177002)   !Contents of A/D DR.

0010       IDLIST(5) = "170440           !Location of D/A DR.

0011       IDLIST(6) = IPEEK("170440)   !Contents of D/A DR.

0012       IDLIST(7) = "170420           !Location of RTC CSR.

0013       IDLIST(8) = IPEEK("170420)   !Contents of RTC DR.

0014       IDLIST(9) = "170422           !Location of BPR Reg.

0015       IDLIST(10) = IPEEK("170422)   !Contents of BPR Reg.

0016       IDLIST(11) = "440             !Location of RTC Int.

0017       IDLIST(12) = IPEEK("440)       !Contents of RTC Int.

0018       IDLIST(13) = 0                 !End of list flag.

C

C

C

C

C

Set initial conditions.

0019       IVEC = "440

0020       ICNT = 1

0021       IPRTY= "7

0022       ID    = 1

C

C

C

C

C

Call device.

0023       CALL DEVICE(IDLIST)



```

C
C
C      Establish interrupt service routine linkage.
C
C
0034      IERR = INTSET(IVEC,IPRTY,ID,ISR)
0035      DO 100 I=1,10000
0036 100      CONTINUE      !Program delay for intset.
0037      IF(IERR.EQ.0) WRITE(7,*)'ISR LINKAGE IS ESTABLISHED.'
0039      IF(IERR.NE.0) WRITE(7,*)'ISR LINKAGE ERROR'
0031      IF(IERR.NE.0) CALL EXIT
C
C
C      Start the real time clock and begin the temperature controller.
C
C
0033      CALL IPOKE("170422,-5)      !Poke DT = 100 Hz.
C
C      Set operating conditions.
C
0034 110      WRITE(7,*)'ENTER THE TARGET TEMPERATURE IN DEGREES C'
0035      READ(7,*) TARTEM
C
C
C
0036      WRITE(7,*)' '
0037      WRITE(7,*)' '
0038      WRITE(7,*)'TO STOP THE CONTROLLER TYPE CTRL C.'
0039      WRITE(7,111) TARTEM
0040 111      FORMAT('1','TARGET TEMPERATURE IS ',F10.1)
0041      WRITE(7,125)
0042 125      FORMAT('0','PRESSURE  KDYNE/CM**2      TEMPERATURE DEGREES C')
0043      WRITE(7,*)' '
0044      CALL IPOKE("170420,"141)      !START CLOCK.
0045 150      READ(7,200) IANS
0046 200      FORMAT(A1)
0047      IF(IANS.EQ.'S') CALL EXIT
0049 145      IF(IANS.NE.'D') GOTO 145
C
C
C
0051      CALL EXIT
0052      END

```

```

      C
      C
      C
      C
      C
0001      SUBROUTINE ISR(ID)
      C
      C
      C      SUBROUTINE ISR IS THE TEMPERATURE CONTROLLING ROUTINE FOR THE
      C      CYROMICROSCOPE STAGE.
      C
      C      A/D CHANNEL 3 IS THE PRESSURE OF ASPIRATION.
      C      A/D CHANNEL 4 IS THE TEMPERATURE OF THE STAGE.
      C
0002      INTEGER ID
0003      COMMON TARTEM, ICNT, TSTART, TFINAL, IFLAGR, TEMPR, DT
      C
      C      TURN OFF THE RTC.
      C
0004      CALL IPOKE("170420,"0)      !CLOCK IS STOPPED.
      C
      C      READ TEMP AND PRESSURE.
      C
0005      CALL IPOKE("177000,"2001)
0006      10  IF((IPEEK("177000).AND."200).EQ.0) GOTO 10
0008      ITEMP= IPEEK("177002)
      C
      C
      C
0009      CALL IPOKE("177000,"1401)
0010      20  IF((IPEEK("177000).AND."200).EQ.0) GOTO 20
0012      IPRES= IPEEK("177002)
      C
      C      PRESSURE TRANSDUCER RANGE +/- 5V LIMITED BY I/O BOX
      C      TEMPERATURE RANGE IS +/- 50mV LIMITED BY I/O BOX
      C
0013      PRESS=IPRES * .0048840049 * 17.2
0014      TEMP = ITEMP * .0048840049 * 10.
0015      TEMDIF=TARTEM-TEMP
0016      SUM = SUM + TEMP
0017      SUM1= SUM1+PRESS
      C
      C      PROPORTIONAL CONTROL SECTION
      C
0018      IF(TEMDIF.LT.0.) CALL IPOKE("170440,"7777)
0020      IF(TEMDIF.GT.10) GO TO 35
0022      IF(TEMDIF.GT.5.) GOTO 36
0024      IF(TEMDIF.GT.2.5) GOTO 37
0026      IF(TEMDIF.GT.0.) GOTO 38
0028      GOTO 41
      C
      C
      C
0029      35  CALL IPOKE("170440,"0)

```

FORTRAN IV

VOL. 5-2

Tue 27-Dec-83 14:43:43

PAGE 002

```
0030      GOTO 41
      C
      C
0031  36      CALL IPOKE("170440,"3777)
0032      GOTO 41
      C
      C
0033  37      CALL IPOKE("170440,"6000)
0034      GOTO 41
      C
      C
0035  38      CALL IPOKE("170440,"7000)
      C
      C
0036  41      IF(ICNT.LT.100) GOTO 50
0038      TEMP = SUM/100.
0039      PRESS=SUM1/100.
0040      WRITE(7,30) PRESS,TEMP
0041  30      FORMAT('+' 5X,F10.1,13X,F10.1)
0042      ICNT = 0
0043      SUM = 0.
0044      SUM1=0.
      C
      C
      C
0045  50      ICNT = ICNT + 1
0046      CALL IPOKE("170420,"141)
0047      RETURN
0048      END
```

the input capability of the I/O box. In addition, to increase the operational temperature bandwidth would require modification to the I/O box. An increase to  $\pm 100^{\circ}\text{C}$  can be obtained by increasing the I/O box input to  $\pm 10$  volts. It should be noted that the current Action Pac model 4150 has a time constant of 130 ms (manufacturer's data). This will affect the performance of the overall temperature controller program. However, the effects of the large time constant of the Action Pac will not be felt as strongly while the program is in the steady state mode. This temperature controller was built primarily for steady state temperature studies.

Figure C4.2 is the Bode plot for the device shown in Figure C4.1. The dots on the gain plot represent actual data taken from the bread-boarded circuit. The gain was measured by inputting a square wave into the input terminals in the range of 10-30 mV, and then observing the output compared to the input on the dual beam oscilloscope.

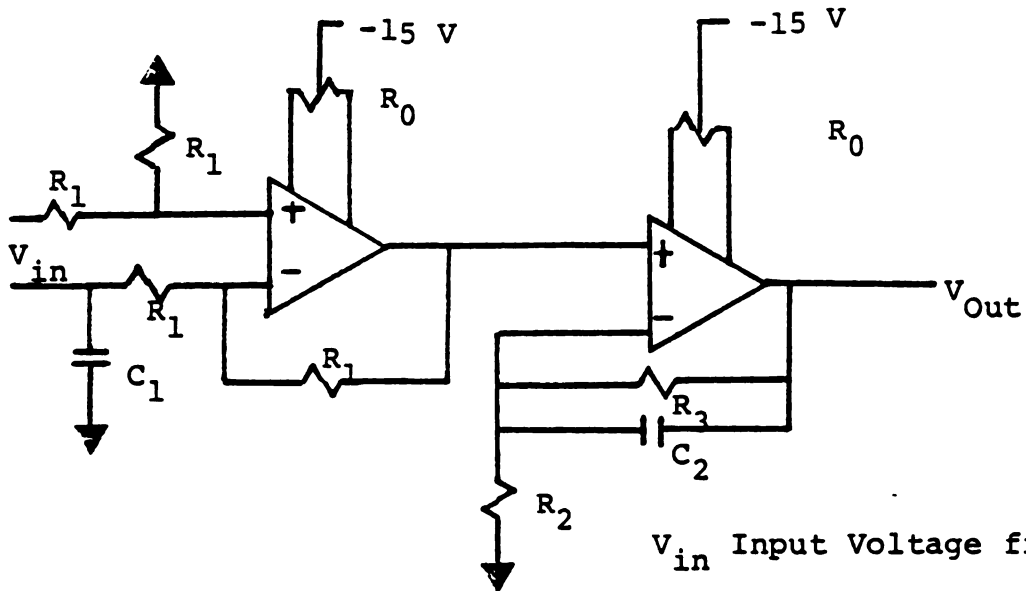
#### C4.2 Digital to Analog Power Amplifier

This device is a power amplifier connected to the D/A converter. This device drives the microscope heater. The darlington pair was taken from the existing analog controller. See the complete controller schematic for complete details (Figure C4.3). The new power amplifier was fabricated and found to be linear.

### C.5 Experimental Results

#### C.5.1 Microscope Stage Characteristics

The cryomicroscope stage can be modeled, accurately, as a first-order system. Figures C5.1 and C5.5 depict the response of the stage to a step input of heating and cooling. When the curves were compared



All Op-Amps LF-351

$V_{in}$  Input Voltage from Action Pack.

$V_{out}$  Output voltage to the I/O box.

$R_0$  10 K -- 10 turn Pot.

$R_1$  1 M Ohm

$R_2$  100 Ohm

$R_3$  10 K Ohm

$C_1$  .01 micro F

$C_2$  .02 micro F

Figure C4.1 Electrical Schematic for Thermocouple Input Signal Conditioner

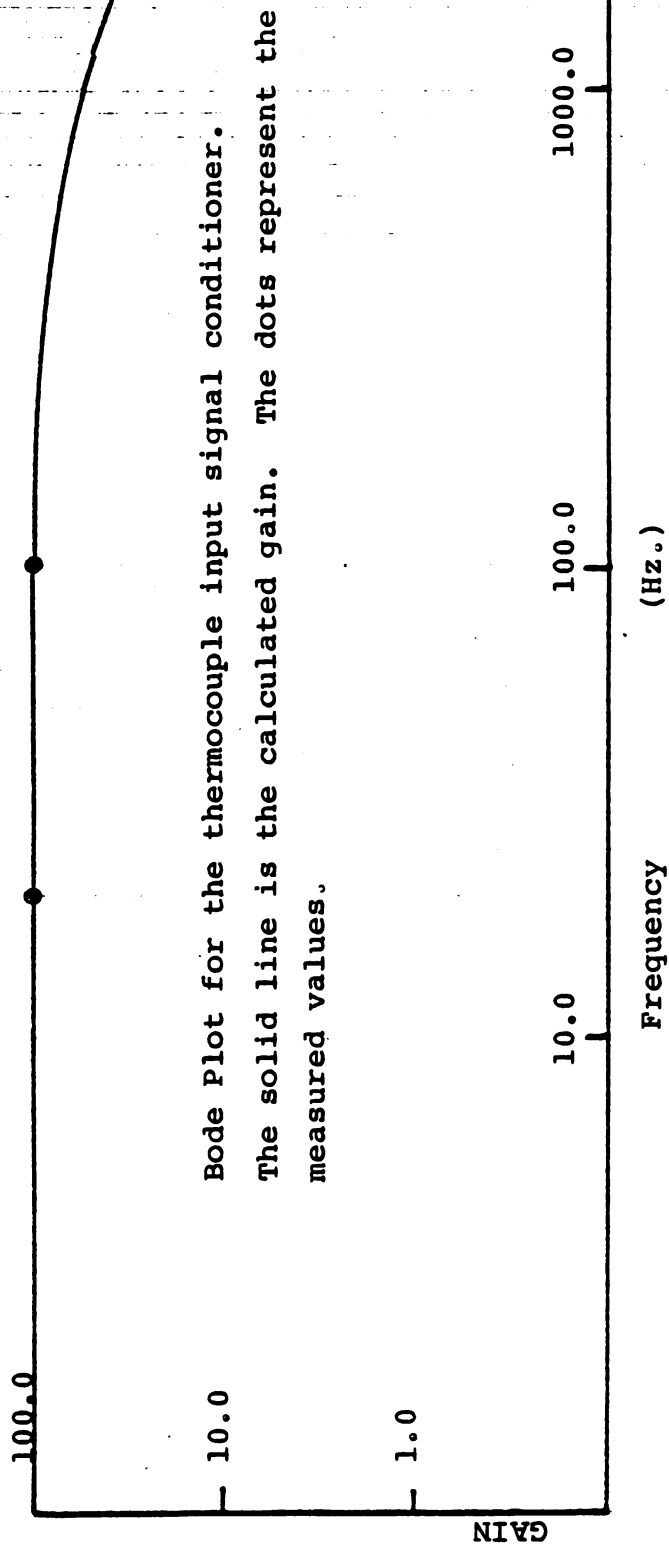


Figure C4.2

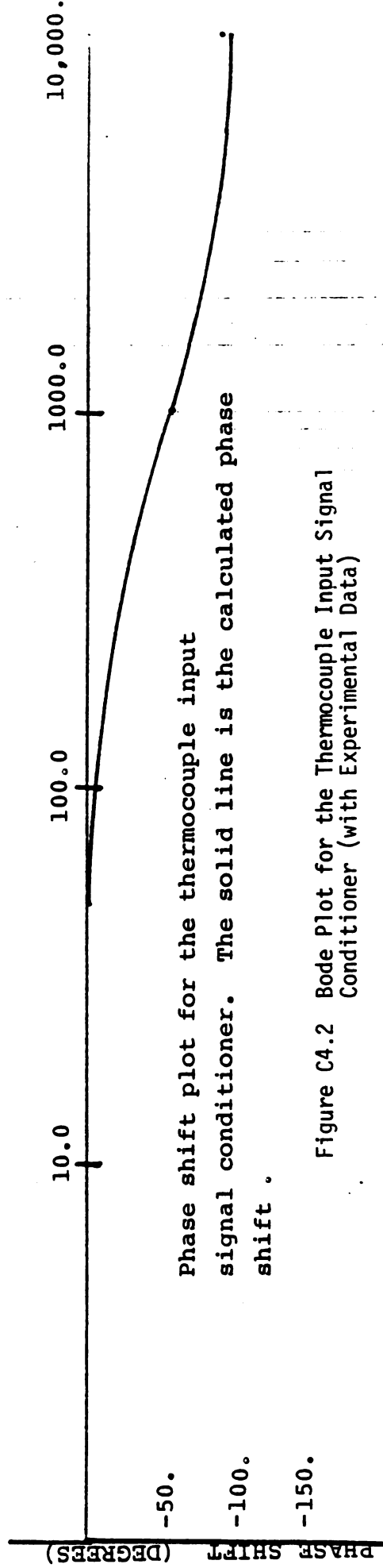


Figure C4.2 Bode Plot for the Thermocouple Input Signal Conditioner (with Experimental Data)

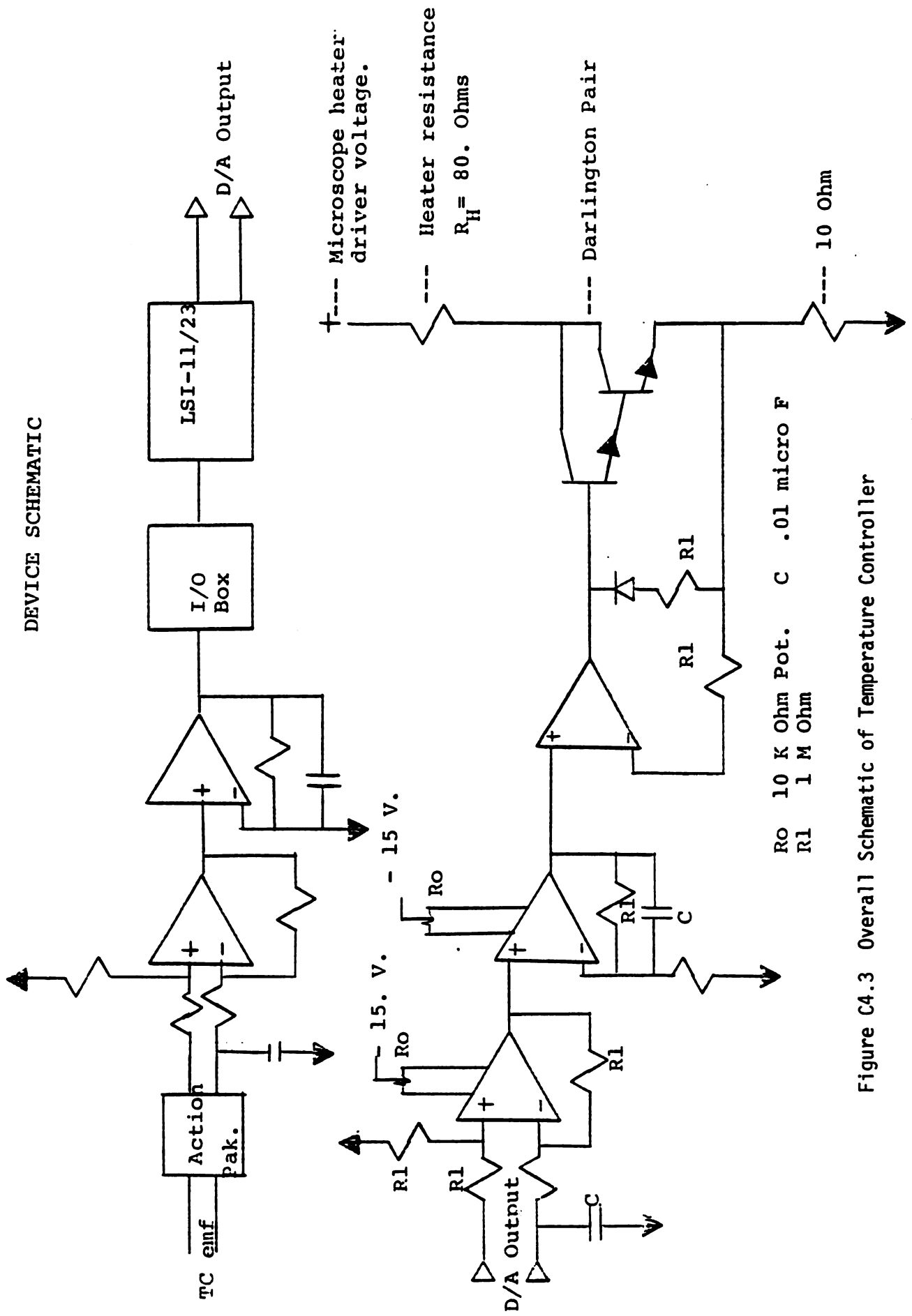


Figure C4.3 Overall Schematic of Temperature Controller

to an exponential function, their respective correlation coefficients were greater than .90. The system time constants in the heating and cooling cycles were found to be 24 and 32 seconds, respectively. It should be noted that these experiments were not conducted on Tu's stage. However, since they were conducted on a much larger stage (Shabana, 1983) (larger thermal mass) one would expect the system time constants to be larger than Tu's, not smaller.

Figure C5.4 is the steady state temperature error at set points from -40 to 40°C. In the current breadboarded configuration, the controller is able to maintain a worst case tolerance of  $\pm .5^{\circ}\text{C}$ . This error can be reduced and this will be discussed in Section 6.

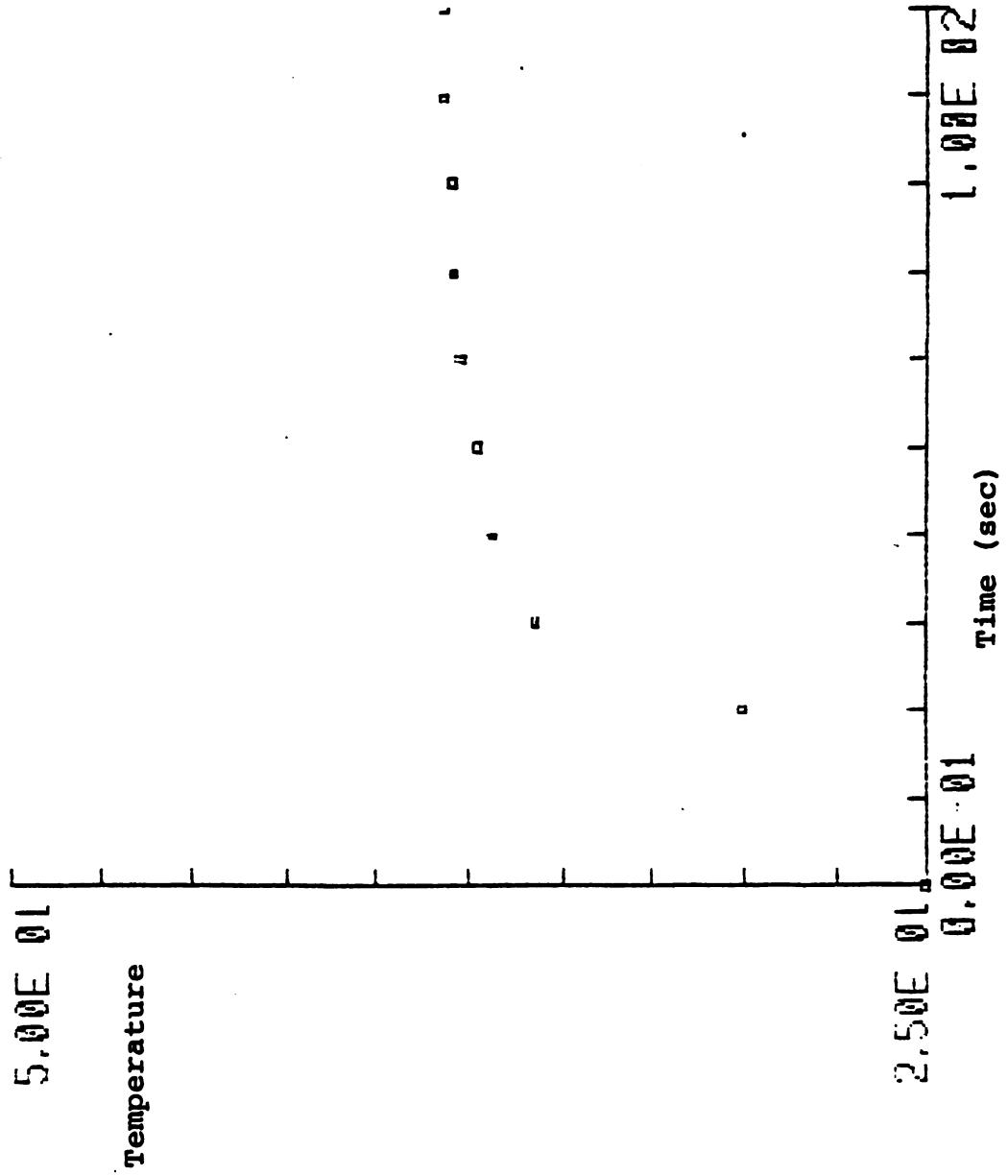
#### C.5.2 Effect of Operation Parameter Variations

The dominant parameter in the operation of the cryomicroscope stage is the stage heater driving voltage. Figures C5.2 and C5.3 demonstrate the effect of the stage heater driving voltage on the system. Figure C5.2 is the time response of the system for various voltage settings. For these experiments the stage heater was subjected to the maximum power the controller would allow for the particular heater driving voltage. This study allowed the definition of Figure C5.3. This figure plots the maximum  $\Delta T$  the stage can experience for a given setting. The current configuration has this voltage set at 34.0 volts.

The effects of various cooling liquids were recorded in Figure C5.5. It is interesting to note that the cooling rate is unchanged when going from liquid nitrogen to ethylene glycol. It should be noted that this effect could be the result of convection to the ambient environment. This effect was not studied in this project.



Figure C5.1 Typical Experimental System Response to a Step Input Current to the Microscope Stage Heater



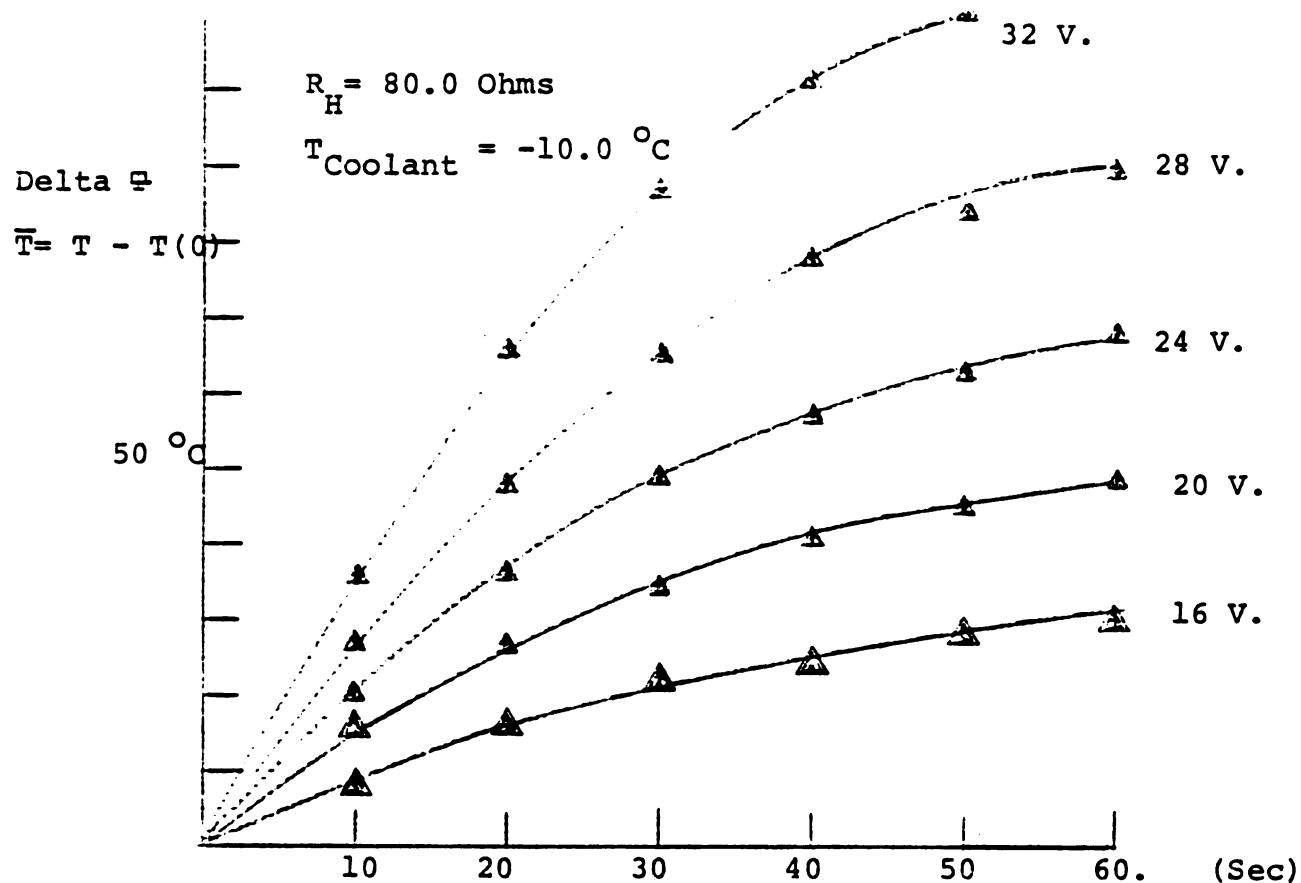


Figure C5.2 System Response as a Function of the Microscope Heater Driver Voltage

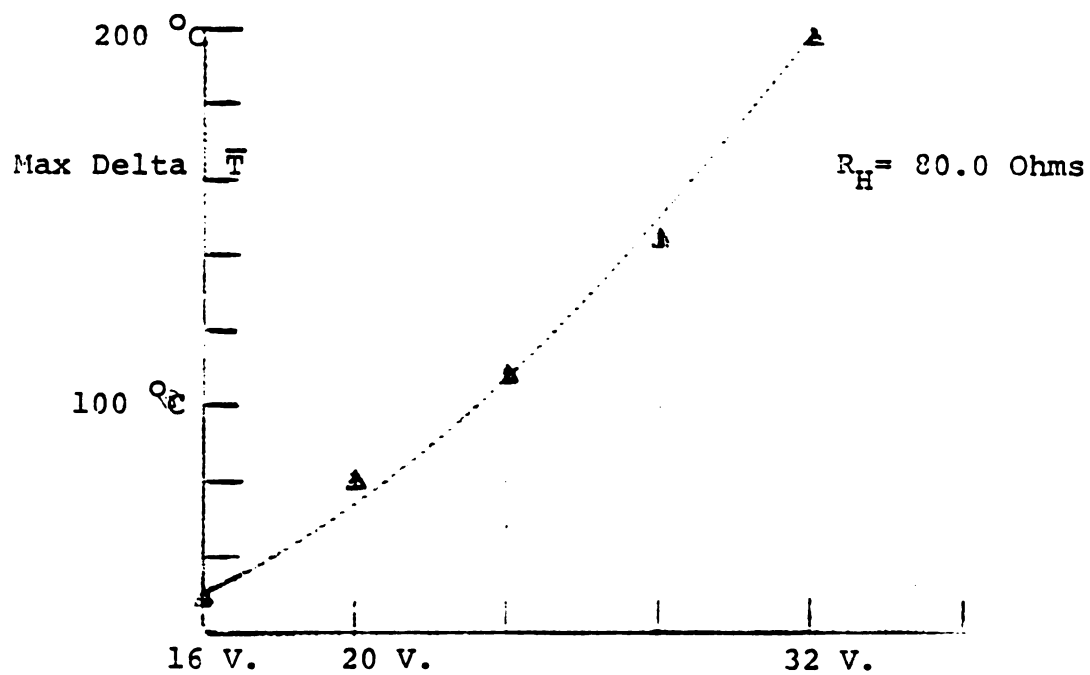


Figure C5.3 Maximum Temperature Rise as a Function of the Microscope Heater Driver Voltage

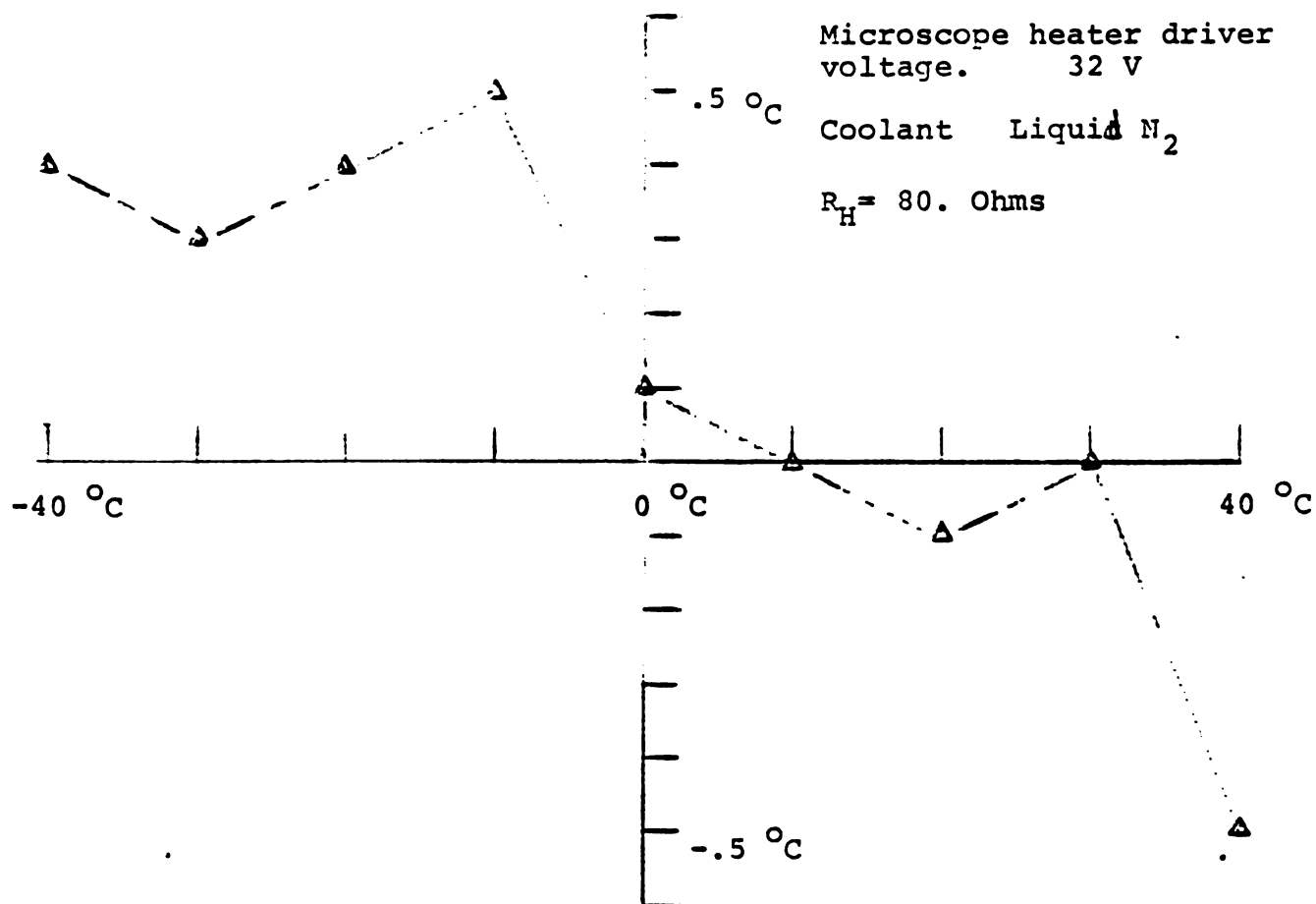


Figure C5.4 Measured Steady State Temperature Error as a Function of Set Point Temperature with Proportional Control

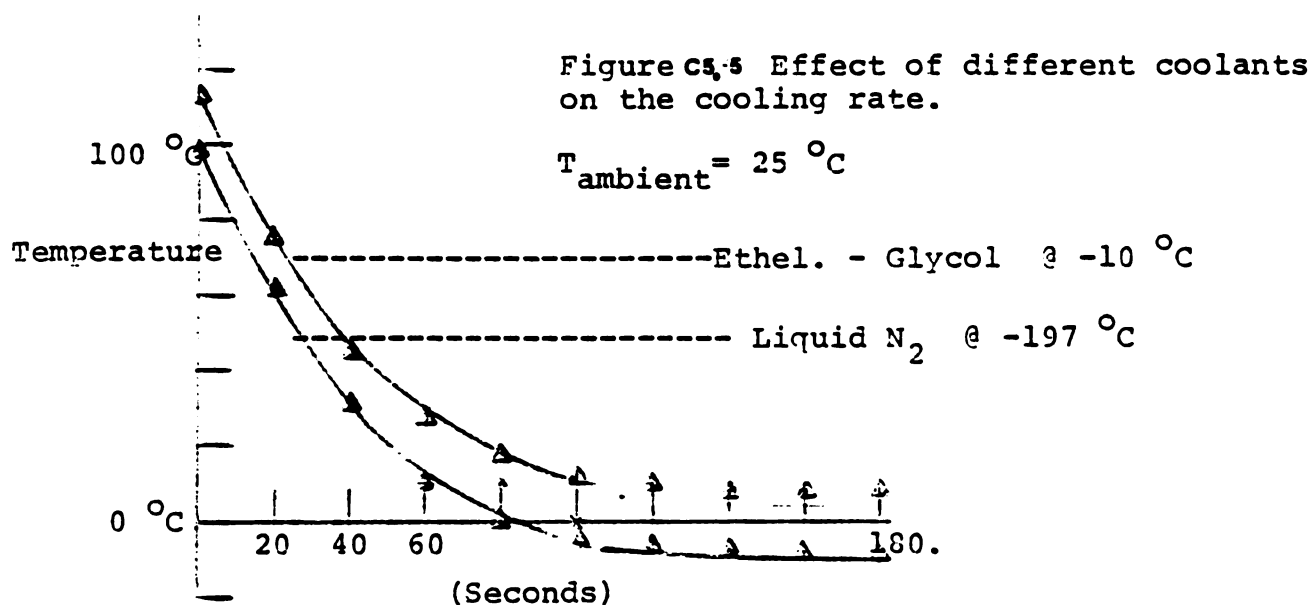


Figure C5.5 Effect of Different Thermal Sink Temperatures on the Stage Cooling Rate

## C.6 Conclusions

### C.6.1 Correlation of the Model to Experiments

The computer program HTRSIM.FOR provided valuable insight into the operation of the digital temperature controller. By performing parameter variation studies, it predicted the maximum source of error would come from the temperature sampling frequency.

The simulation program predictions were verified by experiment. There was an order of magnitude reduction in steady state temperature error when the temperature sampling frequency was increased from 10 to 100 hz. This can be shown from Figure C3.2 and was verified by experiment. As stated previously, the optimal sampling rate, limited by thermocouple time constants, was 100 hz. However, the actual error was larger than the predicted error of the simulation studies.

### C.6.2 Error Sources and Reduction

The simulation program estimated a controller accuracy of  $\pm .1^{\circ}\text{C}$  (Figure C3.4). The actual controller, in the breadboard state, was able to achieve an accuracy of  $\pm .5^{\circ}\text{C}$  as its worst case.

Upon analyzing the output of the thermocouple signal amplifier, it was determined that there was still substantial amounts of electromagnetic noise in the signal. It should be noted that there are numerous filters in the system to remove these errors. This EM noise would cause substantial errors in the temperature the computer reads in the control program. It is felt these EM effects would be eliminated if the controller was constructed on a PC board. There may have also

been a problem of a floating ground since the breadboard ground may have been slightly different than the I/O box, which was used as the common ground. The slight changes in the grounds may have occurred from the distance the device was away from the I/O box and the corresponding cable length.

The preceding work assumed the Action Pac was capable to accurately follow the actual temperature. The temperature control program sampled temperature at a frequency of 100 Hz. However, the time constant of the model 4150 Action Pac was approximately 130 ms. This information was provided by the manufacturer. The large time constant of the Action Pac would induce further errors in the control program. A modified version of the 4150 Action Pac which has a time constant of 5 ms. is available from Action Instruments Company of San Diego, California. The effects of the time constant of the Action Pac will be felt more strongly when the temperature controller is operated in the dynamic mode. Since the controller will be used mainly for isothermal temperature work, the effects of the Action Pac are not as great.

In order to optimize the controller performance, the following procedures should be initiated. First, when in operation, turn off all unnecessary sources of EM noise. Secondly, construct the controller on a PC board and house the board in a Faraday cage. Make all cable runs with grounded shielded cables especially from the Action Pac to the input of the thermocouple signal amplifier. Incorporate the modified Action Pac to allow for greater accuracy in the temperature measurements. When these modifications are made, the controller should operate well within its tolerance of  $\pm .1^{\circ}\text{C}$ .



## APPENDIX D

### EXPERIMENTAL UNCERTAINTY

#### D.1 Uncertainty Analysis for Isothermal Compressibility Modulus Experiment

This uncertainty analysis is based upon the average experimental condition of the liposome. The average conditions are:

$$\bar{T} = 1.601 \text{ dynes/cm}$$

$$\alpha = 0.023$$

$$\Delta L = 5.6 \text{ } \mu\text{m}$$

$$R_L = 23.9 \text{ } \mu\text{m}$$

$$R_p = 6.7 \text{ } \mu\text{m}$$

$$\Delta P = 3440.0 \text{ dynes/cm}$$

The resolution of our experimental apparatus is:

$$d\left(\frac{R_p}{R_c}\right) = 0.029 = \frac{R_p + \Delta R_p}{R_p - \Delta R_p}$$

$$d(\Delta L) = 0.55 \text{ } \mu\text{m}$$

$$d(R_p) = d(R_L) = 0.55 \text{ } \mu\text{m}$$

Using the relationship between aspiration pressure and membrane tension one can derive all the quantities of Equation (3.6.3). Results of this analysis reveals that the term:

$$\frac{\partial \bar{T}}{\partial (\Delta P)} d(\Delta P) = \pm 0.06 \frac{\text{dynes}}{\text{cm}}$$

is the major source of error in Equation (3.6.3).

Equation 3.6.4 can be solved if one uses Appendix A for the relation for  $\alpha$  and incorporates the average properties mentioned earlier. The results of this analysis yield the fact that the terms:

$$\frac{\partial \alpha}{\partial (R_p R_c^{-1})} d(R_p R_c^{-1}) \text{ and } \frac{\partial \alpha}{\partial (\Delta L)} d(\Delta L)$$

are the major sources of error.

Once  $d\alpha$  and  $d\bar{T}$  are found (Equation (3.6.1)) can be solved.

## D.2 Uncertainty Analysis for the Thermal Expansion Coefficient

Equation 3.6.2 is the expression for the uncertainty for  $C_{\bar{T}}$ .

$d\alpha$  and  $d\bar{T}$  must be determined using average conditions that are present during the experiment.  $d\alpha$  is the same as it was in Section D.2.  $d\bar{T}$  is  $\pm 0.5^\circ\text{C}$ .

Finding the values for  $d\alpha$  and  $d\bar{T}$  and using:

$$C_{\bar{T}} = \frac{(\alpha_2 - \alpha_1)}{(\bar{T}_2 - \bar{T}_1)} \quad (\text{D.2.1})$$

One can solve Equation (3.6.2) yielding  $dC_{\bar{T}}$ .

The major source of experimental error was the term:

$$\frac{\partial C_{\bar{T}}}{\partial \alpha} d\alpha$$



## APPENDIX E

### STATE PLANE GENERATION

Equations (4.1.1) and (4.1.3) were used to generate the state planes shown in Figures 4.2 and 4.3, respectively.

$$\gamma(\alpha, T) = K_T \alpha - K_T C_T (T - T_{REF})$$

$$\pi(\alpha, T) = \pi_0 + \frac{d\gamma}{dT} (T - T_{ref}) - K_T \alpha + K_T C_T (T - T_{ref})$$

The state planes were created using parameters experimentally derived from Soy (PC) vesicles. Therefore:

$$K_T = 52.0 \text{ dynes/cm}$$

$$C_T = 0.0036^\circ\text{C}^{-1}$$

$$T_{ref} = 25^\circ\text{C}$$

$$\frac{d\gamma}{dT} = 0.2 \text{ dynes/cm} - ^\circ\text{C}$$

$$\pi_0 \approx 70.0 \text{ dynes/cm}$$

Note the value for  $\frac{d\gamma}{dT}$  was approximated. Little information is available on the quantity.  $\pi_0$  refers to the liposome in the stress free state (Evans and Skalak (1980)).

## BIBLIOGRAPHY

.

## BIBLIOGRAPHY

1. Baret, J. F., (1983) "Progress in Surface and Membrane Science," 14, 291.
2. Blume, A. (1979) Biochimica et Biophysica Acta, 557, 32.
3. Boroske, M., Elwenspoek, F. (1981) Biophysical Journal, 34, 95.
4. Callow, R. (1983) "Thermodynamic Modelling and Cryomicroscopy of Large Unilamellar Liposomes," M.S. Dissertation, Mechanical Engineering Department, Michigan State University.
5. Defay, R. and Prigogine, I. (1966) Surface Tension and Absorption. John Wiley and Sons. New York, New York.
6. Evans, E. and Kwok, R. (1982) Submitted to Biochemistry, unpublished manuscript.
7. Evans, E. and Skalak, R. (1980) Mechanics and Thermodynamics of Biomembranes, CRC Press. Boca Raton, Florida.
8. Evans, E., Waugh, R., and Melnik, L. (1976) Biophysical Journal, 16, 585.
9. Evans, E. and Waugh, R. (1977) Journal of Colloid and Interface Science, 60, 286.
10. Fendler, J. H. (1981) "Membrane Mimetic Chemistry," John Wiley and Sons. New York, New York.
11. Gruen, D. and Wolfe, J. (1982) Biochimica et Biophysica Acta, 688, 512.
12. Israelachvili, J. N., Marle, L. J. A. and Horn, R. G. (1980) Biophysics, 13, 121.
13. Kwok, R. and Evans, E. (1981) Biophysical Journal, 35, 637.
14. Lee, A. (1975) Biochimica et Biophysica Acta, 413, 11.
15. Lehninger, A. (1970) Biochemistry, Worth Publishers, Inc. New York, New York.
16. McGiver, J. L. (1981) Journal of Colloid and Interface Science, 83, 301.

17. Mitchison, J. L. and Swan, M. N. (1954) Journal of Experimental Biology, 31, 443.
18. Nagle, J. F. (1976) J. Membrane Biology, 27, 233.
19. Nowlen, S. (1983) "Non-Equilibrium Thermodynamic Modeling and Parameter Estimation of Phenomenological Coefficients Describing Coupled Transport Across a Membrane," M.S. Dissertation, Mechanical Engineering Department, Michigan State University.
20. Olien, C. R. (1972) J. Theor. Biology, 39, 201.
21. Olien, C. R. (1977) Plant Physiol. 60, 499.
22. Rand, R. P. and Burton, A. C. (1964) Biophysical Journal, 4, 303.
23. Reynolds, J. A., Gilbert, D. B. (1974) Proc. Natl. Acad. Sci., U.S.A., 71, 2925.
24. Shabana, M. (1983) "Cryomicroscope Investigation and Thermodynamic Modeling of the Freezing of Unfertilized Hamster Ova," M.S. Dissertation, Mechanical Engineering Department, Michigan State University.
25. Steponkus (1982) Biochemica et Biophysica Acta. Submitted.
26. Tanford, C. (1973) "The Hydrophobic Effect," John Wiley and Sons, New York, New York.
27. Tanford, C. (1974) Journal of Physical Chemistry, 78, 2469.
28. Tu, S. M. (1983) "Computer Simulation of Two-Dimensional Transient Temperature Field in Cryomicroscope Conduction Stage," M.S. Dissertation, Mechanical Engineering Department, Michigan State University.
29. Yager, P., Sheridan, J. P. and Peticolas, W. L. (1982) Biochemica et Biophysica Acta, 693, 485.

